Structural characterization of FliP,

a component of the type III flagellar protein export gate

Doctoral Thesis
2016

Takuma Fukumura

Graduate School of Frontier Biosciences
Osaka University

Abstract

The bacterial flagellum is a filamentous motile organelle that protrudes from the cell body. For flagellar construction, flagellar component proteins are transported via its specific export apparatus from the cytoplasm to the growing distal end of the flagellar structure. The export gate complex is composed of six inner-membrane proteins, FliO, FliP, FliQ, FliR, FlhA and FlhB and utilizes proton motive force (PMF) as an essential energy source to drive flagellar protein export. However, it remains unknown how the export gate converts PMF to the mechanical work required for protein translocation and how the export gate complex assembles.

This thesis is focused on structure and function of FliP. FliP is an essential component for flagellar protein export and is assumed to be involved in the earliest stage of the assembly of the export gate complex. FliO is assumed to have a role in the regulation of FliP during flagellar assembly although it is not an essential component. To obtain the structural insight into FliP, I solved the structure of the periplasmic domain of FliP ($FliP_P$) from *Thermotoga maritia* at 2.4 Å resolution. The structural feature of Tm-$FliP_P$ and the following *in vivo* experiments suggested that FliP forms a dimer though the $FliP_P$-$FliP_P$ interaction. Structure-based mutational analyses of $FliP_P$ indicated that the $FliP_P$-$FliP_P$ interaction is required for efficient FliP assembly into the export gate.

To clarify that FliP forms oligomer, I purified full-length FliP derived from *Salmonella enterica* and observed it by electron microscopy. Full-length FliP formed the homo-hexameric ring structure. Co-expression of FliP-His with FliO and the following co-purification by Ni-NTA affinity chromatography indicated that FliP directly interacts with FliO. The $FliP_6$ ring dissociated from the FliO/P complex during size exclusion chromatography was more mono-dispersed than FliP alone, suggesting that FliO facilitates hexagonal FliP ring formation. Expression and purification of FliP mutant variants showed that the $FliP_P$-$FliP_P$ interaction is required for efficient FliP ring formation. I propose that the $FliP_6$ ring is a functional unit in the export gate complex.

Abbreviations

ATP : adenosine triphosphate

ADP : adenosine diphosphate

DDM : n-Dodecyl-β-D-maltoside

DNA : deoxyribonucleic acid

DTT : dithiothreitol

EDTA : ethylenediaminetetraacetic acid

EM : electron microscopy

IPTG : isopropyl-1-thio-b-D-galactopyranoside

LB : Luria-Bertani broth

MALDI-TOF : matrix assisted laser desorption ionization time of flight

MPD : 2-Methyl-2,4-pentanediol

OD_{600} : optical density (wavelength 600 nm)

PCR : plymerase chain reaction

PMF : proton motive force

RMSD : root mean square deviation

SAD : single-wavelength anomalous dispersion

S/N : signal/noise

SDS-PAGE : sodium dodecyl sulfate polyacrylamide gel electrophoresis

Tris : tris (hydroxymethyl) aminomethane

TM : transmembrane

Table of contents

Chapter 1
Introduction of the bacterial flagellum

1.1 Bacterial flagellum

Many bacteria can swim in liquid environments by rotating long, herical filamentous organelle called the flagellum (Berg and Anderson, 1973) (**Fig.1-1a**). The flagellum has a rotary motor at the base of its filament. The flagellar motor is driven by the electrochemical potential difference of H^+ (Larsen et al., 1974; Manson et al., 1977; Shioi et al., 1980), Na^+ (Hirota and Imae, 1983), or both H^+ and Na^+ (Terahara et al., 2008) across cytoplasmic membrane. The flagellar motor of *Escherichia coli* and *Salmonella entrica* use the proton influx as the energy source to rotate counterclockwise (CCW) at the maximum speed of 300 revolution per second. When each motors rotate in CCW direction, flagellar filaments form a bundle to produce a thrust for the straight swimming. Quick reversal of motor rotation to clockwise (CW) generates a twist and induces the morphological change of the filament, thereby disrupting the flagellar bundle and so the cells tumble and change their swimming direction (Berg and Brown, 1972; Larsen et al., 1974) (**Fig.1-1b**). This rotational switch is caused by chemotastic signals like chemical attractants, repellents, temperature and pH changes. Therefore, bacteria can move towards more favorable environments from less favorable ones (Cluzel et al., 2000; Sourjik and Berg, 2002).

1.2 Flagellar structure

The flugellum is a large supermoleculer complex composed of 30 different proteins in copy numbers ranging from a few to a few tens of thousands. The flagellar structure can be divided into at least three parts; the basal body, the hook and the filament. The basal body is embedded in the cell membranes and acts as a rotary motor. The basal body contains a specific export apparatus, which exports protein subunits responsible for the formation of the exterior structures beyond the cellular membranes. The filament is a relatively rigid helical structure and functions as a helical propeller. The hook is flexible and acts as a universal joint (Berg, 2003; Macnab, 2003; Sarkar et al., 2009) (**Fig.1-2**).

1.2.1. Basal body

The basal body consists of the C-ring, the MS-ring, the LP-ring and the rod. spans the inner and outer membranes. About 10 stator units assemble around the basal body and so the basal body acts as a bi-directional rotary motor. The MS and C rings act as a rotor of the flagellar motor. The MS-ring is made up of a single cytoplasmic membrane protein, FliF, and works as a base for flagellar assembly. The C-ring is composed of three soluble proteins, FliG, FliM and FliN, and binds to the cytoplasmic face of the MS-ring through an interaction between FliF and FliG. The structure of the C-ring is well characterized by various structural analyses such as X-ray crystallography and cryo-electron microscopy (cryo-EM) to build its functional atomic model (Francis et al., 1992; Francis et al., 1994; Brown et al., 2002; Brown et al,. 2005; Park et al., 2006; Sarkar et al., 2010; Lee et al., 2010; Mianmino et al., 2011; Paul et al., 2011). The C-ring is also called as the switch complex since FliG, FliM and FliN are involved in switching of the direction of flagellar motor rotation. A phosphorelated chemotastic

signal protein, CheY (CheY-P), which is produced by a two-component system activated from extracellular stimuli, regulates the switching frequency of the rotor ring complex. Phosphorelated CheY-P binds to both FliM and FliN to induce a conformational change in the switch complex and hence increases the probability that the motor rotates in the clockwise (CW) direction by (Bai et al., 2010; Sarkar et al., 2010a,b; Paul et al., 2011a,b). However, the detail switching mechanism is not yet clarified and several models are still present (Stock et al., 2012). The P and L rings spans the peptidoglycan layer and the outer membrane, respectively and acts as a bushing by encapsulating the rod that acts as a drive shaft (Akiba et al., 1991; Hizukuri et al., 2006, 2010).

The stator unit consists of two cytoplasmic membrane proteins, MotA and MotB. The stator functions as a proton channel that converts the energy derived from the proton influx through the channel to the rotation work (Suzuki et al., 2004; Thomas et al., 2006; Yonekura et al., 2011). Four copies of MotA and two copies of MotB form a functional stator complex (Braun and Blair, 2001; Kojima and Blair, 2004; Braun et al., 2004). MotA is a polytopic cytoplasmic membrane protein with four transmembrane helices (TM). Two conserved charged residues, Arg-90 and Glu-98, of MotA, which are located in the cytoplasmic loop between TM-2 and TM3, interact electrostatically with charged residues in the C-terminal domain of FliG to generate torque (Zhou and Blair, 1997; Zhou et al., 1998). The electrostatic interaction between MotA and FliG is also required for efficient stator assembly around the rotor. MotB is a bitopic cytoplasmic membrane protein and has a peptidoglycan-binding domain in its large C-terminal periplasmic domain ($MotB_C$). Dynamic conformational changes of $MotB_C$ are required for the binding and anchoring of the stator complex to the peptidoglycan (Kojima et al., 2009), allowing the rotor to rotate relative to the cell wall.

1.2.2. The filament

The filament of *Salmonella* is a substructure of the helical tubular axial structure made of a few tens of thousands of a single protein component, flagellin (FliC or FljB). It grows around the length of 10 - 15 μm. The filament propels the bacterial cell body by its rotation driven by the rotary motor (Fujime et al., 1972). The structure is composed of 11 protofilaments. Each protofilament is predicted to be in either a left-handed (L-type) or a right-handed (R-type) conformation to form the helical structure (Asakura, 1970). This is confirmed by atomic-resolution structural analyses of both L- and R-type the filaments by cryo-EM as well as by X-ray crystallographic analysis of FliC (Samatey et al., 2001; Yonekura et al., 2003; Maki-Yonekura et al., 2010).

1.2.3. The hook

The hook is a herical tubular axial substructure with its length of 55 ± 6 nm and is made of about 120 copies of a single protein, FlgE. The hook acts as a universal joint that smoothly transmits torque generated by the motor to the filament regardless of its orientation (Berg and Anderson, 1973). A whole atomic model of the hook structure is built by docking the atomic model of FlgE fragment solved by X-ray crystallography into a relative high resolution EM-density map of the hook (Samatey et al., 2004; Shaikh et al., 2005; Fujii et al., 2009). The hook subunits are tightly packed in the inner core domain whereas the outer two domains of FlgE are loosely packed in the axial inner subunit interactions in the proto-filament structure due to distinct difference of terminal alpha helices from those of the filament. So, the hook can exert the universal joint function.

1.2.4. Other structures

The filament and the hook are connected by the specific substructure, called junction, which is composed of three proteins, HAP1 (FlgK) and HAP3 (FlgL) and HAP2 (FliD). HAP2 forms the pentameric cap structure at the distal end of the filament to promote filament growth (Macnab, 2003; Berg, 2003).

The rod is a helical tubular structure and acts as a drive shaft connecting the rotor rings and the hook. The rod with an approximate length of 30 nm is a complex structure composed of five proteins, FliE, FlgB, FlgC, FlgF and FlgG. The distal rod freely rotates inside the LP-ring, of which friction is assumed to be low enough for smooth motor rotation (Khan et al., 1985; Akiba et al., 1991). Rod proteins have a strong tendency to form a fibrous structure (Saijo-Hamana et al., 2004). This makes the structural analysis of the rod components by X-ray crystallography difficult. Recently the truncation of the unfolded N- and C-terminal region of FlgG allowed its crystallization (Saijo-Hamano et al., 2013). Although the atomic model of the unusally elongated rod structure called polyrod has been built by docking atomic structure of FlgG fragment into an EM-density map of poly-rod made of FlgG (Fujii, T. 2009), the whole structure of the rod and the mechanism of the smooth rotation remain unknown.

1.3 Flagellar assembly

Flagellar assembly has been clarified by EM observation of each immature structure from various flagellar mutants (Suzuki et al., 1978; Suzuki and Komeda, 1981; Kubori et al., 1992) **(Fig.1-3)**. The assembly of the flagellum begins with the self-assembly of the MS-ring composed of 26 copies of FliF in the cytoplasmic membrane (**Fig.1-3 A**). The export gate complex assembles into the central pore of the

MS-ring during MS ring formation (Morimoto *et al*., 2014). However, the assembly order of the MS-ring and the export gate complex is still unclear (Li and Sourjik, 2011; Wagner et al., 2010; Morimoto et al., 2014). After the formation of the MS-ring, the C-ring assembles at the cytoplasmic face of the MS-ring. Then the soluble components of the flagellar protein export apparatus forms the ATPase ring complex at the flagellar base (**Fig.1-3 B,C**). Recently, the ATPase ring complex has been visualized just outside the C ring by electron cryotomography (Chen *et al.*, 2011; Abrusci *et al.*, 2013; Kawamoto *et al*., 2013). The flagellar axial structure, which consists of the rod, the hook, the junction, the filament cap and the filament, elongates in a tip-growth manner: Flagellar axial proteins are transported via the flagellar export apparatus from the cytoplasm to the distal end of the growing structure where their self-assembly occurs (Namba and Vonderviszt, 1997).

At first, five rod proteins (FliE, FlgB, FlgC, FlgF and FlgG) are exported to the periplasmic side of the MS-ring to form the rod structure with the help of the rod cap protein (FlgJ). The rod passes through the peptidoglycan layer by the peptidoglycan hydrolyzing activity of FlgJ (Nambu et al., 1999) (**Fig.1-3 D**). After the formation of the rod, FlgH and FlgI, which are exported into the periplasm by a general secretion pathway, assemble around the rod to form the LP-ring (**Fig.1-3 E, F**). After completion of the basal body, the hook component protein (FlgE) is transported to the tip of the rod and hook and self-assembles with the help of the hook cap made of five copies of FlgD until its length of 55 ± 6 nm (**Fig.1-3 G,H**) (Ohnishi et al., 1994; Hirano et al., 1994). The hook length is well controlled by an interaction between a ruler protein FliK and an export gate component FlhB. The interaction of the C-terminal domain of FliK with the C-terminal cytoplasmic domain of FlhB induces a conformational change of FlhB to switch substrate specificity of the export apparatus from rod-(FliE, FlgB, FlgC, FlgF,

FlgG, FlgJ) and hook-type (FlgD, FlgE, FliK) to filament-type export substrates (FlgM, FlgK, FlgL, FliD, FliC). Upon hook completion, the hook cap complex is replaced by HAP1 (FlgK) (**Fig.1-3 I**), followed by the attachment of HAP3 (FlgL) on the HAP1 layer to form the hook-filament junction structure (**Fig.1-3 J**). Then the pentameric filament cap complex composed of FliD is formed at the tip of the hook-filament junction to facilitate the polymerization of flagellin (**Fig.1-3 K,L**). Flagellin subunits are transported to the distal end of the growing flagellum (**Fig.1-3 M,R**). The motor begins to rotate after the incorporation of the stator units around the rotor, and the flagellum propels cell body.

1.4 Type III flagellar protein export apparatus

For the construction of the axial flagellar structures, flagellar axial proteins must be exported to their final destination where their assembly occurs. Protein secretion beyond the cell membrane is one of the common mechanisms among all organs to maintain their biological activity. Bacteia have two major secretion pathways to secrete proteins into the periplasm (Wickner and Schekman, 2005; Natele et al., 2007). The general secretion route, termed Sec-pathway, catalyzes the transmembrane translocation of proteins in their unfolded conformation, and then the secreted proteins fold into their native structure at the trans-side of the membrane. Another pathway is the twin-arginine translocation pathway, termed Tat-pathway. It catalyzes the translocation of folded proteins. Both pathways need a specific signal sequence in the N-terminus of substrate proteins. However, among flagellar proteins, only five components FlgH and FlgI (LP-ring components), FlgA (peroplasmic chaperone), FlhE (putative plug or regulator of protone flux of flagellar protein export gate) and FliP (a component of flagellar protein export gate) have the signal peptides and are translocated via the Sec

pathway (Homma et al., 1987; Jones et al., 1987, 1989; Kutsukake et al., 1994a; Nambu et al., 2000; Schoenhalas and Macnab, 1996; Minamino et al., 1994; Ohnishi et al., 1997; Paradel et al.,2004; Lee J et al., 2012; Lee J et al., 2015).

Fourteen flagellar proteins are translocated via its specific export apparatus, named the flagellar type III protein export apparatus from the cytoplasm into the central channel of the growing flagellar structure (Macnab, 2003; Minamino et al., 2008a) (**Fig.1-4**). The export apparatus is beleived to be located in the central pore of the MS-ring. The export apparatus is composed of a water-soluble ATPase complex consisting of FliH, FliI and FliJ, and a transmembrane export gate complex made of FlhA, FlhB, FliO, FliP, FliQ and FliR (Minamino and Macnab, 1999; Minamino and Macnab, 2000). In addition the export apparatus has several flagellar substrate specific chaperons (FlgN, FliA, FliS and FliT) for the ordered flagellar protein export (Vogler et al., 1991; Yokoseki et al., 1995; Mianamino and Macnab, 1999; Fraser et al., 1999; Auvray et al., 2001; Benntt et al., 2001; Aldridge et al., 2003; Minamino et al., 2012; Kinoshita et al., 2013). Recent structural analysis by cryo-electron tomography has revealed the whole complex architecture of the cytoplasmic domain of the export apparatus at low resolution (Murphy et al., 2006; Chen et al., 2011; Raddi et al, 2012; Abrusci et al., 2012; Kawamoto et al., 2013; Hu et al., 2015).

1.4.1. The ATPase complex

The ATPase complex is composed of three soluble components FliH, FliI and FliJ (**Fig.1-5 a**). Among these components, FliI shows the ATPase activity. Both amino acid sequence and structure of FliI shows high similarities with α and β subunit of F-type ATPase (Fan et al., 1996; Vogler et al., 1991; Imada et al., 2007) (**Fig.1-6 a**).

The α and β subunits form the $\alpha_3\beta_3$ ring complex in F-type ATPase whereas FliI forms a homo-hexamer (Claret et al., 2003; Kazetani et al., 2009; Minamino et al., 2006; Chen et al., 2011; Kawamoto et al., 2013; Bai et al; 2014). Although FliJ does not show a significant sequence similarity with components of both F- and V-type ATPase, its coiled-coil structure show extensive structural similarities with both γ subunit of F-type ATPase and D subunit of V-type ATPase, which locate at the central pore of $\alpha_3\beta_3$ and A_3B_3 ring, respectively (Ibuki et al, 2011) (**Fig.1-6 b**). FliJ binds to the central pore of the $FliI_6$ ring to form $FliI_6FliJ$ complex in a way similar to the γ and D subunits. Interestingly, FliJ can bind to the center of the A_3B_3 ring complex to act as a rotary stalk in V-type ATPase, suggesting that the type III export apparatus and F- and V-type ATPase families share the same evolutional origin (Kishikawa et al, 2013) (**Fig.1-6 c,d**). FliJ binds to not only FliI but also FliH and the axial components to prevent their aggregation in cytoplasm. The amino acid sequence of FliH also shows high similarities with b and δ subunit of F-type ATPase (Pallen et al., 2006).

Previous biochemical analysis has revealed that FliH binds to FliI to form the $FliH_2FliI$ complex in the solution (Minamino and Macnab, 2000; Auvray et al., 2002). Since FliH interacts with a C-ring component FliN and the export gate component FlhA through its N-terminal domain, FliH is proposed to stabilize the localization of the $FliI_6FliJ$ ring complex at the base of the flagellum (González-Pedrajo et al., 2002; Minamino et al., 2009; Hara et al., 2012). Since the $FliH_2FliI$ complex bind to export substrates and chaperone-export substrate complexes (Thomas et al., 2004; Imada et al., 2010; Minamino et al., 2012a), the $FliH_2FliI$ complex is proposed to deliver the export substrates to the export gate complex.

1.4.2. The export gate complex

The trasnmembrane export gate complex is composed of six integral inner membrane proteins, FlhA, FlhB, FliO, FliP, FliQ and FliR and is believed to be located in the central pore of the MS-ring (Mianmino and Macnab, 1999) **(Fig.1-5 b)**. In contrast to the cytoplasmic ATPase complex, these components do not show any amino acid sequence similarities.

FlhA is the most conserved component among these proteins. Previous genetic and biochemical study indicated that FlhA interacts with all of other export gate components and the MS-ring component, FliF (Kihara et al., 2001; McMurry et al., 2004; Hara et al., 2011; Li and Sourjik, 2011; Barker and Samatey, 2012). FlhA has a large cytoplasmic domain ($FlhA_C$) (Minamino et al, 1994). X-ray crystallographic analysis of $FlhA_C$ revealed $FlhA_C$ consists of four subdomains, D1, D2, D3 and D4 and a flexible linker connecting $FlhA_C$ with the N-terminal transmembrane domain with eight TM helices (Saijo et al., 2010; Bange et al., 2010). A highly conserved hydrophobic dimple located at an interface between D1 and D2 is involved in the interaction with flagellar secretion chaperones FlgN, FliS and FliT (Mianmono et al., 2012b; Kinoshita et al., 2013). FlgN, FliT and FliS are chaperons specific for FlgK/L, FliD and FliC respectively, and their binding affinities for $FlhA_C$ increase when they form a complex with their substrates. The binding affinity of the FlgN/FlgK complex for $FlhA_C$ is slightly higher than that of the FliT/FliD complex and is about 14-fold higher than that of the FliS/FliC complex. This suggests that $FlhA_C$ interacts with the FlgN/FlgK and FlgN/FlgL complexes prior to the FliT/FliD and FliS/FliC complexes to form the hook-filament junction zone upon completion of hook assembly (Evdokimov et al., 2003; Imada et al., 2010; Mianmono et al., 2012 Kinoshita et al., 2013). The cytoplasmic domain of FlhA homologue, MxiA, formed the nonameric ring structure in

the crystal. Structure-based mutagenesis has revealed that $MxiA_C$ ring formation is required for protein translocation. The electron densities corresponding $MxiA_C$ and $FlhA_C$ were observed by cryo-electron tomography, indicating that FlhA forms a nonamer in the MS-ring in a way similar to MxiA (Abrusci et al., 2012; Kawamoto et al., 2013). FlhB has a large cytoplasmic domain ($FlhB_C$), too and is involved in export specificty swiching from rod/hook-type to filament-type export class (Mianmino et al., 2000). Self-cleavage of $FlhB_C$ and the following interaction with the C-terminal domain of FliK after the hook completion result in the conformational change of $FlhB_C$ to swich the export specificity (Kutsukake et al., 1994; Williams et al., 1996; Minamino and Macnab, 2000; Ferris et al., 2005; Moriya et al., 2006). Therefore, both $FlhA_C$ and $FlhB_C$ play important roles in coordinating protein export with flagellar assembly. In contrast to $FlhA_C$ and $FlhB_C$, the function and structure of the transmembrane regions of FlhA and FlhB remain unknown.

Little of functions and structures of FliO, FliP, FliQ and FliR is known by the same reason. FliO is a 13 kDa bitopic membrane protein. FliO is not essential for flagellar construction (Barker et al., 2014). Indeed, several bacteria do not have the *fliO* gene in their genome. All bypass mutations isolated from a *fliO* null mutant have been found in the *fliP* gene, indicating that FliO has something important role to regulate FliP function (Barker et al., 2010). FliO has a large C-terminal cytoplasmic domain and is assumed to be involved in flagellar protein export. FliP is a 25 kDa polytopic cytoplasmic membrane protein and has a signal peptide at its N-terminus (Malakooti et al., 1994; Ohnishi et al., 1997). FliP is translocated and inserted in the cytoplasmic membrane by the Sec pathway. The N-terminal signal peptide of FliP is cleaved during membrane insertion, producing mature FliP with the molecular weight of 23 kDa (Ohnishi et al., 1997; Pradel et al., 2004). The mature form of FliP is predicted to have

four TM helices and have a 10 kD periplasmic domain ($FliP_P$) between TM-2 and TM-3. FliP is identified in purified basal body and about four copies of FliP molecules are estimated to associate with the MS-ring (Fan et al., 1997). FliQ has two TM helices and its molecular weight is 10 kDa. The function and structure of FliQ are almost unknown. FliR is a 29 kDa cytoplasmic membrane protein and is predicted to have six TM helices. FliR is visualized to associate with the MS ring by immno-electron microscope (Fan et al., 1997). Since a fusion protein of FliR and FlhB is functional, the stoichiometry of FliR and FlhB is assumed to be 1 to 1 (Van Arnam et al., 2010).

It has been shown that the FliI ATPase activity is dispensable for flagellar protein export and that proton motive force (PMF) across the cytoplasmic membrane is a primary energy source (Minamino and Namba, 2008; Paul et al., 2008). The export gate complex can utilize only the membrane potential ($\Delta\psi$) of the PMF when FliJ interacts with the linker region of FlhA in the presence of FliH and FliI (Minamino et al., 2011). Since FliJ can work a rotary stalk in the A_3B_3 ring complex of V-type ATPase (Kishikawa et al., 2013), FliJ could rotate in the $FliI_6$ ring by ATP hydrolysis to induces a conformational change of FlhA thorough the interaction of FliJ with FlhA, allowing the gate to drive flagellar protein export in a $\Delta\psi$-dependent manner (Kishikawa et al., 2013; Minamino et al., 2014) (**Fig.1-7**).

1.5 Aims and outline of my Ph.D work

Genetic and biochemical studies of the assembly mechanism of the injectisome of *Salmonella*, which is a highly homologous structure of the FBB, indicate that the export gate complex assembles in a coordinated manner prior to the assembly of the inner ring complex of the injectisome, which corresponds to the MS-ring of the FBB (Wagner et al., 2010). SpaP (FliP homologue) and SpaR (FliR homologue) form a

stable complex, which is followed by the assembly of SpaQ (FliQ homologue) and SpaS (FlhB homologue) and finally InvA (FlhA homologue). The export gate complex allows the inner ring of the injectisome to be more efficiently formed around the gate. It has been shown that FliO contributes to the protein stability of FliP within the cytoplasmic membrane (Barker et al., 2010). The assembly of FlhA-YFP into the export gate complex is dependent on FliO, FliP, FliQ and FliR but not on FlhB (Morimoto et al., 2014), raising the possibility that the assembly of the flagellar export gate complex begins with FliO and FliP, followed by FliQ and FliR, and finally FlhA and FlhB.

To understand the assembly mechanism of the export gate complex in more detail, my Ph.D work is focused on the structural characterization of FliP. Because FliP has a large periplasmic domain between TM-2 and TM-3 (**Fig.1-8**), I first characterized the structure and function of the $FliP_P$ (Chapter 2). I solved the crystal structure of $FliP_P$ from *Thermotoga maritima*. Structure-based mutational analyses reveal that FliP forms a homo-dimer through the $FliP_P$-$FliP_P$ interaction *in vivo*. To clarify the oligomeric state of FliP, I over-expressed and purified full-length FliP of *Salmonella*. I show that FliP efficiently assembles into a hexagonal ring oligomer with the help of FliO and that the $FliP_P$-$FliP_P$ interaction is required for FliP ring formation (chapter 3). Based on these results, I will discuss the assembly mechanism of FliP. Finally, I establish the co-expression system of the FliO/P/Q/R-FlhB/A-FliF/G complex to clarify the further detail molecular mechanism of the export gate assembly in the future (chapter4).

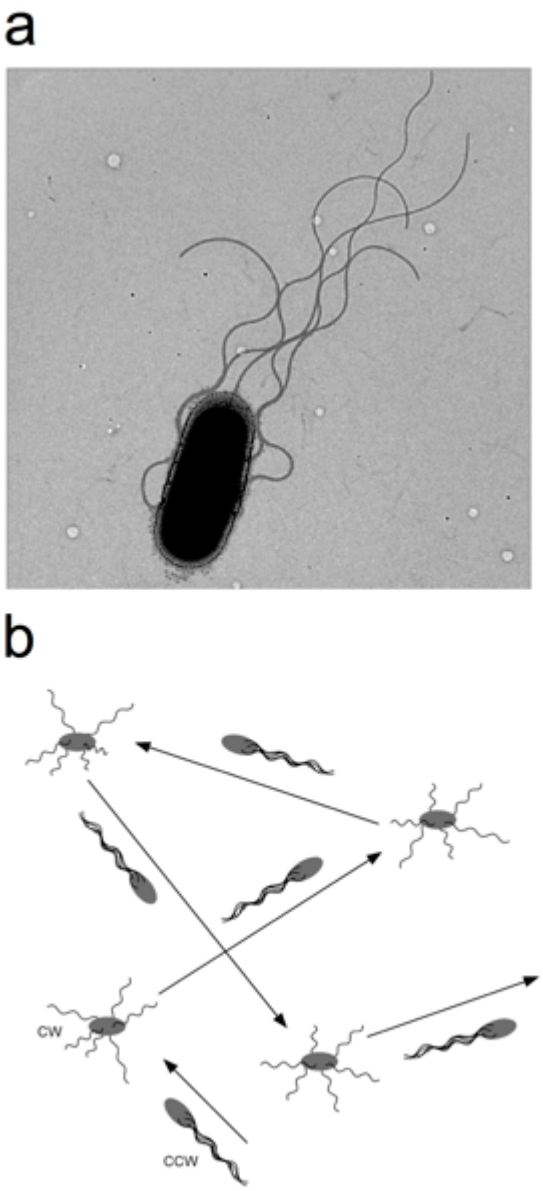

Figure1-1. Bacterial flagellum.

(a) Electron micrograph of *Salmonella enterica* serovar Typhimurium. Typical size of the cell body is about 2 μm. In this micrograph, five flagellar filaments form a bundle. (b) A typical swimming pattern of *Salmonella* cells.

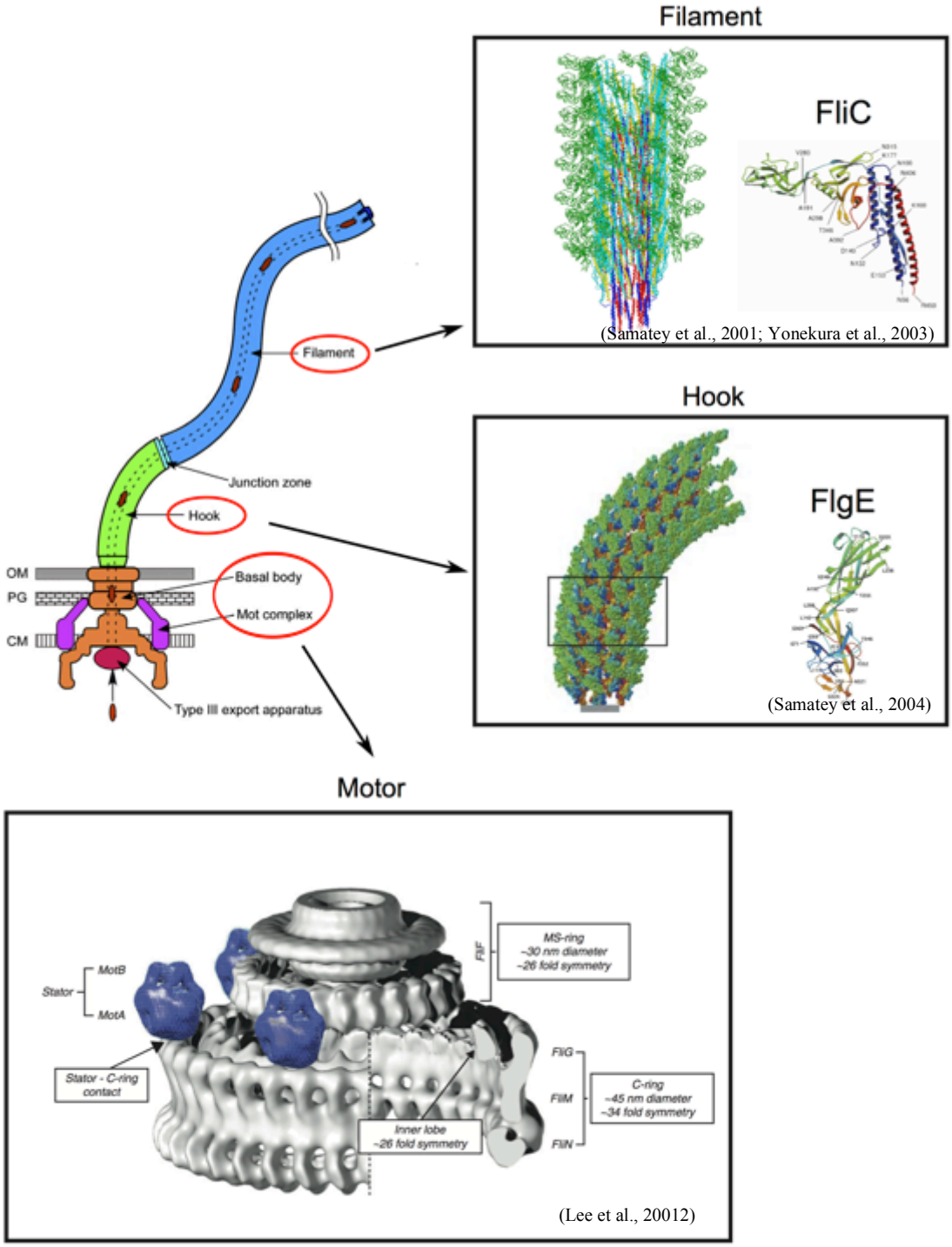

Figure1-2. Major substructures of flugellum..

Schematic diagram of the bacterial flagellum and substructures. The filament is composed of tens of thousands of a single component, FliC. The hook is composed of a single component, FlgE. At least 10-12 stator complexes surround the rotor complex. (Samatey et al., 2001;

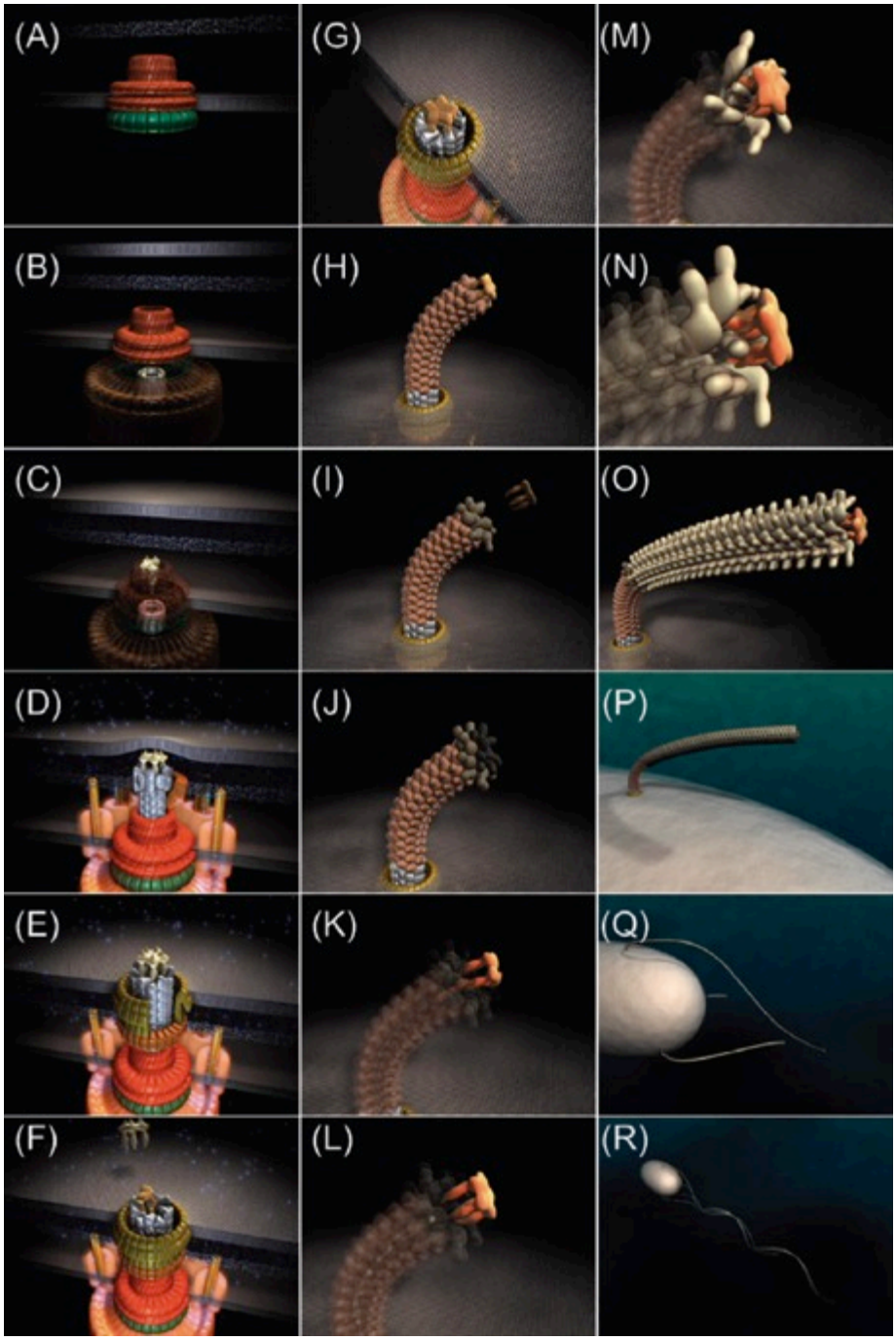

Figure1-3. The assembly process of the flagellum proceeds from (a) to (r).

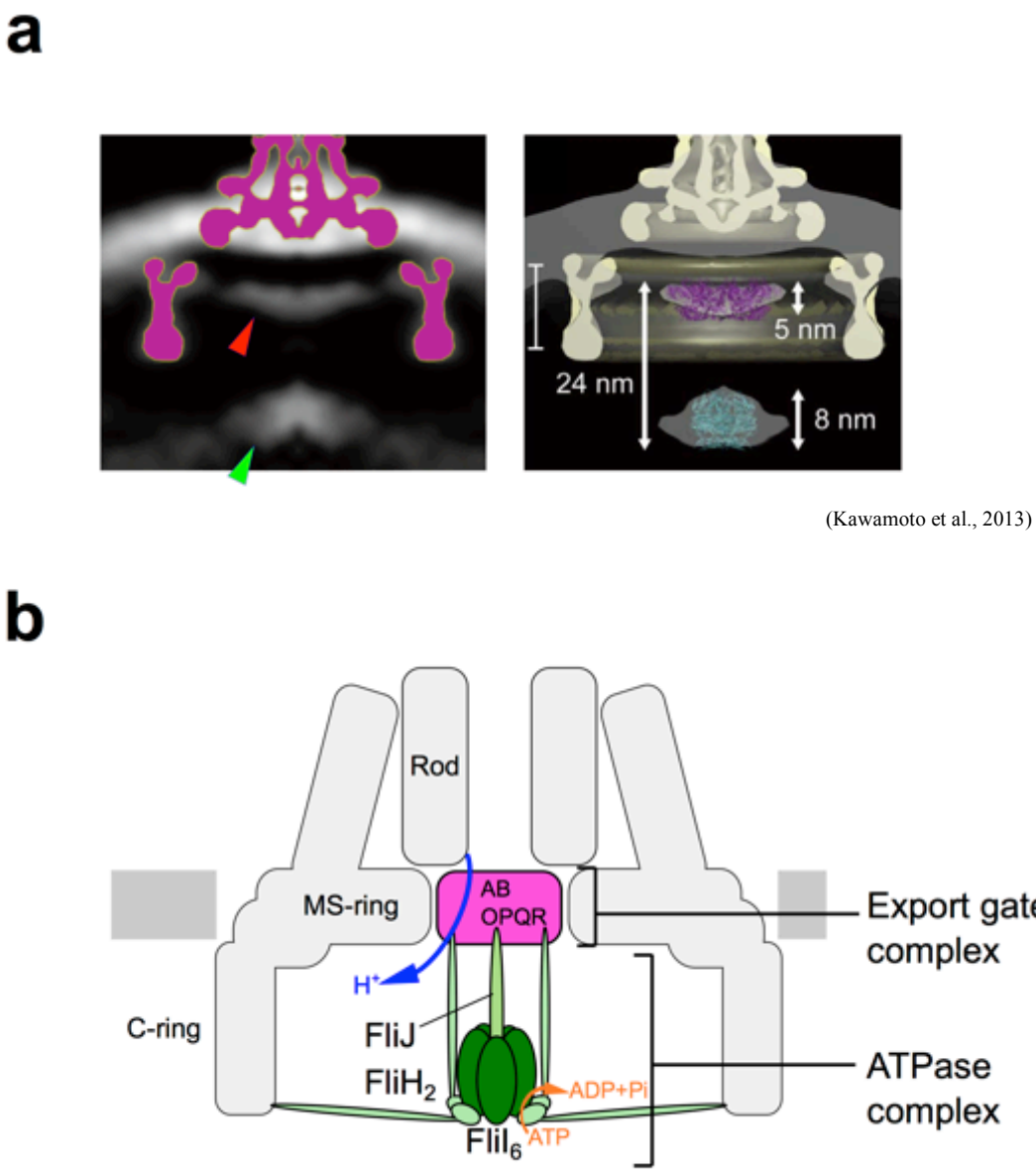

Figure1-4. Architecture of flagellar protein export apparatus.

(a) *In situ* structure of the basal body revealed by the cryo-electron tomography. Red arrow indicates the cytoplasmic domain of FlhA. Green arrow indicates the FliI ATPase ring complex. (b) Schematic architecture of the flagellar protein export apparatus. The export gate utilizes proton motive force as an essential energy source. The FliI ATPase activity is required for efficient flagellar protein export.

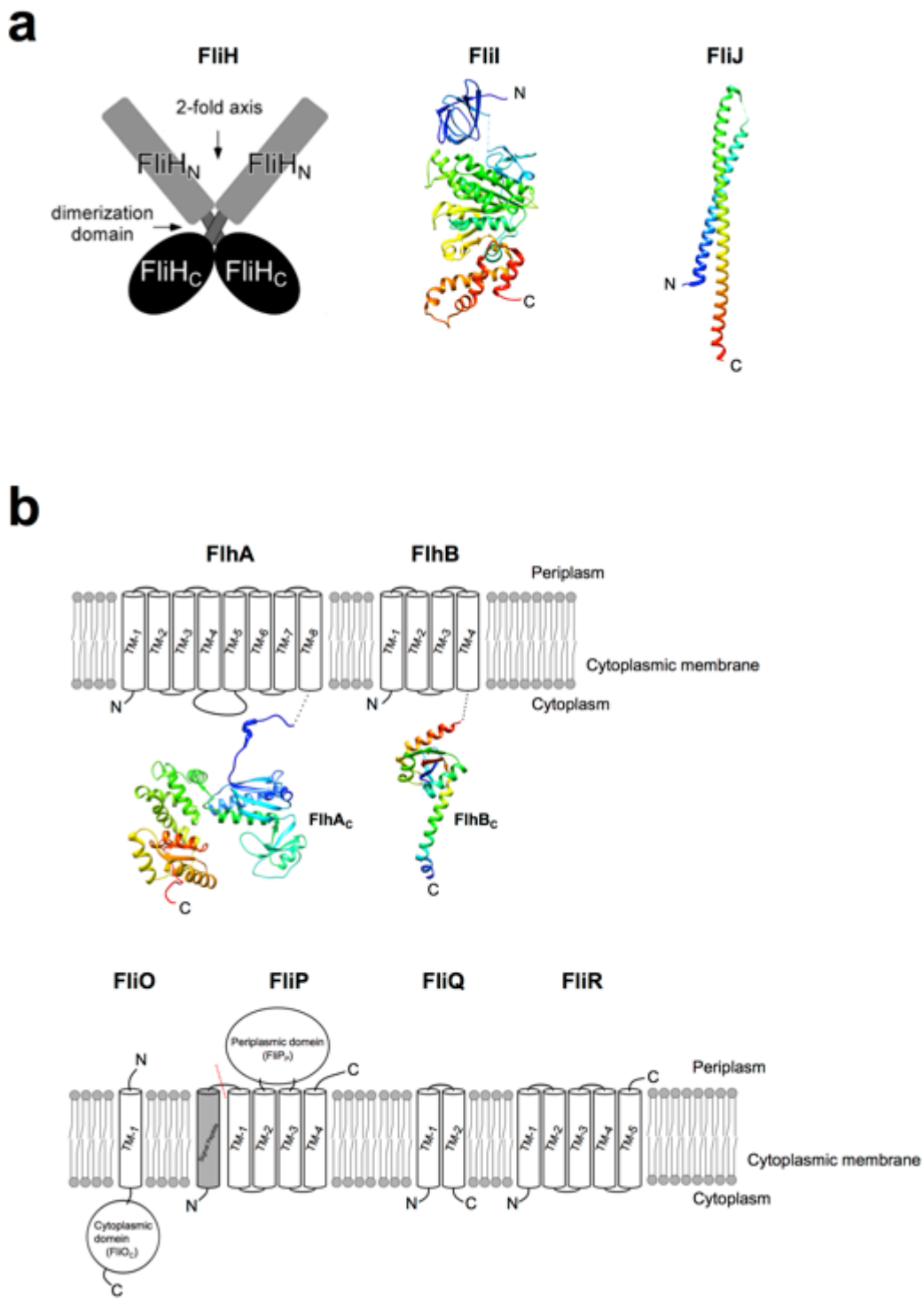

Figure1-5. Components of the export apparatus

(a) Components of the cytoplasmic ATPase complex. Crystal structures of FliI (PDB ID: 2DPY) and FliJ (PDB ID: 3AJW) are shown in rainbow. (b) Topology model of export gate components. Crystal structures of $FlhA_C$ (PDB ID : 3A5I) and $FlhB_C$ (PDB ID: 3B0Z) are depicted in rainbow.

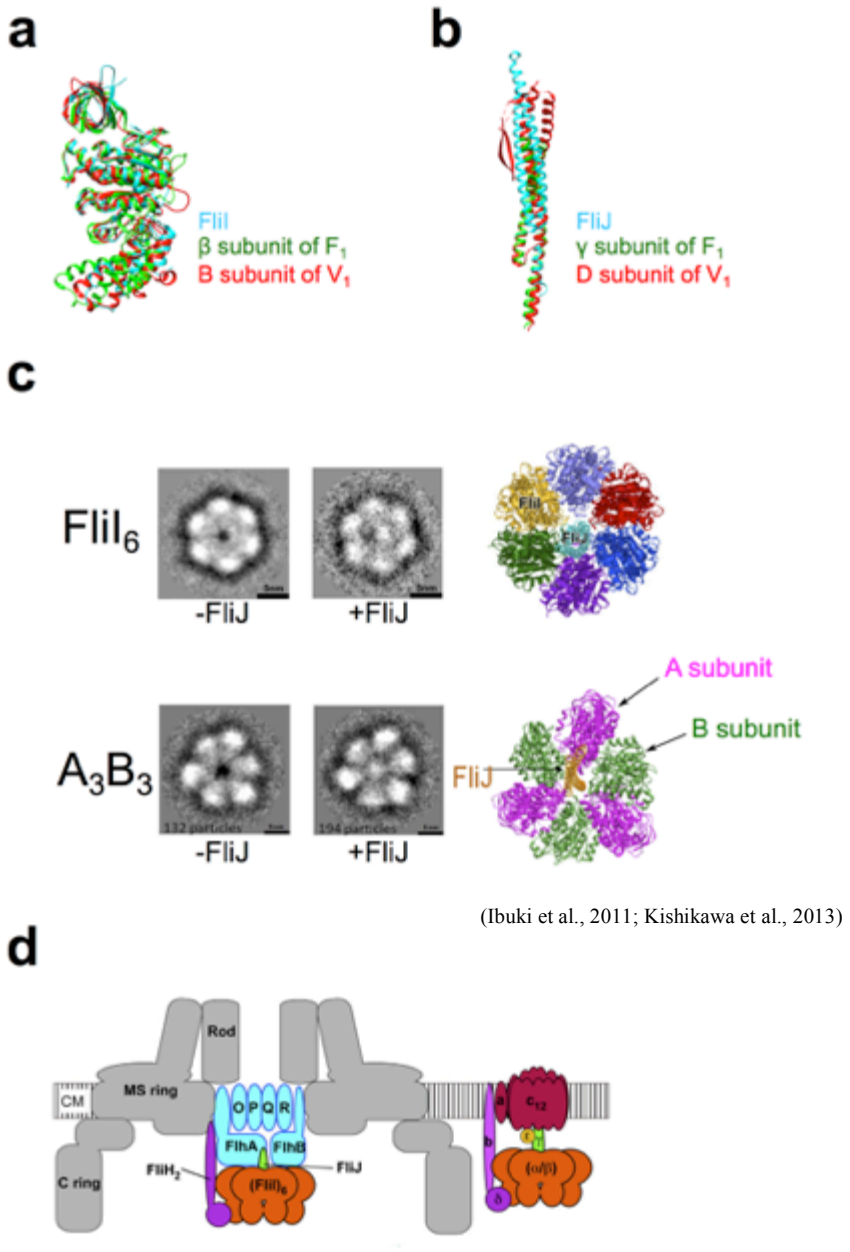

(Ibuki et al., 2011; Kishikawa et al., 2013)

Figure1-6. Structural similarity between the flagellar cytoplasmic ATPase complex and F- and V-type rotary ATPases.

(a) Superimposition of FliI (cyan) onto the β subunit of F-type ATPase (green, PDB ID: 1BMF) and the B subunit of V-type ATPase (red, PDB ID: 3VR6). (b) Superimposision of FliJ (cyan) on the γ subunit of F-type ATPase (green) and the D subunit of V-type ATPase (red). (c) 2-D cryo-EM average images of $FliI_6$ and A_3B_3 with or without FliJ. The structural models of $FliI_6J$ and A_3B_3J are shown on the right. (d) Comparison between the architecture of the export apparatus and F_O-F_1 ATPase.

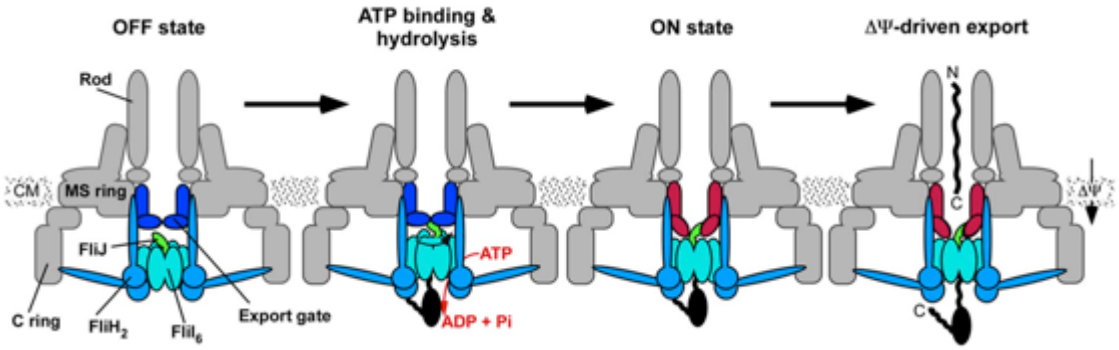

(Minamino et al., 2014)

Figure1-7. Current model of flagellar protein export mechanism

ATP hydrolysis by FliI activates the export gate through an interaction between FliJ and FlhA, allowing the export gate complex to efficiently utilize the membrane potential ($\Delta\psi$) of proton motive force to unfold and transport export substrates into the central channel of the flagellar axial structure.

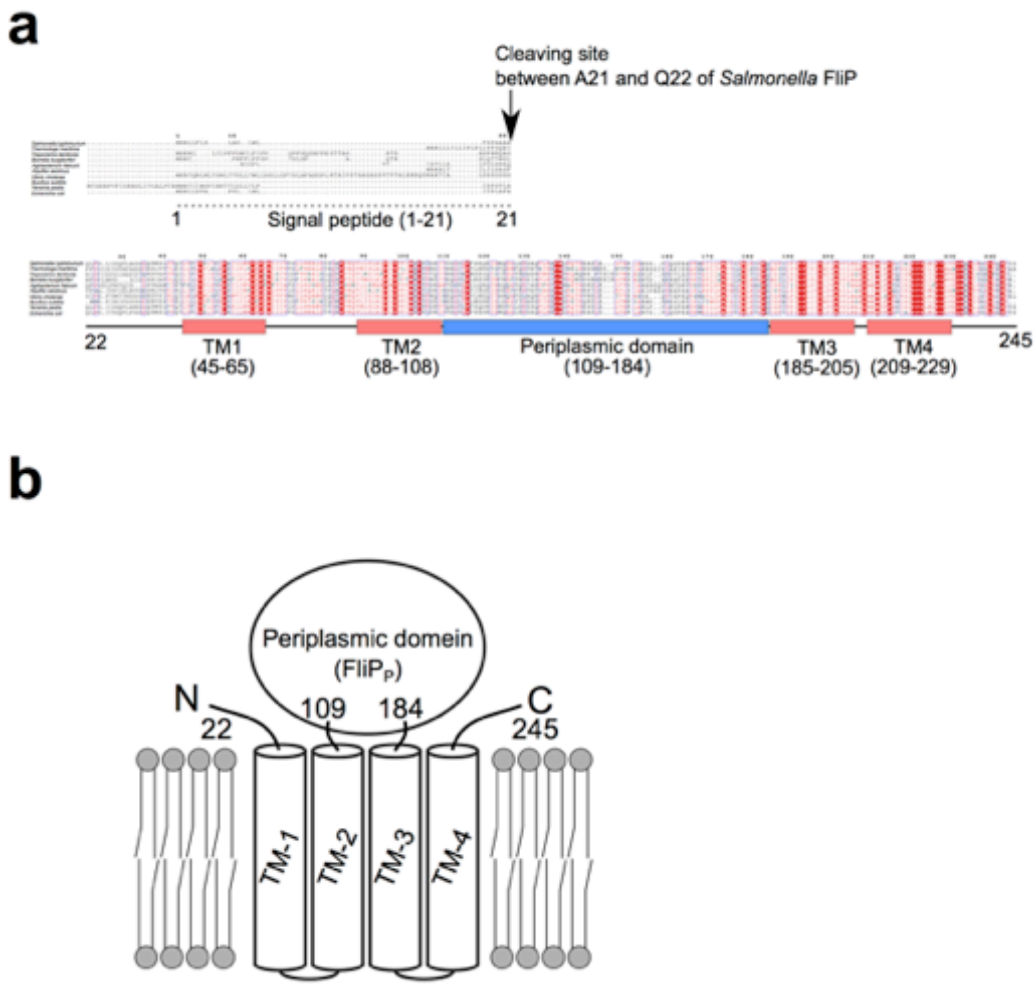

Figure1-8. Multiple sequence alignment of FliP homologues and topology model of FliP

Chapter 2
Structural and functional characterization of the periplasmic domain of FliP

2.1. Introduction

It has been reported that overexpression of full-length FliP causes a remarkable growth arrest of *E. coli* host cells (Kinoshita, M., Imada, K. and Minamino, T. personal communications). This makes it difficult to carry out biochemical analysis of FliP. Therefore, to clarify the role of FliP in flagellar protein export, I first carried out structural and functional characterization of a relatively large periplasmic domain of FliP ($FliP_P$), which is predicted to be located between TM-2 and TM-3. Although we use *Salmonella* as a model organism for flagellar research, $FliP_P$ from *Salmonella typhimurium* was expressed as an inclusion body and strongly tends to aggregate during its refolding and purification (Fukumura, T. 2013). In contrast, $FliP_P$ from *Thermotoga maritima* (Tm-$FliP_P$) was highly soluble, and so I obtained the hexagonal crystal of Tm-$FliP_P$ and detemined its crystal structure at 2.4 Å resolution. In this chapter, I will show the details of the Tm-$FliP_P$ structure. I also show that the $FliP_P$-$FliP_P$ interaction is critical for FliP function. Based on the obtained results, I will discuss a biological unit of FliP and will also discuss how the $FliP_P$-$FliP_P$ interaction contributes to FliP assembly into the export gate complex.

2.2. Materials and Methods

1.2.1. Bacterial strains, plasmids and media

Bacterial strains and plasmids used in this chapter are listed in Table 2-1. Compositions of media used in this study are as follows:

- Luria-Bertani Broth (LB) medium : H_2O 1 l, Bacto™ Tryptone (Becton, Dickinson and Company) 10 g, Bacto™ Yeast Extract (Becton, Dickinson and Company) 5 g, NaCl 5 g
- 2×YT medium : H_2O 1 l, Bacto™ Tryptone 16 g, Bacto™ Yeast Extract 10 g, NaCl 5 g
- Terrific Broth (TB) medium : H_2O 1 l, Bacto™ Tryptone 12 g, Bacto™ Yeast Extract 24 g, glycerol 8 ml, K_2HPO_4 9.4 g, KH_2PO_4 2.2 g
- LA plate : LB 1 l, Bacto™ Agar (Becton, Dickinson and Company) 15 g
- Soft tryptone agar plate : H_2O 1 l, Bacto™ Tryptone 10 g, Bacto™ Agar 7 g, NaCl 5 g
- SeMet minimal medium : H_2O 1 l, NH_4Cl 1 g, KH_2PO_4 3 g, $Na_2HPO_4 \cdot 12H_2O$ 8 g, glucose 20 g , $MgSO_4 \cdot 7H_2O$ 0.6 g, $Fe_2(SO_4)_3$ 10 mg, thiamine 10 mg, L-SeMet 50 mg (Guerrero *et al*, 2001; Sakane, 2008)

To maintain plasmids in the bacterial host cells, ampicillin were added to each media at a final concentration of 50-100 μg/ml

1.2.2. DNA manipulations

To construct a plasmid for the crystallization, a DNA fragment encoding $FliP_P$ (Tm-$FliP_P$) consisting of residues 110-188 of *T. maritima* FliP was generated by PCR with a plasmid pGS1-*TmfliP* (Gene Design Inc.) as a template. The amplified PCR product was inserted into the *Nde*I and *Bam*HI sites of the pET15b vector.

To construct pUC19-based plasmids for both disulfide cross-linking experiments and genetic characterization, a DNA fragment encoding *fliP* was amplified by PCR with genomic *Salmonella* DNA as a template. The amplified DNA fragment was inserted into the *Nde*I and *Bam*HI sites of the pET3c vector. Then, the DNA fragment encoding the *fliP* gene with a ribosome-binding site of the pET3c vector was subcloned into the *Xba*I-*Bam*HI sites of pUC19. Each mutation for disulfide cross-linking experiments and genetic characterization was generated by quickChange site-directed mutagenesis method as described in the manufacturer's instruction (Strategene).

To construct pBAD24-based plasmids for genetic characterization, a DNA fragment encoding *fliP* with the 30 bp upstream region was amplified by PCR with genomic DNA of *Salmonella* as a template. The amplified DNA fragment was inserted into the *EcoR*I and *Kpn*I sites of the pBAD24 vector. Each mutation for genetic characterization was generated by site-directed mutagenesis.

DNA sequence reactions were carried out using BigDye v3.1 (Applied Biosystems) and DNA sequencing was performed with an Applied Biosystems 3130 Genetic Analyzer (Applied Biosystems).

1.2.3. Protein expression and purification

To purify Tm-FliP$_P$ for crystallization, a 30 ml overnight culture of *Escherichia coli* strain BL21 (DE3) harboring a plasmid encoding TmFliP$_P$ with a hexahistidine tag attached at its N-terminus (pKY045) was inoculated into 2.5 l LB medium. Cells were grown at 30 °C until the culture density had reached an OD_{600} = 0.4 - 0.8. Expression of $_{His}$Tm-FliP$_P$ was induced by isopropyl β-D-1-thiogalactopyranoside (IPTG) at a final concentration of 0.4 mM, and then culture was incubated for another 6

h. The cells were harvested by centrifugation (6,400 g, 10 min, 4 ºC) and stored at -80 ºC. The cells were thawed, suspended in Buffer A (50 mM Tris-HCl pH 8.0, 300 mM NaCl) containing 20 mM imidazole and sonicated (ASTRASON model XL2020 sonicator, Misonix Inc.). The cell lysate was centrifuged (110,000 g, 40 min, 4 ºC) to remove cell debris. The supernatant was loaded onto a Ni-NTA agarose resin (QIAGEN) equilibrated with Buffer A containing 20 mM imidazole. Protein was then eluted with a 50–300 mM imidazole gradient in Buffer A and fractions containing $_{His}$TmFliP$_P$ were collected. The His_6 tag was removed by thrombin (GE Healthcare) to the $_{His}$Tm-FliP$_P$ solution. The reaction mixture was dialyzed overnight at 4 ºC against Buffer A with 200 mM imidazole, followed by Buffer A with 100 mM imidazole and finally buffer A with 20 mM imidazole. Tm-FliP$_P$ was purified using a HisTrap HP 5 ml (GE Healthcare) to remove the N-terminally His-tagged polypeptide, non-cleaved $_{His}$Tm-FliP$_P$ and thrombin. The eluted fractions containing Tm-FliP$_P$ was concentrated using a Vivaspin 20 (30,000 MWCO, Sartorius), dialyzed overnight against Buffer B (10 mM sodium phosphate pH 7.0, 100 mM NaCl) and loaded a HiLoad Superdex 75 (26/60) column (GE Healthcare) equilibrated with Buffer B. Fractions containing TmFliP$_P$ were collected. The purity of the product was examined by SDS-PAGE and MALDI-TOF mass spectrometry (Voyager DE/PRO, Applied Biosystems).

To purify a SeMet derivative of Tm-FliP$_P$ (SeMet_Tm-FliP$_P$) for phase determination, we used the *E. coli* B834 (DE3) strain as a host. Cells grown overnight in LB at 30 ºC were harvested by centrifugation (5,000 g, 5 min, 4 ºC), washed and suspended in 0.5%(w/v) NaCl. The cells were inoculated into the SeMet minimal medium and grown at 37 ºC until the cell density had reached an OD_{600} of 0.4. Expression of SeMet-labelled $_{His}$Tm-FliP$_P$ was induced with 0.4 mM IPTG and the culture was continued for another 4 h. The cells were harvested by centrifugation (6,400

g, 10 min, 4 ºC) and stored at 4 ºC. SeMet_Tm-FliP$_P$ was purified in the same way with native Tm-FliP$_P$. Incorporation of SeMet into TmFliP$_P$ was confirmed by MALDI-TOF mass spectrometry.

1.2.4. Analytical ultracentrifugation of Tm-FliP$_P$

Analytical ultracentrifugation was carried out using a Beckman Optima XL-A analytical ultracentrifuge with an AnTi 60 rotor. The protein samples were extensively dialyzed against Buffer B prior to analytical ultracentrifugation. Sedimentation equilibrium measurements were performed at 4 ºC at speeds of 22,000, 24,000 and 26,000 rpm on a sample at an initial concentration of 0.85 mg/ml, using a two channel charcoal-filled epon and quartz windows. Scans were collected at a wavelength of 280 nm at a spacing of 0.001 cm in step mode with twenty averages per step. The equilibrium of the system was judged by superimposition of the three scans. Sedimentation equilibrium data of TmFliP$_P$ whose partial specific volume v-bar was calculated to be 0.736 ml/g from the amino acid composition of the protein were analyzed for the average molecular weight by the program OptimaTM XL-A/XLI version 6.04.

1.2.5. Crystallization of Tm-FliP$_P$

Purified Tm-FliP$_P$ was concentrated and passed through a 0.20 μm Millex-LG syringe filter (Millipore). The protein concentration was estimated based on its Abs_{280} of 0.47 for a 1 mg ml^{-1} solution. Initial crystallization screening of Tm-FliP$_P$ was performed at 4 ºC and 20 ºC by the sitting-drop vapor-diffusion technique using NeXtal Evolution plates (QIAGEN) and the following screening kits: Wizard I and II, Cryo I and II (Emerald Biostructures) and Crystal Screen I and II (Hampton Research). Each

drop was prepared by mixing 1.0 µl protein solution (20 mg ml^{-1} Tm-$FliP_P$, 10 mM sodium-phosphate pH 7.0, 100 mM NaCl) with 1.0 µl reservoir solution, and equilibrated against 60 µl reservoir solution. The crystallization conditions were optimized by varying the precipitant concentration, pH and additives using the hanging-drop method with VDX plates (Hampton Research). Finally, crystals suitable for X-ray analysis were obtained from drops prepared by mixing 1.5 µl protein solution (5 mg ml^{-1}) with 1.5 µl reservoir solution containing 0.1 M phosphate-citrate pH 4.4, 36% 2-Methyl-2,4-pentanediol (MPD) at 4 ºC within a week.

1.2.6. X-ray diffraction data collection and processing

All X-ray diffraction data were collected at SPring-8 beamline BL41XU (Harima, Japan). Crystals were mounted into nylon cryo-loops (Hampton Research). Since the concentration of MPD in the crystallization drops was high enough for cryoprotection, the crystals were directly transferred into liquid nitrogen for freezing. The diffraction data were recorded on a MX225HE CCD detector (Rayonix) at -173 ºC using a nitrogen gas flow to reduce radiation damage. The diffraction data were indexed, integrated and scaled using the programs iMOSFLM (Battye et al., 2011) and SCALA (Evans, 2006) from the CCP4 program suite (Winn et al., 2011). The statistics of data collection are summarized in Table 1. The model was determined and refined with PHENIX (Adams et al., 2010). The missing residues in the auto-built model were manually added in COOT (Emsly et al., 2010). All structural figures were prepared by Chimera (https://www.cgl.ucsf.edu/chimera/).

1.2.7. In vivo disulfide cross-linking and immunoblotting

Salmonella cells were exponentially grown in 50 ml LB at 30 ºC with shaking. The cells were harvested and resuspended in 5 ml of PPBS. For oxidization, iodine was added to the suspended *Salmonella* cells at a final concentration of 0.2 mM and incubated for 5 min at room temperature. To block disulfide bond formation for the remaining cyctein, N-ethylmalemide was added to the cell suspensions at a final concentration of 20 mM and incubated for 5 min at room temperature. The cells were washed with PBS and resuspended in 10 ml of PBS, and then disrupted by sonication (ASTRASON model XL2020 sonicator, Misonix Inc.). The cell lysate was centrifuged at 20,000g for 15 min to remove cell debris. Supernatant was ultracentrifuged at 110,000 g for 30 min to isolate the membrane fraction. The membrane fractions were resuspended in PBS to adjust the total membrane protein concentration of 10 mg ml^{-1}. The membranes were mixed with non-reducing SDS loading buffer. After sodium dodecyl sulfate-polyacrylamide gel electrophoresis (SDS-PAGE), immunoblot was carried out with monoclonal anti-HA antibody and detected by an ECL immunoblotting detection kit (GE Healthcare).

1.2.8. Motility assay

Fresh transformant colonies were inoculated onto soft tryptone agar plates and incubated at 30°C. For the induction from pBAD24, 0.2 % arabinose was added to soft tryptone agar plates. The motility rings were analyzed by imageJ.

1.2.9. Preparation of whole cell fractions and immunoblotting

Salmonella cells were grown at 30°C with shaking until the cell density had reached an OD_{600} of 1.2–1.8. Aliquots of culture proteins containing a constant number of cells were clarified by centrifugation. Cell pellets were resuspended in SDS-loading

buffer normalized by cell density to give a constant amount of cells. After SDS-PAGE, immunobloting was carried out with monoclonal anti-HA antibody and detected by an ECL immunoblotting detection kit (GE Healthcare).

1.2.10. Multiple sequrnce aliginment

Multiple sequence alignment was performed by CLUSTAL-Ω (http://www.ebi.ac.uk/Tools/msa/clustalo/). Depection of the multiple sequence alignment was carried out by similarity coloring scheme of %equivalent in ESprint3 server (http://espript.ibcp.fr/ESPript/ESPript/).

Table 1-1. Strains and plasmids used in this study of this chapter.

Strains or Plasmids	Relevant properties	Source or reference
E.coli		
BL21 (DE3)	Host for overexpression from the T7 promoter	Novege
Salmonella		
SJW1103	Wild type for motility and chemotaxis	(Yamaguchi et al., 1984)
TH	ΔfliP	
Plasmids		
pET3c	Cloning vector	Novagen
pET15b	Expression vector	Novagen
pBAD24	Expression vector	(Guzman et al., 1995)
pUC19	Expression and cloning vector	Invitrogen
pKY045	pET15b/TmFliP$_{110\text{-}188}$	This study
pKY049	pET3c/$_{HA}$FliP	This study
pKY041	pBAD24/$_{HA}$FliP	This study
pKY050	pBAD24/$_{HA}$FliP(F137A)	This study
pKY051	pBAD24/$_{HA}$FliP(M138A)	This study
pKY052	pBAD24/$_{HA}$FliP(Q141A)	This study
pKY053	pBAD24/$_{HA}$FliP(Y174A)	This study
pKY054	pBAD24/$_{HA}$FliP(E178A)	This study
pKY010	pUC19/$_{HA}$FliP	This study
pKY014	pUC19/$_{HA}$FliP(F137A)	This study
pKY055	pUC19/$_{HA}$FliP(M138A)	This study
pKY056	pUC19/$_{HA}$FliP(Q141A)	This study
pKY019	pUC19/$_{HA}$FliP(Y174A)	This study
pKY021	pUC19/$_{HA}$FliP(E178A)	This study
pKY057	pUC19/$_{HA}$FliP(G130C-A182C)	This study
pKY058	pUC19/$_{HA}$FliP(P133C-A182C)	This study
pKY059	pUC19/$_{HA}$FliP(P133C-E178C)	This study
pKY060	pUC19/$_{HA}$FliP(P133C-T181C)	This study
pKY061	pUC19/$_{HA}$FliP(F137C)	This study
pKY062	pUC19/$_{HA}$FliP(F137C-E178C)	This study
pKY063	pUC19/$_{HA}$FliP(R140C)	This study
pKY064	pUC19/$_{HA}$FliP(E144C)	This study
pKY065	pUC19/$_{HA}$FliP(M123C-L153C)	This study

pKY066	pUC19/$_{HA}$FliP(M123C-T176C)	This study
pKY067	pUC19/$_{HA}$FliP(Q124C-S156C)	This study
pKY068	pUC19/$_{HA}$FliP(L127C-P172C)	This study

Table 1-2. Primers used in this study of this chapter

Primers	Sequence
Tm-FliPp.Fw	GGAATTCCATATGTACAACAATGCCATAACGCCG
Tm-FliPp.Re	CGCGGATCCTCATTTGAAGGCAACTTCCAGTTC
FliP_NdeI.Fw	acacaagcatATGCGCCGTTTGTTTGTTATTCCT
FliP_BamHI.Re	cgcggatccCTAACTGTAAAAGCTTTGGG
FliP+30bp_EcoRI.Fw	ccggaattcgagcttactcaagcgttccg
FliP_KpnI.Re	cggggtaccCTAACTGTAAAAGCTTTGGG
SigPep_HA.Fw	CCGCCGCCGCTGCGCAAtacccatacgatgttccagattacgctCTGCCGGGGCTTATCAG
SigPep_HA.Re	CTGATAAGCCCCGGCAGagcgtaatctggaacatcgtatgggtaTTGCGCAGCGGCGGCGG
FliP_F137A.Fw	GCGCAACCGTTACGCGCGgcCATGCTGCGCCAAACCCGC
FliP_F137A.Re	GCGGGTTTGGCGCAGCATGgcCGCGCGTAACGGTTGCGC
FliP_M138A.Fw	CAACCGTTACGCGCGTTCgcGCTGCGCCAAACCCGCGAAG
FliP_M138A.Re	CTTCGCGGGTTTGGCGCAGCgcGAACGCGCGTAACGGTTG
FliP_Q141A.Fw	CGCGCGTTCATGCTGCGCgcgACCCGCGAAGCCGATCTG
FliP_Q141A.Re	CAGATCGGCTTCGCGGGTcgcGCGCAGCATGAACGCGCG
FliP_Y174A.Fw	CGTATCCTCCTGCCCGCTgcgGTCACCAGCGAATTAAAG
FliP_Y174A.Re	CTTTAATTCGCTGGTGACcgcAGCGGGCAGGAGGATACG
FliP_E178A.Fw	CCCGCTTATGTCACCAGCGcATTAAAGACGGCGTTTCAG
FliP_E178A.Re	CTGAAACGCCGTCTTTAATgCGCTGGTGACATAAGCGGG
FliP_M123C.Fw	GCGAGCAGAAAATTTCTtgcCAGGAAGCGCTGGATAAAG
FliP_M123C.Re	CTTTATCCAGCGCTTCCTGgcaAGAAATTTTCTGCTCGC
FliP_Q124C.Fw	GAGCAGAAAATTTCTATGtgcGAAGCGCTGGATAAAGGC
FliP_Q124C.Re	GCCTTTATCCAGCGCTTCgcaCATAGAAATTTTCTGCTC
FliP_L127C.Fw	GAAAATTTCTATGCAGGAAGCGtgtGATAAAGGCGCGCAACCG
FliP_L127C.Re	CGGTTGCGCGCCTTTATCacaCGCTTCCTGCATAGAAATTTTC
FliP_G130C.Fw	CAGGAAGCGCTGGATAAAtGCGCGCAACCGTTACGCGCG
FliP_G130C.Re	CGCGCGTAACGGTTGCGCGCaTTTATCCAGCGCTTCCTG
FliP_P133C.Fw	CTGGATAAAGGCGCGCAAtgcTTACGCGCGTTCATGCTG
FliP_P133C.Re	CAGCATGAACGCGCGTAAgcaTTGCGCGCCTTTATCCAG
FliP_F137C.Fw	GCGCAACCGTTACGCGCGTgCATGCTGCGCCAAACCCGC
FliP_F137C.Re	GCGGGTTTGGCGCAGCATGcACGCGCGTAACGGTTGCGC
FliP_R140C.Fw	GTTACGCGCGTTCATGCTGtGCCAAACCCGCGAAGCCGAT
FliP_R140C.Re	ATCGGCTTCGCGGGTTTGGCaCAGCATGAACGCGCGTAAC
FliP_E144C.Fw	CATGCTGCGCCAAACCCGCtgcGCCGATCTGGCGCTGTTTG

FliP_E144C.Re	CAAACAGCGCCAGATCGGCgcaGCGGGTTTGGCGCAGCATG
FliP_L153C.Fw	CTGGCGCTGTTTGCCCGTtgcGCCAATAGCGGTCCGTTAC
FliP_L153C.Re	GTAACGGACCGCTATTGGCgcaACGGGCAAACAGCGCCAG
FliP_S156C.Fw	GTTTGCCCGTCTGGCCAATtgcGGTCCGTTACAGGGACCG
FliP_S156C.Re	CGGTCCCTGTAACGGACCgcaATTGGCCAGACGGGCAAAC
FliP_L172C.Fw	GATGCGTATCCTCCTGtgcGCTTATGTCACCAGCGAATTAAAG
FliP_L172C.Re	CTTTAATTCGCTGGTGACATAAGCgcaCAGGAGGATACGCATC
FliP_T176C.Fw	GTATCCTCCTGCCCGCTTATGTCtgcAGCGAATTAAAGACGGCG
FliP_T176C.Re	CGCCGTCTTTAATTCGCTgcaGACATAAGCGGGCAGGAGGATAC
FliP_E178C.Fw	CCCGCTTATGTCACCAGCtgcTTAAAGACGGCGTTTCAG
FliP_E178C.Re	CTGAAACGCCGTCTTTAAgcaGCTGGTGACATAAGCGGG
FliP_T181C.Fw	GTCACCAGCGAATTAAAGtgcGCGTTTCAGATCGGTTTTAC
FliP_T181C.Re	GTAAAACCGATCTGAAACGCgcaCTTTAATTCGCTGGTGAC
FliP_A182.Fw	ACCAGCGAATTAAAGACGtgcTTTCAGATCGGTTTTACG
FliP_A182.Re	CGTAAAACCGATCTGAAAgcaCGTCTTTAATTCGCTGGT

Table 1-3. Summary of the data statistics.
Values in parentheses indicate statistics for the highest resolution shell.

Data collection

	Native	SeMet derivative
Space group	$P6_222$	$P6_222$
Cell dimensions		
a,b,c (Å)	114.9, 114.9, 193.8	115.3, 115.3, 193.6
α,β,γ (°)	90, 90, 120	90, 90, 120
Wavelength (Å)	1	0.9791
Resolution (Å)	43.6 - 2.4 (2.53 - 2.4)	43 - 2.8 (2.95 - 2.8)
No. of reflections	214552	257930
No. of unique reflections	30262	18573
Rmerge	0.088 (0.357)	0.097 (0.23)
I/σI	13.5 (5.5)	17.0 (5.4)
Completeness (%)	99.9 (100.0)	95.1 (67.6)
Redundancy	7.1 (7.2)	7.5 (2.4)
Figure of Merit		0.48

$^{\#}R_{\text{merge}} = \Sigma_{\mathbf{h}} \Sigma_l |I_{\mathbf{h}l} - \langle I_{\mathbf{h}} \rangle| / \Sigma_{\mathbf{h}} \Sigma_l \langle I_{\mathbf{h}} \rangle$, where I_l is the lth observation of reflection **h** and $\langle I_{\mathbf{h}} \rangle$ is the weighted average intensity for all observations l of reflection **h**.
$^{+}R_{\text{ano}} = \Sigma_{\mathbf{h}} |\langle I(\mathbf{h}+) \rangle - \langle I(\mathbf{h}-) \rangle| / \Sigma_{\mathbf{h}} (\langle I(\mathbf{h}+) \rangle + \langle I(\mathbf{h}-) \rangle)$, where $\langle I(\mathbf{h}+) \rangle$ and $\langle I(\mathbf{h}-) \rangle$ correspond to the average intensities of each Friedel pair for reflection **h**.

Table 1-4. X-ray refinement statistics.
Values in parentheses indicate statistics for the highest resolution shell.

Refinement	
Measurement	Value
Resolution (Å)	42.9 - 2.4
No. of reflections	30084
Rwork/Rfree	0.211 / 0.258
No. atoms	
Protein	4354
Water	397
B-factor	
Protein	43.6
Water	52
R.m.s deviations	
Bond lengths (Å)	0.004
Bond angles (°)	0.778

エラー! リンクが正しくありません。

$R_w = \sum ||F_o| - |F_c|| / \sum |F_o|$, same as R_{free} but calculated on 5% of data set aside for refinement.

2.3. Results

2.3.1. Purification and crystallization of Tm-FliP$_P$

The size exclusion chromatography showed that the molecular weight of eluted Tm-FliP$_P$ is about 40 kDa (**Fig.2-1a**). Since the molecular weight of Tm-FliP$_P$ was deduced about 10 kDa, purified Tm-FliP$_P$ would form a tetramer. To confirm whether Tm-FliP$_P$ is actually in a tetrameric state in solution, I carried out sedimentation equilibrium analytical ultracentrifugation. A single species model with the molecular weight of 39.7 kDa produced the best fit (**Fig.2-1b**). Therefore, I conclude that Tm-FliP$_P$ forms a homo-tetramer in solution. Some of the tetramers, however, were dissociated into dimers in a few days. To stabilize the tetramer, I varied pH and NaCl concentrations and found that the tetramer is quite stable at pH less than 7.0. I obtained Tm-FliP$_P$ crystals under several conditions that contain low molecular weight compounds as a precipitant at low pH (less than 8.0). The crystals were especially well grown in a solution containing 0.1 M phosphate-citrate pH 4.4, 36% MPD at 4 ºC (**Fig.2-2**). The TmFliP$_P$ crystals diffracted to 2.4 Å resolution and belonged to the hexagonal space group $P6_222$. SeMet_Tm-FliP$_P$ crystals were obtained under the same condition as the native Tm-FliP$_P$ ones. The shape and size of the SeMet_Tm-FliP$_P$ crystals were almost the same as those of the native ones and its space group was also $P6_222$.

2.3.2. Crystal structure of Tm-FliP$_P$

Tm-FliP$_P$ is composed of four α helices (α1, α2, α3 and α4) (**Fig.2-3a**). The N-terminal 13 residues were not visible in the electron density map presumably due to its conformational flexibility. Therefore, an atomic model of Tm-FliP$_P$ contained residues from Gly-123 to Lys-188, which correspond to Gly-122 and Gln-184

respectively in $FliP_P$ of *Salmonella*. The asymmetric unit contained eight Tm-$FliP_P$ molecules (**Fig.2-4a**). All chains in the asymmetric unit show no structural difference (**Fig.2-4b**). The most closely contact allows four chains to form a tetramer unit (**Fig.2-5a**). The electrostatic potential map and hydrophobicity map of the tetramer surface show that the surface is polarized and hydrophilic (**Fig.2-5b,c)**. Since sedimentation equilibrium analytical ultracentrifugation measurements showed that Tm-$FliP_P$ forms a tetramer in solution, I conclude that the tetramer structure observed in the crystal is equivalent to that in solution.

2.3.3. Disulfide cross-linking of $FliP_P$

Two two-fold axes cross orthogonally at the center of the tetramer structure (two-fold axis1 and axis2) (**Fig.2-6a).** As a result, only two of the four C-termini of the Tm-$FliP_P$ chains of the tetramer can be connected to the cytoplasmic membrane region in the same orientation when the tetramer is put on the cytoplasmic membrane so as to connect the C-terminus of Tm-$FliP_P$ directly to the cytoplasmic membrane. (**Fig.2-6b)**. Therefore, I assumed that full-length FliP would form a dimer through the $FliP_P$-$FliP_P$ interaction. There were two self-interaction interfaces in the tetramer structure (Interface1 and Interface2) (**Fig.2-6a, 2-7**). In order to investigate which interface is actually exist in full-length FliP, I replaced pairs of amino acid residues, which are in close proximity to each other at the interfaces of Tm-$FliP_P$, with cysteine to performed *in vivo* disulfide cross-linking using full-length FliP of *Salmonella*. I selected eight pairs of residues for the tight interface and four residues for the loose interface that would be possible to form a disulfide bond when they were substituted with cysteine. A *Salmonella fliP* null mutant cells that express $_{HA}$FliP with a pair of cysteine substitutions from pUC19, were exponentially grown in LB media at 30 ºC and then, disulfide

cross-linking was induced by adding iodine, followed by SDS-PAGE and finally western blotting with anti-HA antibody. In the case of the Interface1, cross-linking products were detected under an oxidizing condition but not at a reducing condition (**Fig2-8a**). The cross-linking product was about 50 kDa that would correspond to a dimer of $_{HA}$FliP. Almost all pairs of the Cys variants produced the cross-linking products except for $_{HA}$FliP(P133C/E178C). The motility of the $_{HA}$FliP(P133C/E178C) and $_{HA}$FliP(F137C/E178C) was not restored at all, indicating E178 is critical for for FliP function. Therefore, I suggest that full-length FliP forms a dimer through the Interface1. In contrast, any FliP protein expression was not observed at the Interface2 (**Fig2-8b**), raising the possibility that these residues is critical for the protein stability of FliP. Therefore, we cannot rule out the possibility that the interactions at the Interface2 contribute to efficient export gate formation and/or export activity.

2.3.4. Mutational characterization of $FliP_P$

Phe-138 and Phe-178 forms T-shaped benzene dimer at the interface1 of the *Thermotoga* $FliP_P$ structure. Glu-142 and Glu-182 form a salt bridge with Arg-134. Met-127 and Val-131 make hydrophobic interactions with Leu-183, Ala-182 and Phe-187 at the edge of the interface1 (**Fig2-9)**. To clarify where these interactions are physiologically important, I selected conserved amino acid residues among the above residues and then replaced each of them by alanine in *Salmonella* full-length FliP (**Fig2-10)**. To evaluate the mutational impact on FliP function, I measured the motility of the *fliP* null mutants transformed with a plasmid encoding each of the FliP point mutant proteins in soft agar. FliP mutant variants were expressed from an arabinose-inducible promoter of the pBAD24 vector by adding 0.2 % arabinose. FliP(M138A) and FliP(Q141A) restored motility to a significant degree, FliP(F137A)

and FliP(Y174A) to some degree, and FliP(E178A) did not (**Fig2-11)**. Next, I overexpressed FliP variants from the pUC19 vector. Immunoblotting with anti-HA antibody revealed that the expression levels of FliP(F137A) and FliP(Q141A) are almost the same as that of wild-type FliP and that the expression levels of FliP(M138A), FliP(Y174A) and FliP(E178A) were much lower than, the wild-type level. Except for FliP(E178A), almost all variants restored the motility to the wild-type level when they were expressed from the pUC19 vector (**Fig2-11)**. Furthermore, all FliP variants did not show dominant negative effect at all (**Fig2-12)**.

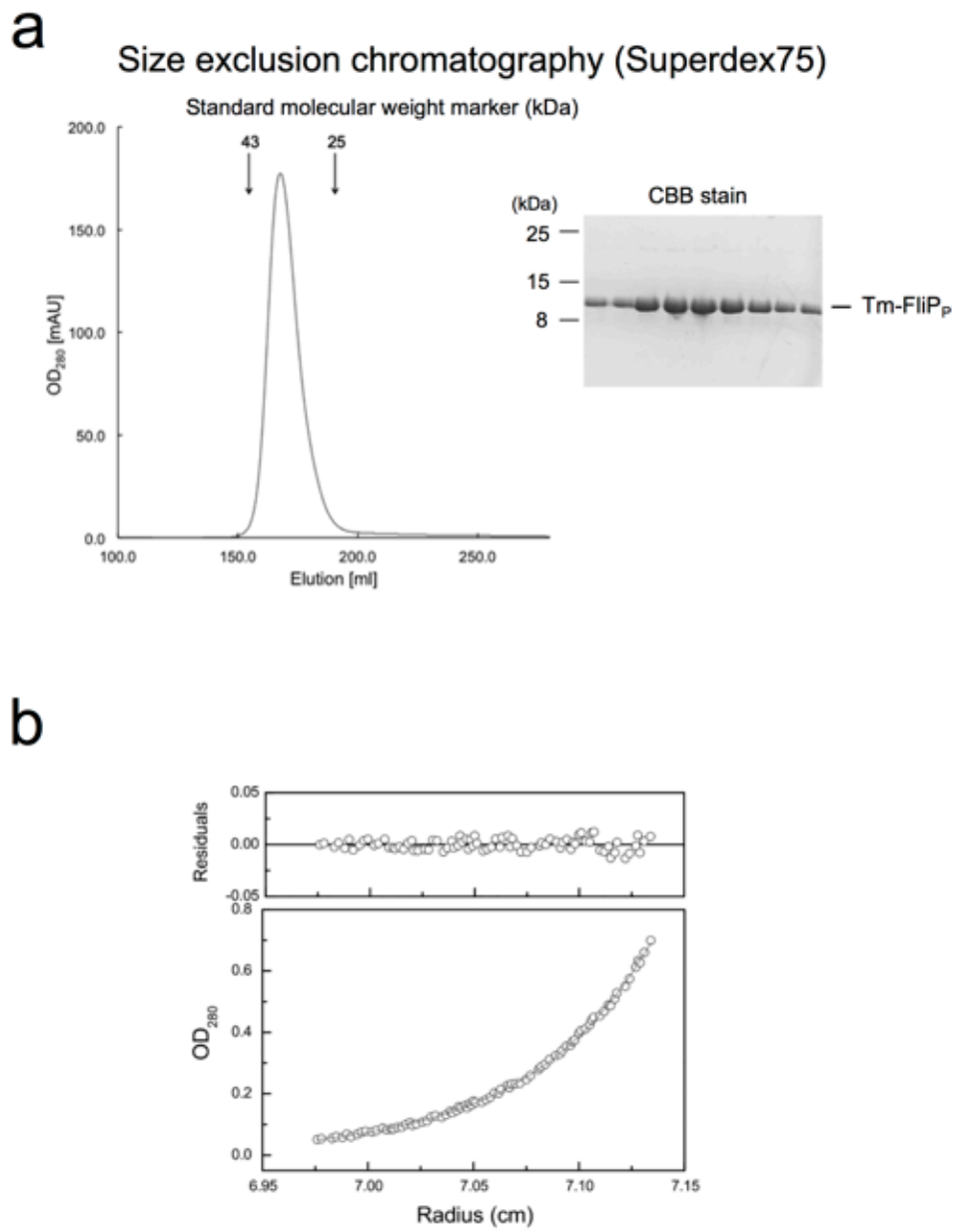

Figure 2-1. Purification profie of Tm-FliP$_P$.

(a) Purification of Tm-FliP$_P$ by size exclusion chromatography using a Superdex75 column. Eluted protein in the peak fraction was conformed by SDS-PAGE. (b) Sedimentation equilibrium analysis of Tm-FliP$_P$. The initial protein concentration was 0.85 mg/ml. Open circles are data points, and the solid line is a model fit. Data points are fitted to a single species model with a molecular mass of 39.7 kDa. Measurements were done at 4 ºC.

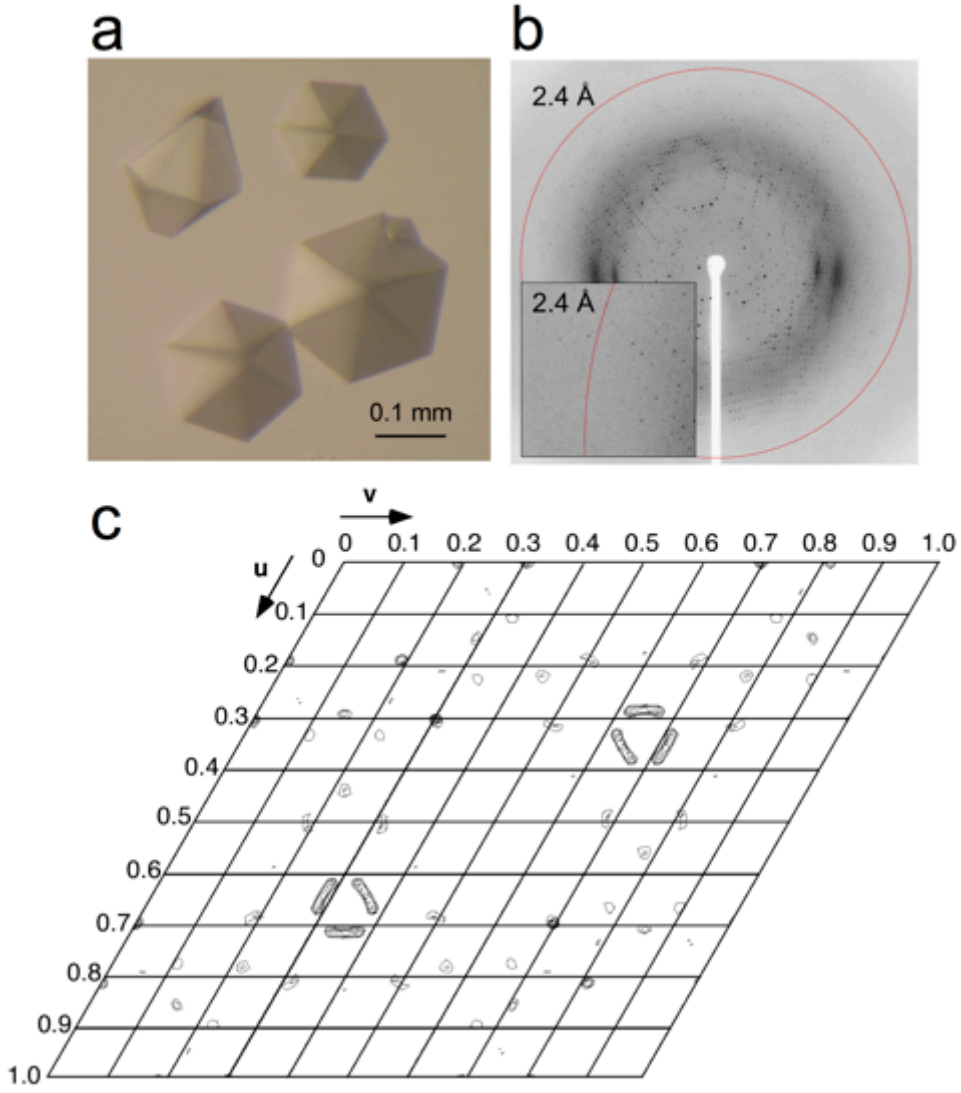

Figure 2-2. Crystals of native Tm-FliP$_P$ and its X-ray diffraction pattern.

(a) Crystals of native Tm-FliP$_P$. Crystals obtained using 36% MPD, 0.1 *M* phosphate-citrate pH 4.4. (b) Diffraction image of the Tm-FliP$_P$ crystal grown from the optimized condition. A typical X-ray diffraction pattern of the TmFliP$_P$ crystal collected at SPring-8 beamline BL41XU. The inset shows a close up view of the diffraction image. (c) Bijvoet Difference Patterson map at w = 0.33 Harker section calculated from the Tm-FliP$_p$ Se-Met derivative data at 3.5 Å resolution. The contour lines are drawn from 2.0 s to 6.0 s with an increment of 0.5 s.

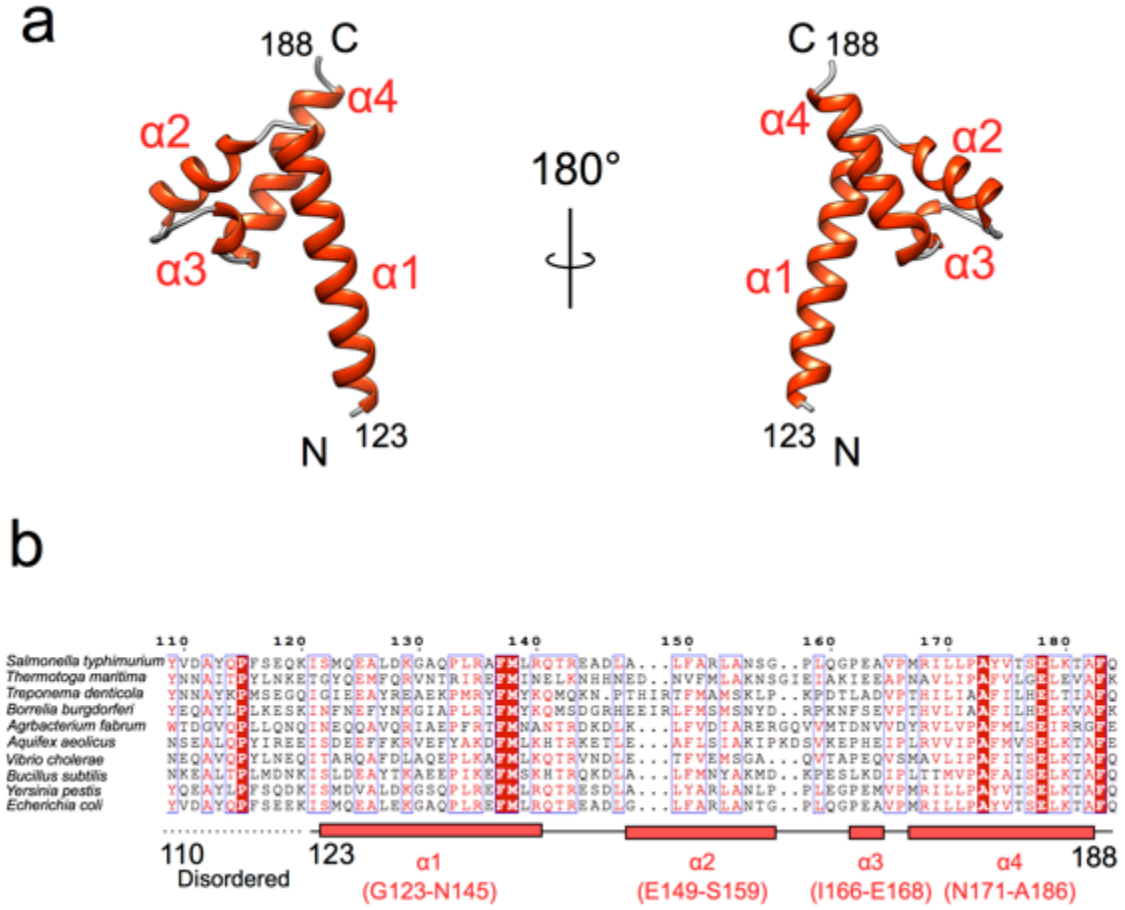

Figure 2-3. Crystal structure of Tm-FliP$_P$

(a) The Tm-FliP$_P$ monomer is shown in ribbon model, viewed from two different angles rotated 180° along the vertical axis. The N-terminal 13 amino acids were disordered. (b) Multiple sequence alignment of FliP$_P$. Uniprot accession numbers: *Salmonella* (P54700); *Thermotoga* (Q9WZG2); *Agrobacterium* (Q44344); *Aquifex* (Q67750); *Yersinia* (Q8D0A8); *Escherichia* (P0AC05); *Bacillus* (P35528); *Pseudomonas* (Q51468); *Vibrio* (A0A085SGD5).

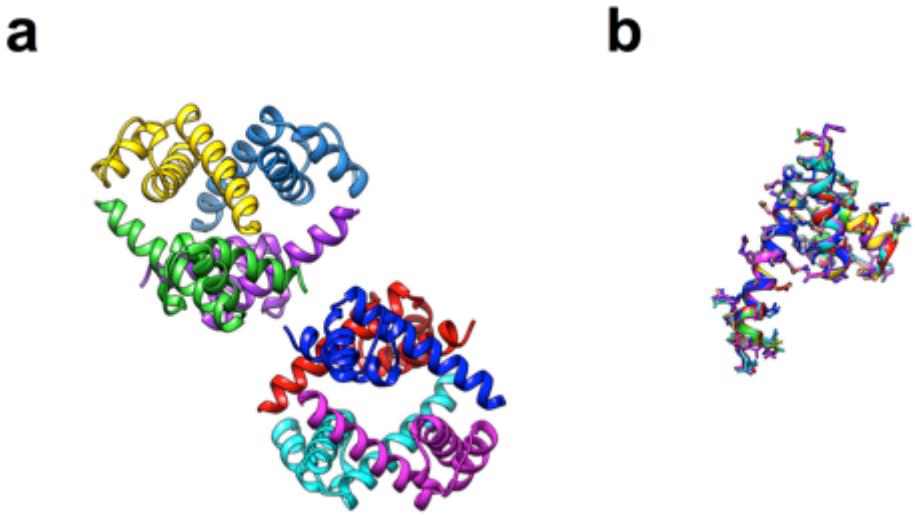

Figure 2-4. Unit cell and crystal contact

(a) The asymmetric unit contains eight Tm-FliP$_P$ chains. Each chain is shown in different colors. (b) Superimposition of all Tm-FliP$_P$ in the asymmetric unit.

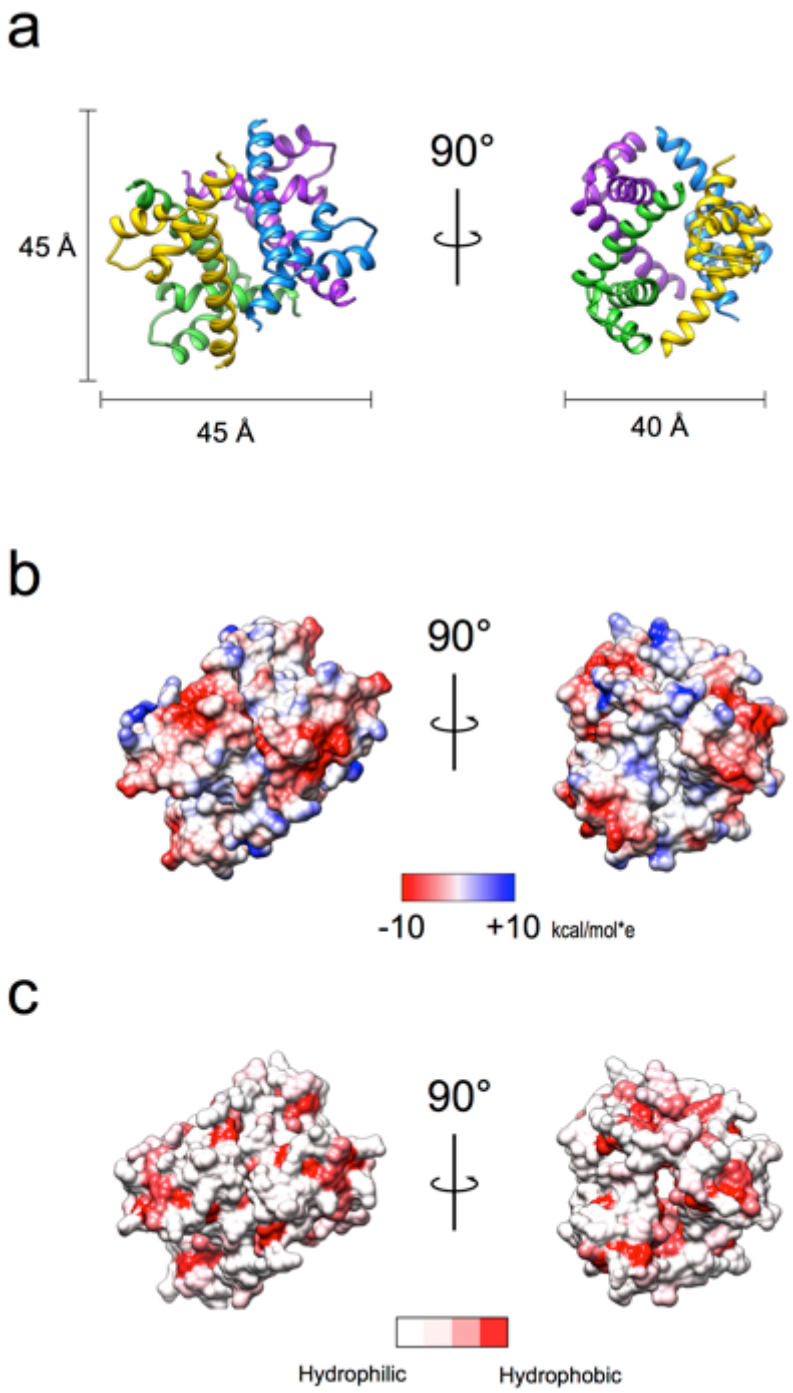

Figure 2-5. Tm-FliP$_P$ tetramer in the crystal

(a) Ribbon model of the Tm-FliP$_P$ tetramer structure, viewed from two different angles rotated 180° along the vertical axis. (b) Electrostatic potetial surface coloring of the tetramer, viewed from the same orientations with (a). (c) Hydrophobicity surface coloring of the tetramer, viewed from the same orientations with (a).

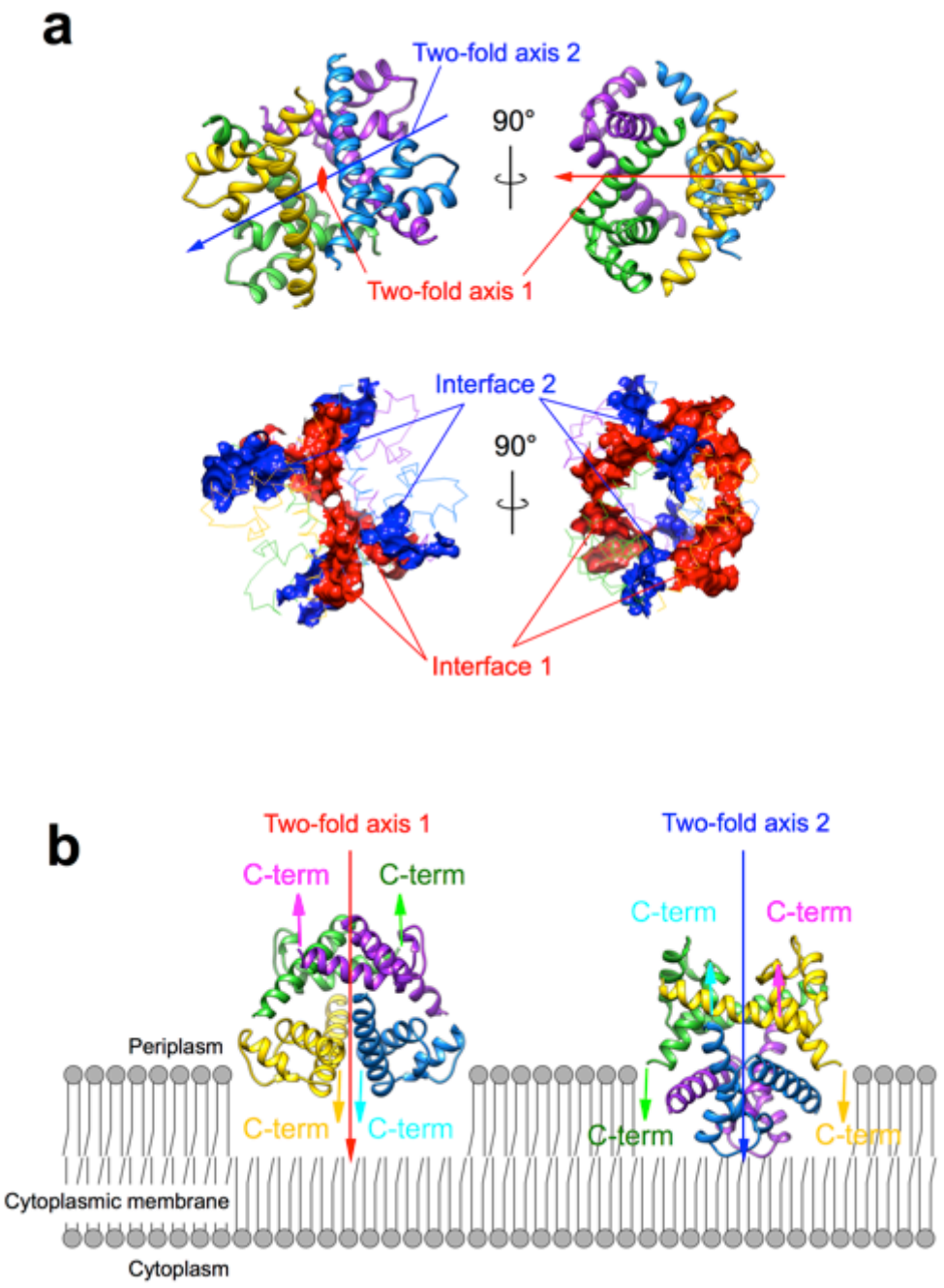

Figure 2-6. The symmetry axes in the tetramer.

(a) The two two-fold axes cross at the center of the tetramer. Two kinds of interfaces are present in the tetramer (red and blue). (b) The orientations of each C-terminus of Tm-FliP$_P$ chains in the tetramer structure are shown as arrows. The tetramer structure is put on the cytoplasmic membrane so as to directly connect the C-terminus of Tm-FliP$_P$ to the cytoplasmic membrane region. The two-fold axis1 and axis2 cross the cytoplasmic membrane orthogonally in the left and the right in the figure respectively.

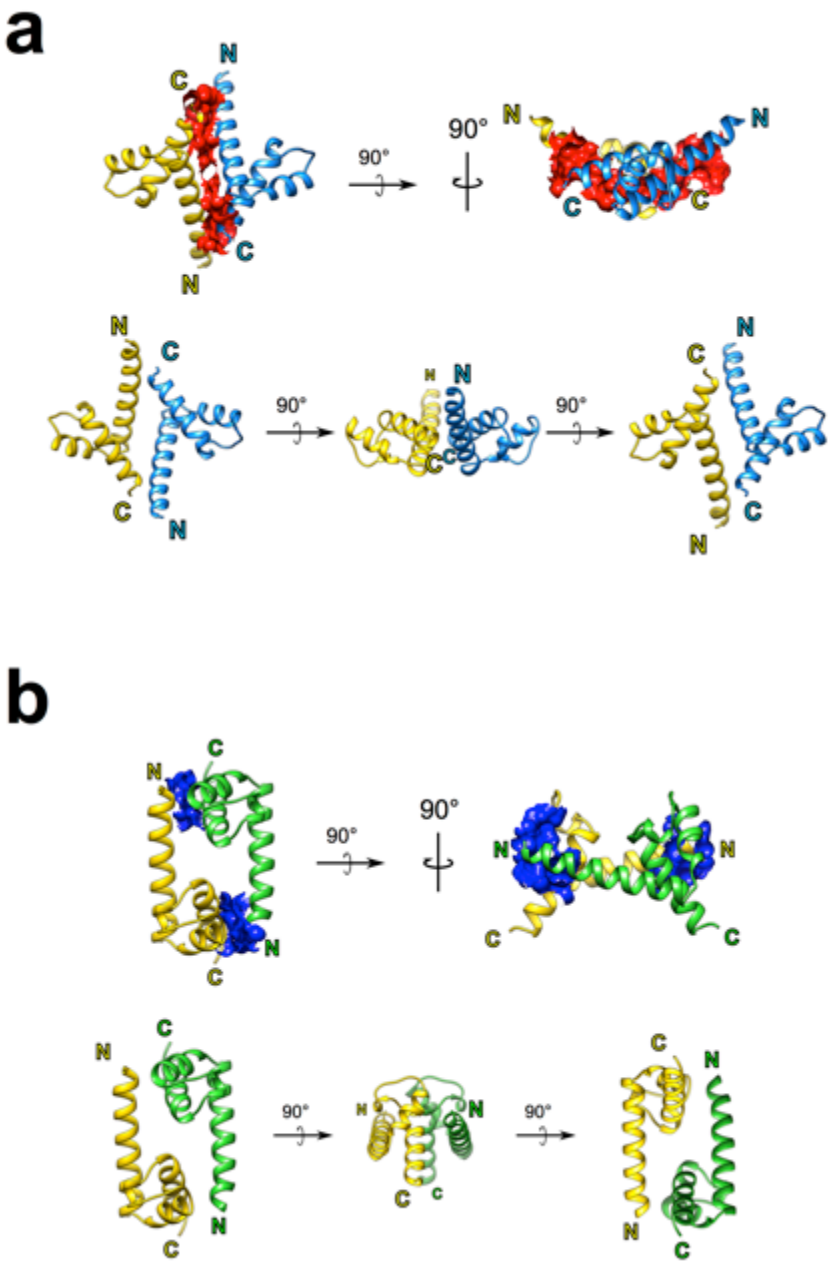

Figure 2-7. The interfaces in the tetramer structure.

(a) The red surface indicates interface1 and the blue indicates interface2. (b) The dimer formation that forms interface1. (c) The dimer formation that forms interface2.

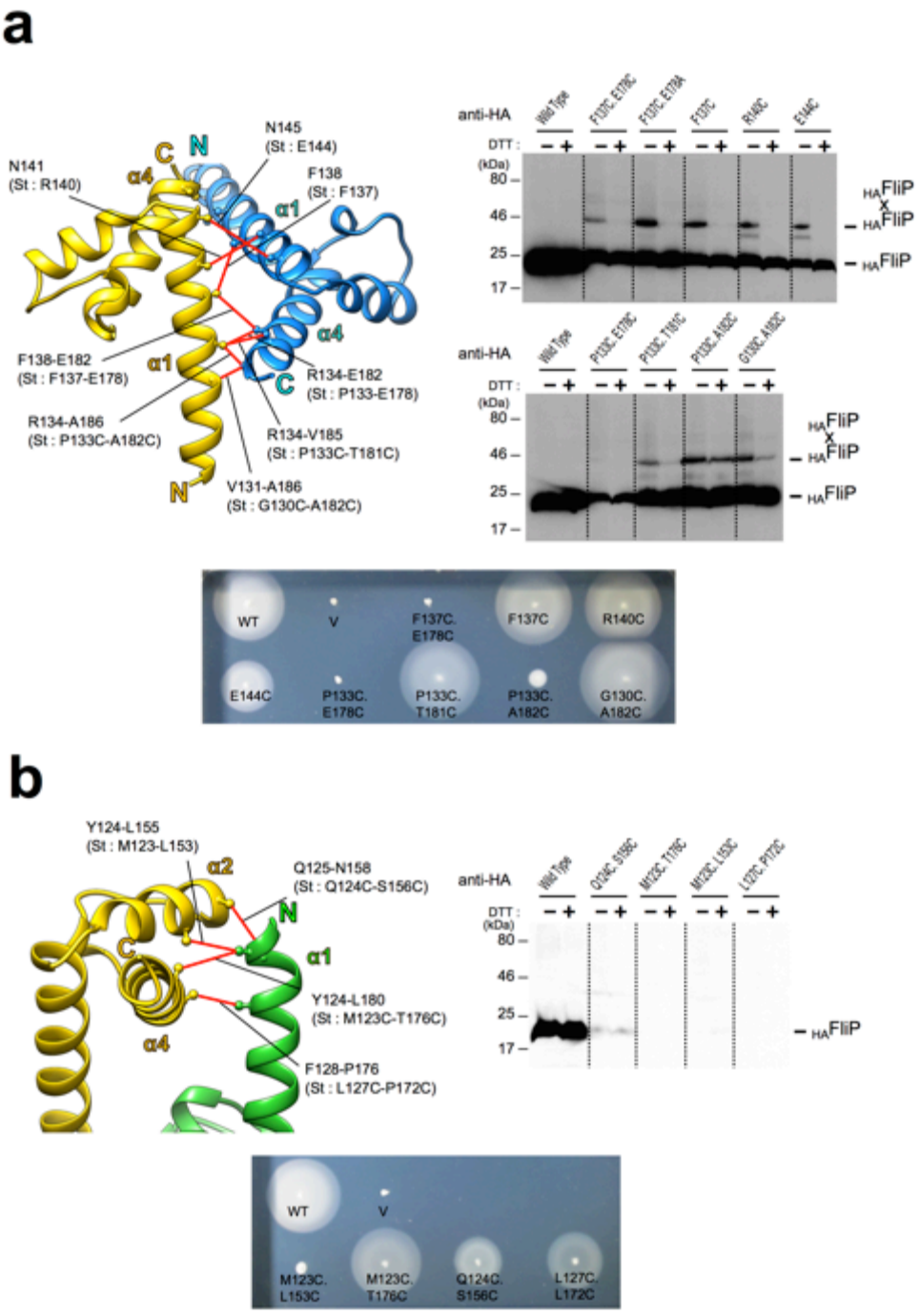

Figure 2-8. Disulfide cross-linking experiments

Results of disulfide cross-linking and the mutational effects of the cysteine replacement; (a) Interface1; (b)Interface2.

Mutational sites selected for cross-linking of *Salmonella* are mapped on the Tm-FliP$_P$ structure. C$_\beta$ of the residues of the variants are shown as sphere. Pairs of cross-linking are shown as red lines.

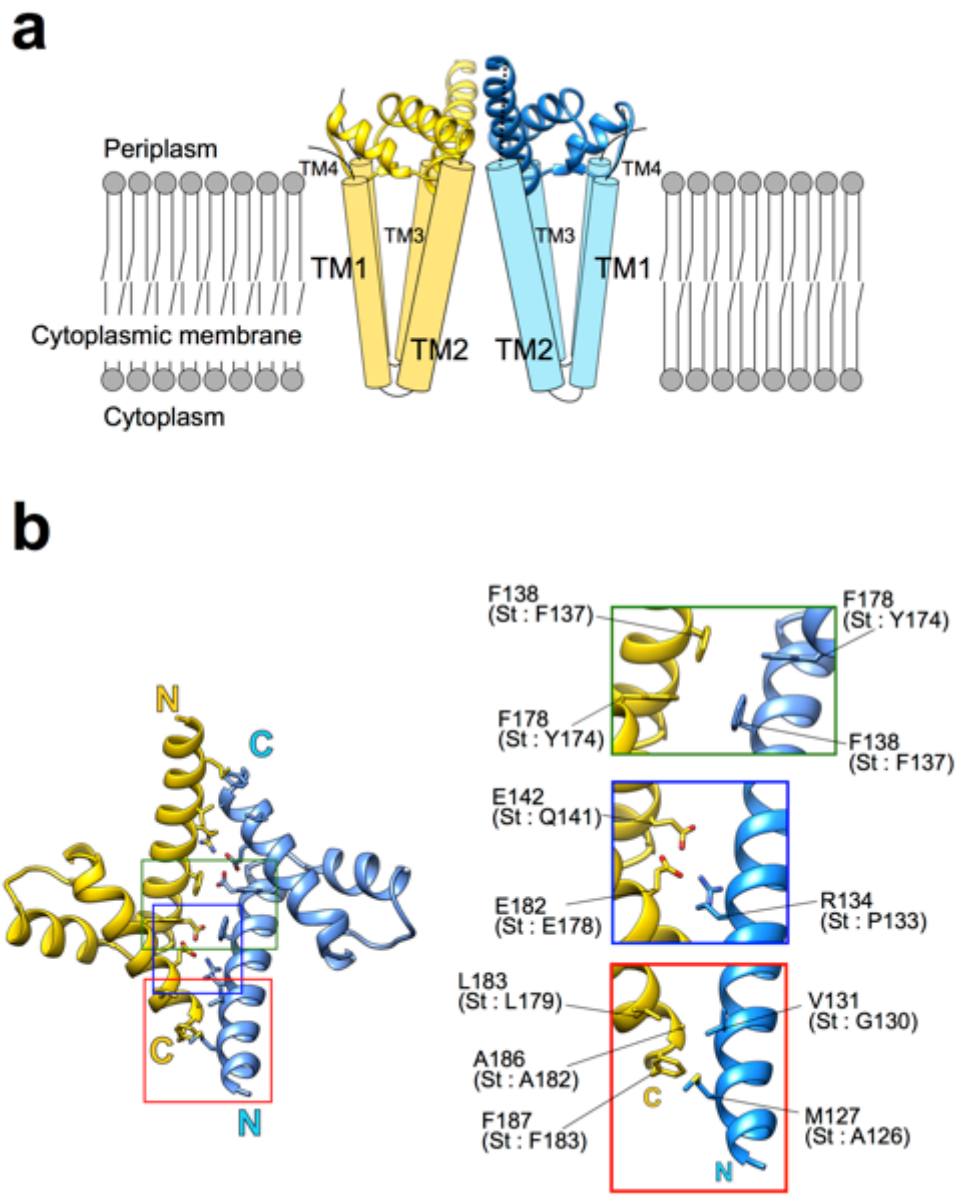

Figure 2-9. Dimer model of full-length FliP and the interactions at the interface1.
(a) Dimer model of fill-length FliP through the Interface1 in the cytoplasmic membrane. (b) Interactions in the interface1. Close-up view of green square indicates T-stacking, blue indicates salt bridge and red indicates hydrophobic interaction. The contributing residues of *Thermotoga* (and corresponding residues of *Salmonella*) are mapped on the Tm-FliP$_P$ structure. St : *Salmonella*

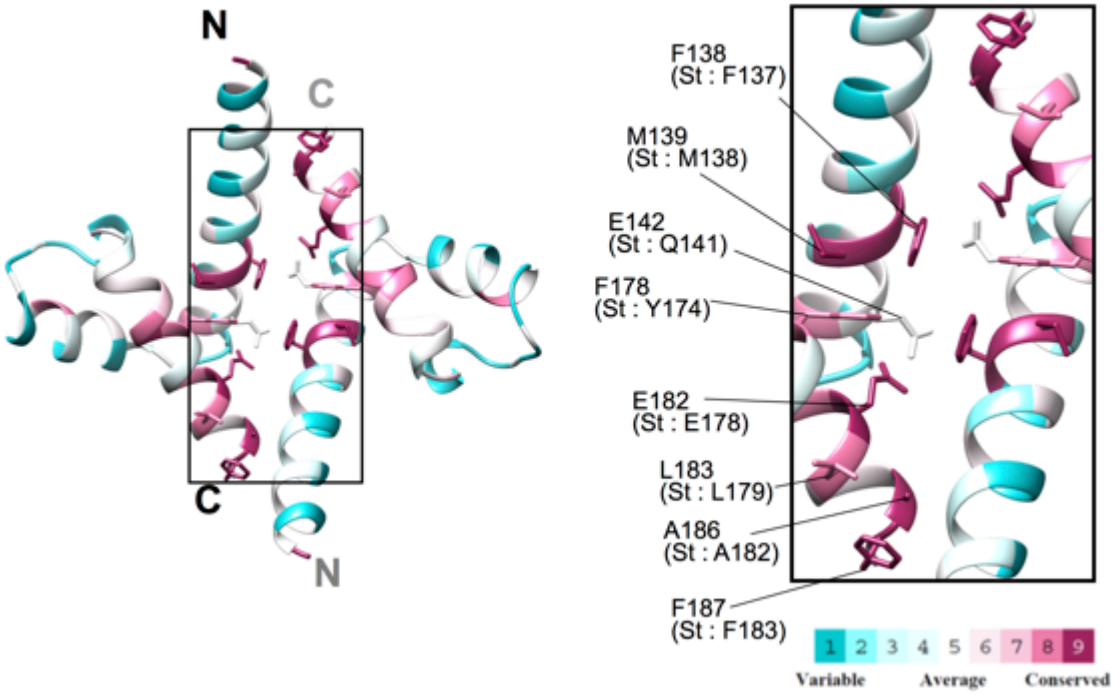

Figure 2-10. Evolutionary conserved residues of $FliP_P$.

The figure was prepared by ConSurf (http://consurf.tau.ac.il/). The mutational sites of *Thermotoga* (and corresponding residues of *Salmonella*) are mapped on the Tm-$FliP_P$ structure. St : *Salmonella*

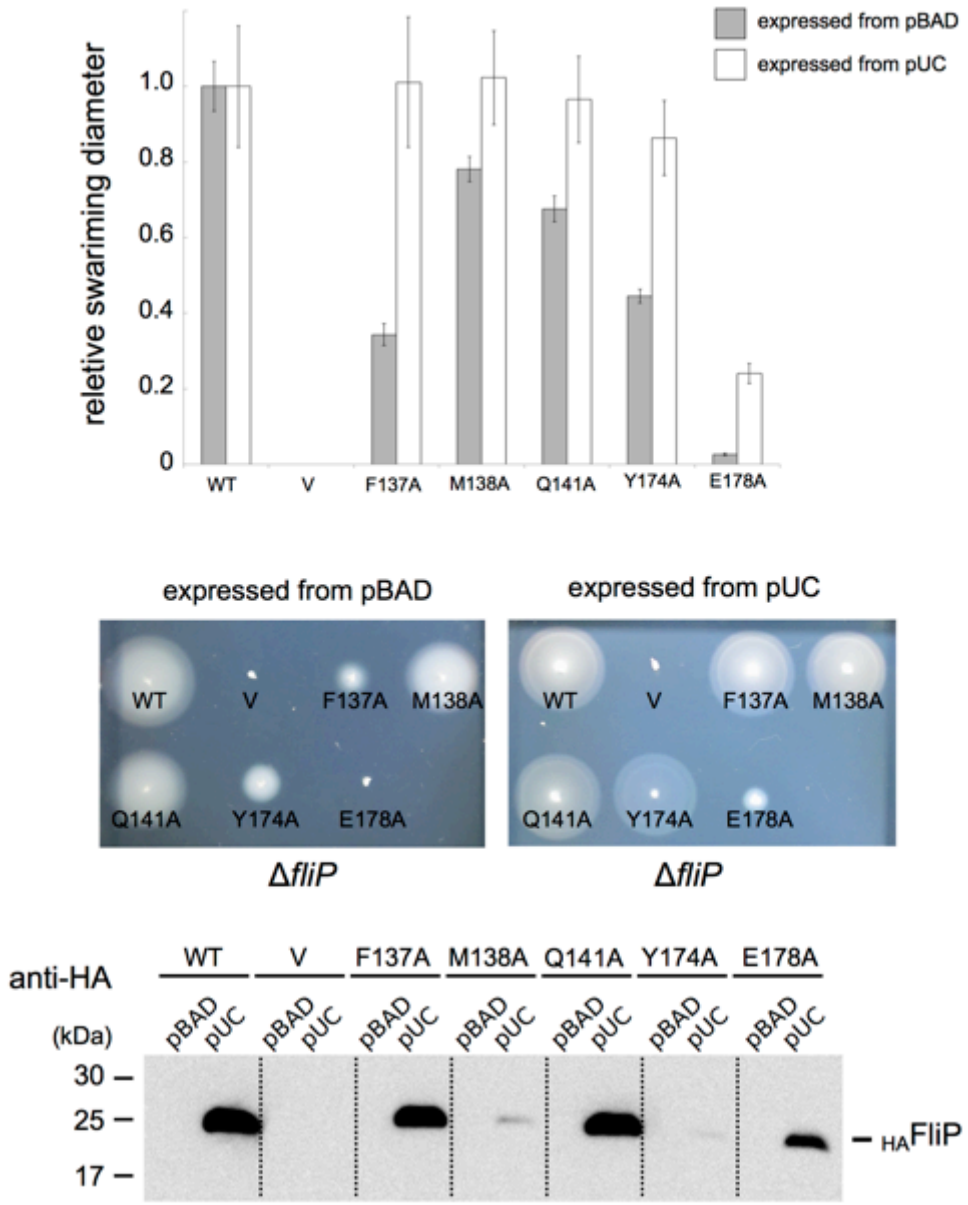

Figure.2-11. Effect of alanine substitutions in $FliP_P$ on motility

(a) Relative motility and representative swarming motility of a *Salmonella* Δ*fliP* mutant transformed with pBAD- and pUC-based plasmids encoding alanine substitution variants of $_{HA}$FliP. WT, wild type FliP; V, pBAD24 or pUC19 (b) Expression level of wild-type FliP and its point variants in the Δ*fliP* null mutant transformed with the above plasmids as judged by immunoblotting with polyclonal anti-HA antibody.

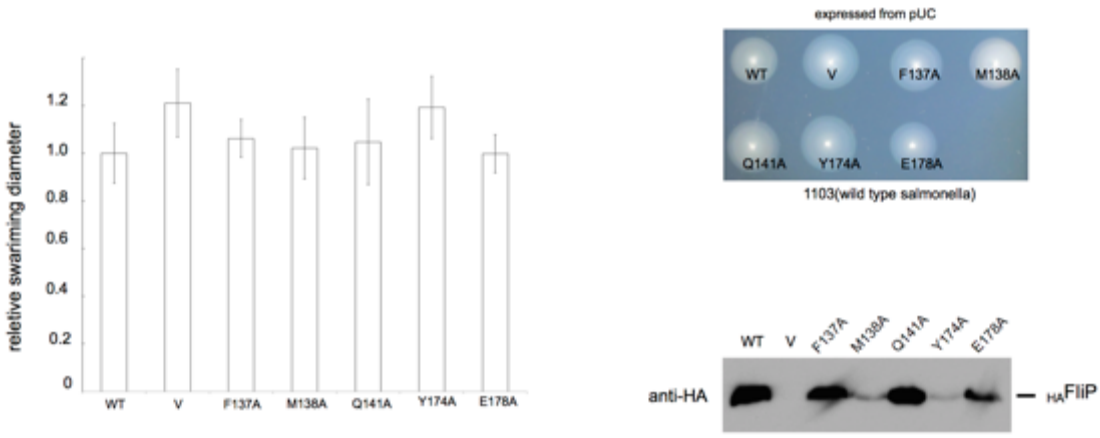

Figure.2-12. Dominant negative effect of alanine substitutions in $FliP_P$

(a) Relative motility and representative swarming motility of wild-type cells transformed with pUC-based plasmids encoding alanine substitution variants of $_{HA}$FliP. WT, wild type FliP; V, pUC19; (b) Expression of wild-type and variant FliP in wild-type cells transformed with the above plasmids.

2.4. Discussion

2.4.1. Relevance between the solubility and the structure of Tm-FliP$_P$

Salmonella FliP$_P$ was expressed as an inclusion body whereas $_{His}$Tm-FliP$_P$ was expressed in a soluble fraction. One side of the molecular surface of Tm-FliP$_P$ monomer or dimer is high hydrophobic. However, the hydrophobic surfaces face was covered in the tetramer and hence then the hydrophobic surfaces of Tm-FliP$_P$ are isolated from water solvent. Therefore, I suppose that *Salmonella* FliP$_P$ might not be able to form a tetramer in a way similar to Tm-FliP$_P$. This might be a reason why the protein solubility is quite different between FliP$_P$ from *Salmonella* and *Thermotoga*.

$_{His}$Tm-FliP$_P$ still tends to form highly aggregates during its purification. However, the removal of an N-terminal His-tag greatly improved its solubility. The N-terminal region of Tm-FliP$_P$ has a flexible conformation. This is in agreement with the secondary structure prediction of FliP$_P$ indicating that N-terminus of FliP$_P$ would form loop or turn. Since a His-tag itself tends to aggregate in general, I assume that Tm-FliP$_P$ forms a large aggregate through its N-terminus region with His-tag. Because alanine substitution of the P133 residue, which is located in the disordered N-terminus region of Tm-FliP$_P$, showed a significant reduced motility of *Salmonella* cells, I suggest that the conformational flexibility of the N-terminal region of FliP$_P$ may have important roles in FliP function.

2.4.2. The role of the FliP$_P$-FliP$_P$ interation

The role of FliP in flagellar protein export remains unknown. In this study, I found that the overexpression of FliP point mutant variants restores the motility to the wild-type level. Since these mutated residues are involved in the FliP$_P$-FliP$_P$ interaction at the Interface1, over-expression of FliP mutant variants could increase the probability

of FliP dimer formation, thereby fully exerting their FliP function. In agreement with this, these FliP variants did not show a dominant negative effect on wild-type motility. Therefore, I propose that the $FliP_P$-$FliP_P$ interaction at the interface 1 is critical for efficient export gate formation. Since the export gate complex is located in a highly limited space within the MS-ring, the number of FliP molecules in the export gate would not increase even if the FliP variants were over-expressed. Therefore, it is possible that the $FliP_P$-$FliP_P$ interaction is not directly involved in the protein export process. However, over-expression of FliP(E178A) did not restore motility to the wild-type level although its cellular level was slightly higher than that of FliP(Y174A), of which over-expression conferred wild-type motility. This raises the possibility that a highly conserved Glu-178 residue is also involved in the protein export process.

2.4.3. Effect of each mutation to the $FliP_P$ structure

Among the point mutnant variants, FliP(F137A) reduced the motility at almost same degree with FliP(Y174A) when they were expressed from the pBAD24 vector. These residues formed T-stacking at the Interface1, suggesting that the T-stacking interaction strongly contributes to form the Interface1. The aromatic part of Phe-178 (St: Tyr-174) forms a hydrophobic core with Met-139 (St : Met-138) for the folding of α-1 and α-2. Since both expressions of FliP(M138A) and FliP(Y174A) variants were quite lower than wild type FliP, the hydrophobic core formed by Phe-178 (St: Tyr-174) and Met-139 (St : Met-138) would be important to stabilize the $FliP_P$ structure. Glu-184 (St : Glu-178) forms a salt bridge with Arg-134 (St : Pro-133) in the crystal structure for $FliP_P$-$FliP_P$ interaction (**Fig.2-9, 2-13**). Since Arg-134 (St : Pro-133) is not conserved among the FliP homologues, this salt bridge contributes to the thermal stabilization of *Thermotoga* $FliP_P$. Multiple sequence alignments indicated that this

Arg-134 of Tm-FliP corresponds to the Pro residue among many species and to Pro-133 of *Salmonella* FliP (**Fig.2-14**). However, FliP(E178A) variant showed the most decreased motility among the variants. The secondary structure prediction showed that the region close to Pro-133 of *Salmonella* FliP is expected to form a small random coil domain (**Fig.2-14**). These results suggest that the region of Pro-133 of *Salmonella* FliP has flexibility and Glu-178 would play an important role at the flexible region.

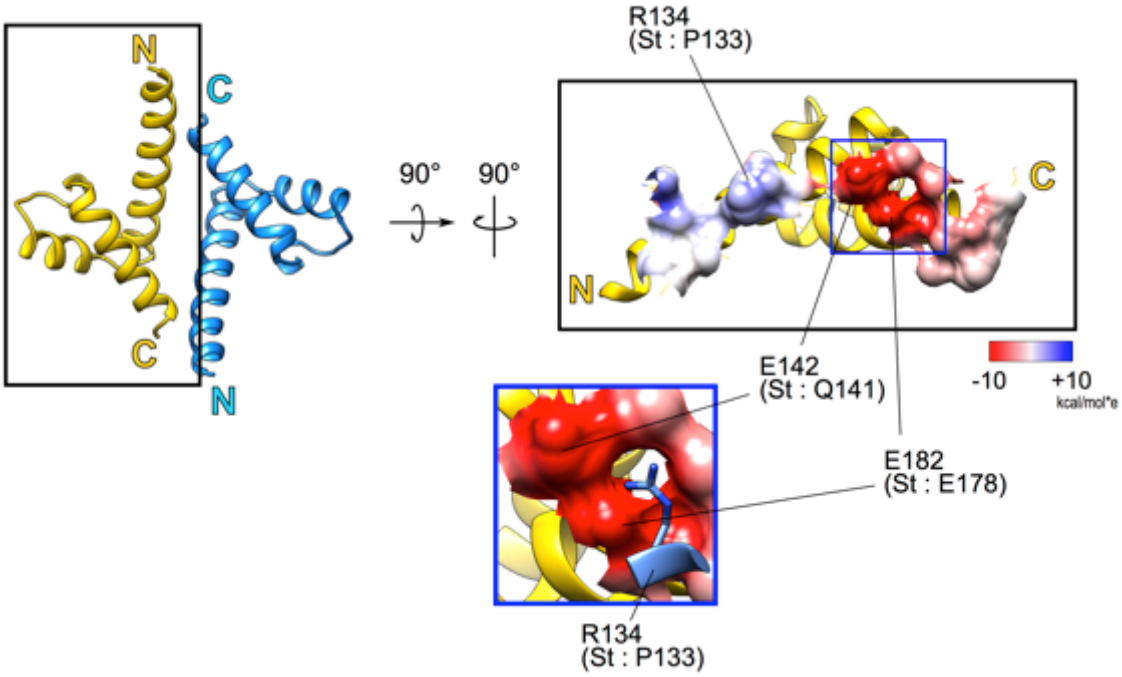

Figure 2-13. Electrostatic potential map of the Interface1

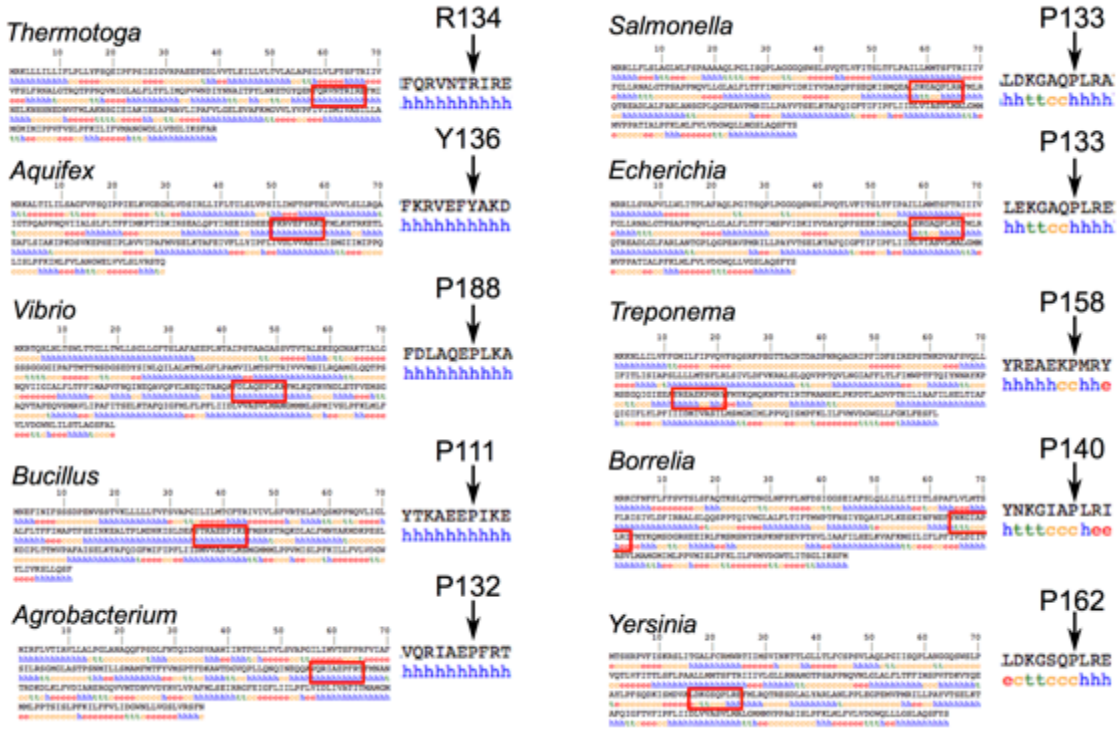

Figure 2-14. Secondary structure prediction of FliP used for the multiple sequence alignment. h: helix, b: beta bridge, e: extended strand, t: beta turn, s: bend region, c: random coil. The prediction was carried out by SPOMA.

Chapter 3
FliP forms the hexagonal ring structure and FliO facilitates FliP ring formation

3.1. Introduction

In the previous chapter, I have suggested that FliP forms a homo-dimer though the $FliP_P$-$FliP_P$ interaction to efficiently assemble into the export gate complex. It has been reported that that 4-5 copies of FliP molecule are identified in the purified FBB of *Salmonella* (Fan et al., 1997), raising the possibility that *Salmonella* FliP forms a dimer of dimer or a trimer of dimer in the export apparatus. To clarify it, I expressed and purifed *Salmonella* FliP. Although purified FliP was not mono-dispersed, EM observation revealed that FliP formed a ring-shaped oligomer.

Previous genetic analyses of a *fliO* null mutant have suggested that FliO interacts with FliP to regulate FliP function (REF). In this study, to clarify that FliO directly interacts with FliP to regulate FliP ring formation, I constructed the FliO/P co-expression system. By the purification from this co-expression system, I found that FliO directly interact with FliP to form FliO/P complex. Furthermore, the FliP ring dissociated from the FliO/P complex shows a high mono-dispersion. 2D-EM image classification reveals that the FliP ring is hexagonal. These results let me suggest that FliP forms a homo-hexamer and that FliO act as a scaffold for efficient FliP ring formation.

3.2. Materials and Methods

3.2.1. Bacterial strains, plasmids and media

The bacterial strains and plasmids used in the chapter are listed in Table 3-1 Compositions of media used in this chapter are essentially the same as those in chapter 2.

3.2.2. DNA manipulations

To construct a pTrc99A-based plasmid, a DNA fragment encoding *fliO*, *fliP* or *fliO-fliP* was amplified by PCR with chromosomal DNA of *Salmonella* as a template. The amplified DNA fragment was inserted into the *Nde*I and *Bam*HI sites of the pTcc99A vector. Mutations for biochemical characterization were generated by site-directed mutagenesis as described in chapter 2. Peptide insertions were performed by inverse-PCR method. All substitutions and insertions were confirmed by DNA sequencing as described in chapter 2.

3.2.3. Protein expression and purification

For expression and purification of FliP, the expression vectors encoding $_{His}$FliP (pTF) were transformed into a *S.typhimurium flhDC* null strain (Δ*flhDC*). The resulting transformants were grown in 2×YT medium containing 100 μg ml^{-1} at 30 ℃ until OD_{600} = 0.4-1.0 and then incubated at 16℃ for another 24 h to express $_{His}$FliP without any induction. Cells were harvested by centrifugation at 6,400 *g* for 10 min and stored at -80 ºC. The cells were thawed, resuspended in a lysis buffer containing 20 mM Tris-HCl pH 8.0, 3 mM EDTA and sonicated. The cell lysates were centrifuged at 20,000*g* for 15 min to remove cell debris. The supernatants were ultracentrifuged at 110,000*g* for 1 hour to isolate the membrane fractions. Harvested membranes were

stored at -80 ℃. For purification, the membranes were solubilized in the solubilization buffer containing 50 mM Tris-HCl pH 8.0, 300 mM NaCl, 5 % glycerol, 20 mM imidazole and 1% n-dodecyl b-D-maltoside (DDM) at 4 ℃ for 30 min and centrifuged at 110,000g for 30 min to remove the insoluble membranes. The solubilized membranes were loaded onto a Ni-NTA agarose resin and washed extensively with the wash buffer containing 50 mM Tris-HCl pH 8.0, 300 mM NaCl, 5 % glycerol, 20 mM imidazole and 0.1% DDM. Protein was then eluted with a 50–400 mM imidazole gradient and fractions containing $_{His}$FliP were collected. $_{His}$FliP was concentrated and then purified by size exclusion chromatography (Superdex 200 10/300) in a buffer containing 20 mM Tris-HCl pH 8.0, 150 mM NaCl, 2 mM EDTA, 5 % glycerol and 0.1% DDM.

For co-expression of FliO/P, the expression vectors encoding FliO-$_{His}$FliP (pTF) were transformed into the *Salmonella* Δ*flhDC* cells. The same expression and purification procedures were applied except for using a Superose 6 10/300 column for size exclusion chromatography purification. To obtain mono-dispersed FliP from the FliO/P complex, eluted fraction of FliO/P after Ni-NTA affinity purification was incubated at room temperature for 1day, resulting in the dissociation of FliP from the complex. Further size exclusion chromatography purification was carried out in the same way as FliP alone.

3.2.4. Motility assay

Fresh transformant colonies were inoculated onto soft tryptone agar plates as described in chapter 2.

3.2.5. Preparation of whole cell fractions and immunoblotting

Salmonella cells were exponentially grown at 30°C with shaking. Aliquots of

culture proteins containing a constant number of cells were clarified by centrifugation. Cell pellets were resuspended in SDS-loading buffer normalized by cell density to give a constant amount of cells. After sodium dodecyl sulfate-polyacrylamide gel electrophoresis (SDS-PAGE), immunoblot detection was done with an ECL immunoblotting detection kit (GE Healthcare).

3.2.6. Negatively stained EM observation and image processing

Samples were applied to carbon-coated copper grids and negatively stained with 1.0% (w/v) uranyl acetate. Micrographs were recorded at a magnification of ×50,000 with a JEM-1011 transmission electron microscope (JEOL, Tokyo, Japan) operated at 100 kV. 4,663 particle images were selected with BOXER (Ludtke *et al*., 1999) and the boxed particle images were aligned and classified using the REFINE2D.PY (Ludtke *et al*., 1999).

Table 3-1. Strains and plasmids used in this study of this chapter

Strains or Plasmids	Relevant properties	Source or reference
Salmonella		
SJW1368	Δ(cheW-flhD); master operon mutant	(Ohnishi et al.,1994)
	ΔfliO	
	ΔfliP	
Plasmids		
pTrc99AFF4	Modified trc expression vector	(Ohnishi et al.,1994)
pKY069	pTrc99AFF4/$_{His}$FliP	This study
pKY070	pTrc99AFF4/FliO.$_{His}$FliP	This study
pKY071	pTrc99AFF4/FliO.$_{His}$FliP(F137A)	This study
pKY072	pTrc99AFF4/FliO.$_{His}$FliP(E178A)	This study
pKY073	pTrc99AFF4/FliO	This study
pKY074	pTrc99AFF4/$_{HA}$FliP	This study
pKY075	pUC19/$_{HA}$FliP	Chapter 2

Table 3-2. Primers used in this study of this chapter

Primers	Sequence
FliO_NdeI.Fw	gggaattccatATGATGAAGACAGAAGCCAC
FliO_BamHI.Re	cgcggatccTCAGGATCTCCCGGAACGCTTG
FliP_BamHI.Re	cgcggatccCTAACTGTAAAAGCTTTGGG
SigPep_QLHis_FliP.Fw	GCCGCCGCTGCGCAACTTcatcatcaccatcaccacCTGCCGGGGCTTATCAGC
SigPep_QLHis_FliP.Re	GCTGATAAGCCCCGGCAGgtggtgatggtgatgatgAAGTTGCGCAGCGGCGGC
FliP_F137A.Fw	GCGCAACCGTTACGCGCGgcCATGCTGCGCCAAACCCGC
FliP_F137A.Re	GCGGGTTTGGCGCAGCATGgcCGCGCGTAACGGTTGCGC
FliP_E178A.Fw	CCCGCTTATGTCACCAGCGcATTAAAGACGGCGTTTCAG
FliP_E178A.Re	CTGAAACGCCGTCTTTAATgCGCTGGTGACATAAGCGGG

3.3. Result

3.3.1. Expression for full-length FliP of *Salmonella*

FliP can be expressed from a *ptac* promoter of the pTrc99A vector in Salmonella even in the absence of IPTG. The rate of the expression of FliP was quite slow and so the growth arrest did not occur. The expression level of FliP was detected by immunoblotting but not by CBB staining but by from the cell lysate (**Fig. 3-1a**). Therefore, I decided to attach a tag such as a His-tag and a HS-tag to the N and C-terminus of mature FliP for affinity chromatography. However, most of peptide tags dramatically reduced the FliP expression level except for an N-terminal HA tag. Therefore, I tried to modify the FliP construct by optimizing tags, signal peptides required for efficient FliP insertion into the cytoplasmic membrane, insertion positions of a tag and their combinations (**Fig. 3-1b**). All constructs that have a C-terminal tag destabilized FliP whereas some constructs that have a N-terminal hexa-histidine tag were stable. Next, I tested whether these constructs were functional. I checked motility of a *fliP* null mutant that expresses each FliP recombinant in soft agar. Almost all constructs that have a chimeric signal peptide showed high toxicity to *Salmonella* cells. A FliP construct, which has a hexa-histidine tag with a N-terminal single leuceine (LHHHHHH) located between Q22 and L23, was both functional and stable, and the amino acid composition was the simplest among all of the constructs (**Fig. 3-1c**). I used this construct as $_{His}$FliP for the following experiments.

3.3.2. Purification and EM observation of FliP full length

Total isolated membranes were solubilized by DDM. I carried out Ni-NTA affinity chromatography, followed by size exclusion chromatography. Purified FliP was not mono-dispersed and the highest molecular weight of eluted FliP was estimated to be

about 200 kDa as judged by size exclusion chromatography (**Fig. 3-2a**). Since purified membrane proteins are embedded in detergent micelles, they generally behave as up to two times larger than their molecular weight. Therefore, purified FliP oligomer was speculated to contain 4 to 8 copies of FliP monomer.

Next, I observed each major peak fraction of FliP (peak1 and peak2) by negatively stained electron microscope in order to visualize the FliP shape. In the peak1 fraction, I clearly observed the ring-shape structure (**Fig.3-2b**). However, the amounts of the ring structures were much lower in the peak2 fraction than in the peak 1 fraction and quite smaller fragments were seen in the peak2 fraction (**Fig.3-2b**). These results indicated that FliP forms an oligomeric ring structure and that there were several oligomeric states of FliP in the purified sample.

3.3.3. Co-expression, purification and EM observation of FliO/P

To succeed in both functional and structural analysis, the purification of a mono-dispersed protein is quite important. In general, it is necessary to carry out detergent screening to obtain mono-dispersed membrane proteins. I examined DDM, DM (n-decyl-β-D- maltopyranoside), SLl (sucrose monolaurate), SMc (sucrose monocaprate), OG (n-octyl -β-glucoside), CHAPS (3-[(3-Cholamidopropyl)dimethylammonio]-1-propane- sulfonate), LMNG (lauryl maltose neopentyl glycol) and DMNG (decyl maltose neopentyl glycol) for the first screenig. Only DDM and SMl made FliP dispersion but not mono-dispersion. Other detergents made FliP insoluble or soluble aggregation (void fraction in size exclusion chromatography). It is also known that some proteins are more stable when they form a complex with other components. FliP was assumed to interact with FlO, FliR and FlhA (REFS). Especially, recent genetic study indicated that FliO is not an essential

component for flagellar construction among the export gate components, and bypass mutations, which allows a *fliO* null mutant to form flagella to a considerable degree, are identified in the *fliP* gene (Barker et al., 2010; Barker et al., 2014). Furthermore, the cellular level of FliP is increased when FliP is co-expressed with FliO. Therefore, FliO is assumed to interact with FliP in direct via its transmembrane region to stabilize FliP in the cytoplasmic membrane. To test this, I co-expressed and purified FliP with FliO. I expressed FliO and FliP as an operon from the p*trac* promoter of the pTrc99A vector because antibiotics except for ampicillin dramatically decreased both the FliO and FliP expression levels. I took the same purification method and condition for the FliO/P complex as FliP alone and so succeeded in the purification of the FliO/P complex. It has been reported that FliO is expressed as two forms, a long form and a short form (REF). Interestingly, both two forms of FliO were co-purified with FliP (**Fig.3-3a**). Although purified FliO/P complex seemed to be mono-dispersed in size exclusion chromatography, EM observation of the complex revealed that a couple of the FliP rings connect with each other presumably through an interaction between the FliP ring and FliO (**Fig.3-3b**). Surprisingly, I was also able to obtain the highly mono-dispersed and homogenous FliP rings from the FliO/P complexes rather compared to FliP alone (**Fig.3-3a**). These results suggest that FliO directly interacts with FliP to facilitate FliP ring formation.

We performed 2D classification image analysis of the FliP ring isolated from the FliO/P complexes. 4663 particles were picked up and classified into 100 classes. Many of the classes revealed the hexagonal ring with a diameter of 2nm (**Fig.3-4**).

3.3.4. Purification and EM observation of FliP variants

To test if the $FliP_P$-$FliP_P$ interaction is required for FliP ring formation, I

decided to express and purify FliP(F137A), FliP(Y174A) and FliP(E178A) because these FliP mutations reduced motility (**Fig. xx**). I found that the expression levels of FliP(Y174A) and FliP(E178A) are lower than the wild-type level. Therefore, I constructed plasmids co-expressing these FliP point mutant variants with FliO because the steady cellular level of FliP is increased considerably by its co-expression with FliO. Unfortunately, I could not obtain a plasmid encording FliO and FliP(Y174A) on the pTrc99A vector presumably because high-expression of the FliO/P(Y174A) complex confers toxicity to the host cells. Therefore, I expressed and purified the FliO/P(F137A) and FliO/P(E178A) complexes in the same way with wild-type FliO/P. Both FliP(F137A) and FliP(E178A) co-purified with FliO. However size exclusion chromatography revealed that the molecular weight of each FliP variants were smaller than wild-type FliP (**Fig.3-5a**). Furthermore, FliP(E178A) dissociated from FliO much easier than wild-type FliP and FliP(F137A), indicating that the E178A mutation reduces the binding affinity of FliP for FliO. Therefore, I suggest that $FliP_P$ contributes to a stable association of FliP with FliO.

Next, I observed purified FliP variants by negatively stained EM. Compared to wild-type FliP, the FliP(F137A) and FliP(E178A) rings were not observed efficiently compared to wild-type FliP although their much small particles were seen. These results suggest that the F137A and E178A mutations significantly reduces the probability of FliP ring formation (**Fig.3-5b**). Therefore, I suggest that the $FliP_P$-$FliP_P$ interaction is required for efficient FliP ring formation.

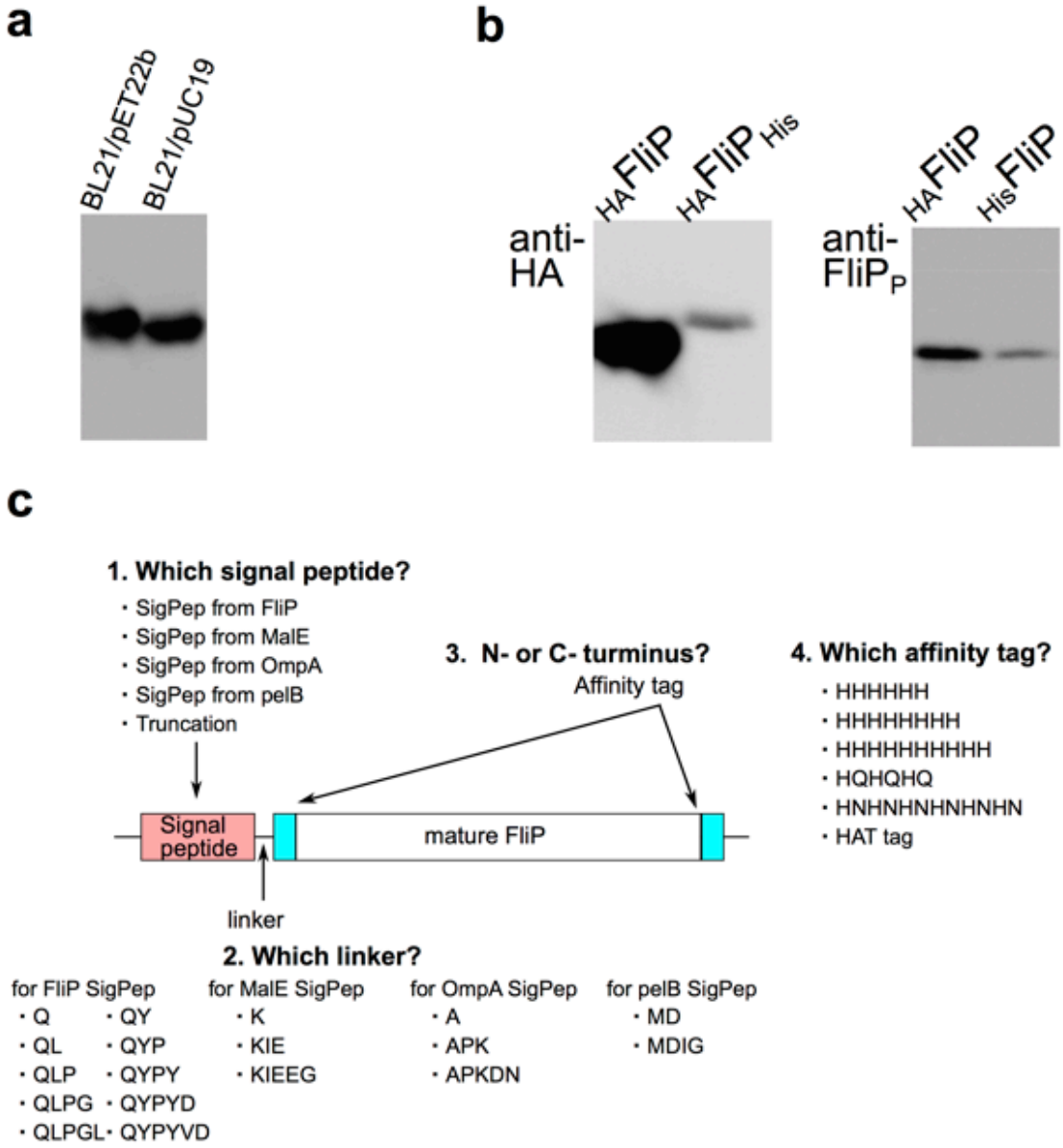

Figure 3-1. Expression of FliP full length

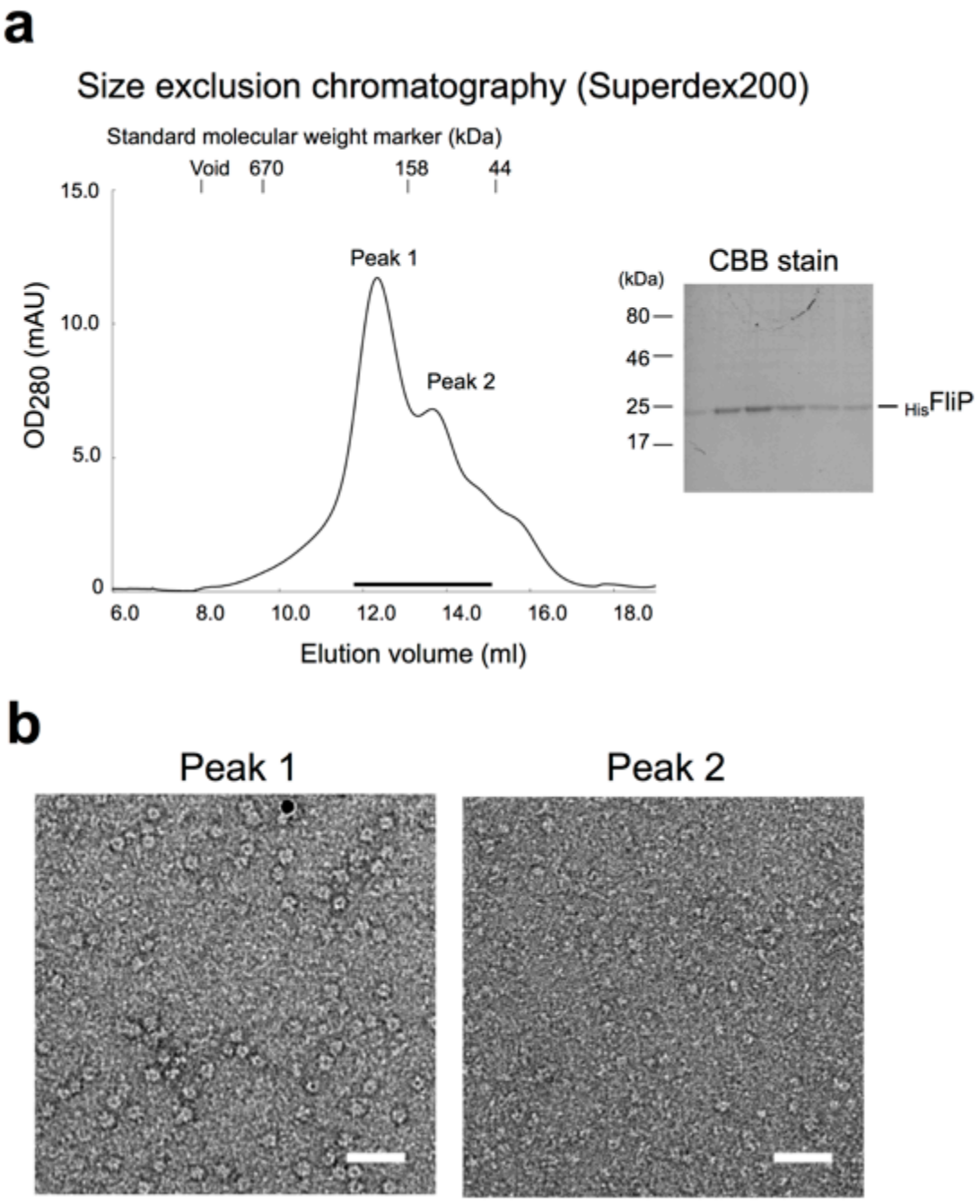

Figure 3-2. Purification and EM-observation

(a) Size exclusion chromatography (Superdex200) of FliP. Eluted protein in each peak fraction was confirmed by CBB stain. (b) Representative negatively stained EM images of peak1 and peak2. Scale bar shows 50 nm.

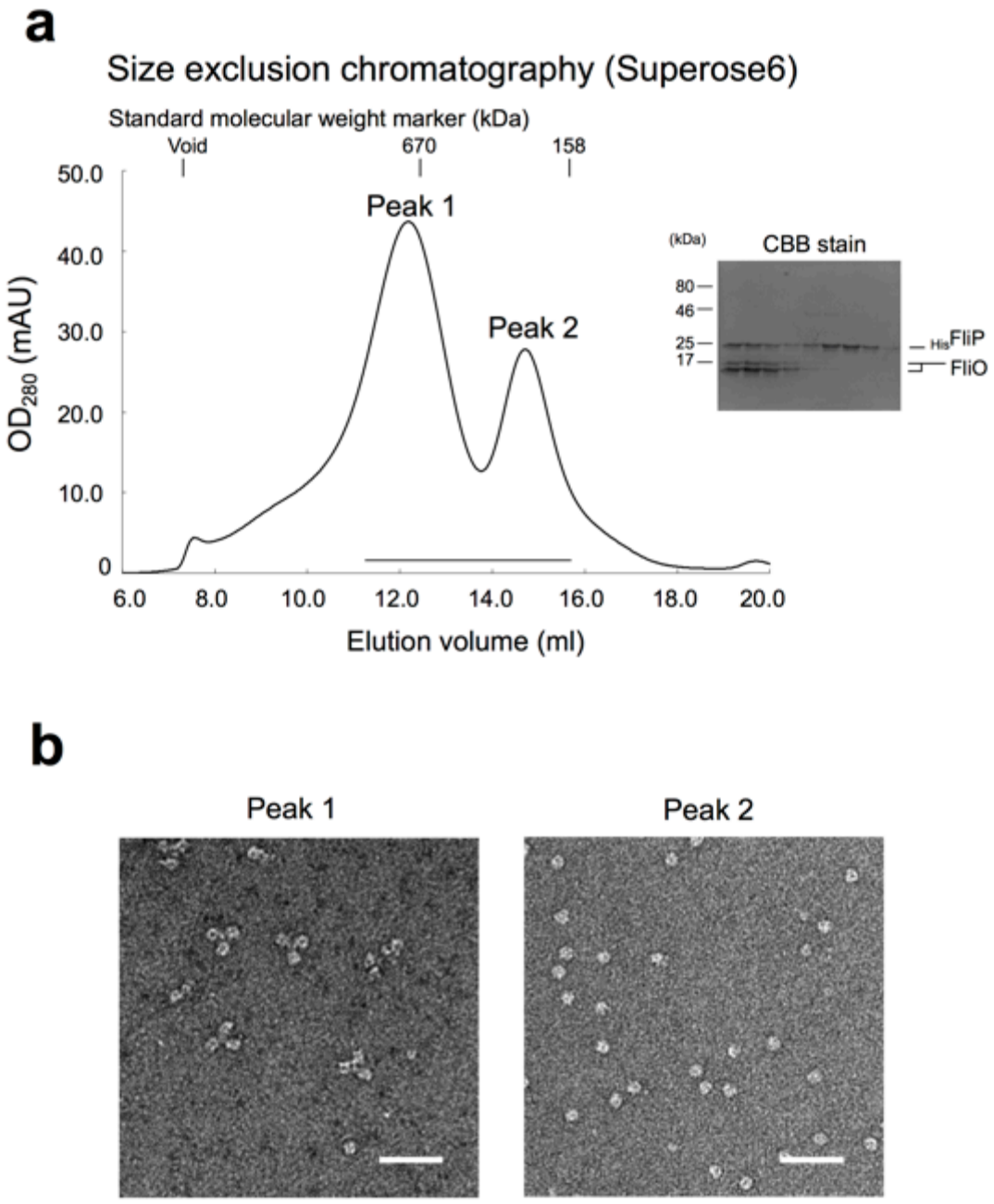

Figure 3-3. Purification and EM-observation of FliO/P

(a) Size exclusion chromatography (Superose6) of FliO/P. Eluted protein in each peak fraction was confirmed by CBB stain. (b) Representative negatively stained EM images of peak1 and peak2. Scale bar shows 50 nm.

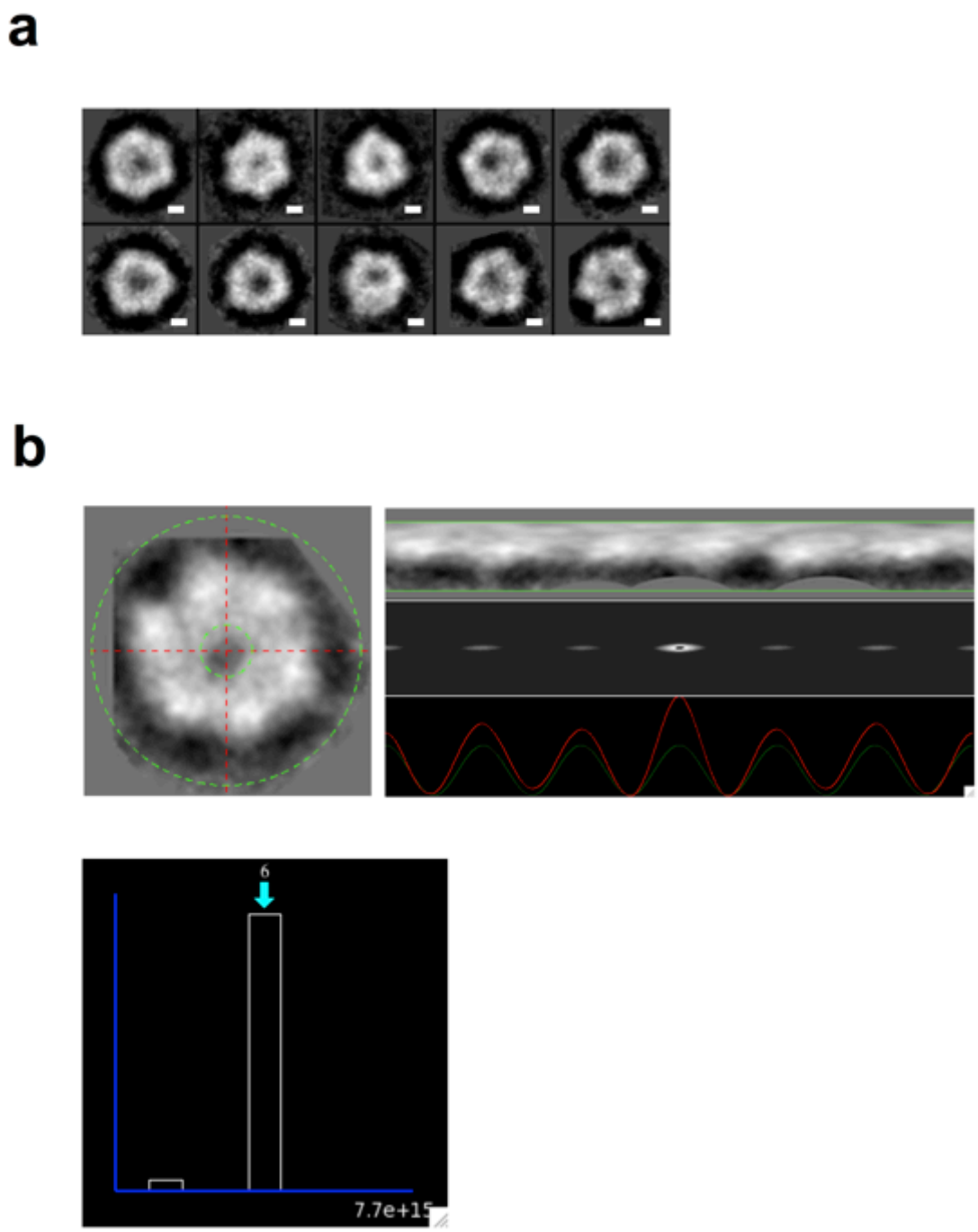

Figure 3-4. 2D classification

(a) Enlarged views of 10 representative 2D class averages show hexagonal ring structures. Scale bar shows 2 nm. (c) Auto-correlation analysis of the 2D class averaged image of the FliP ring.

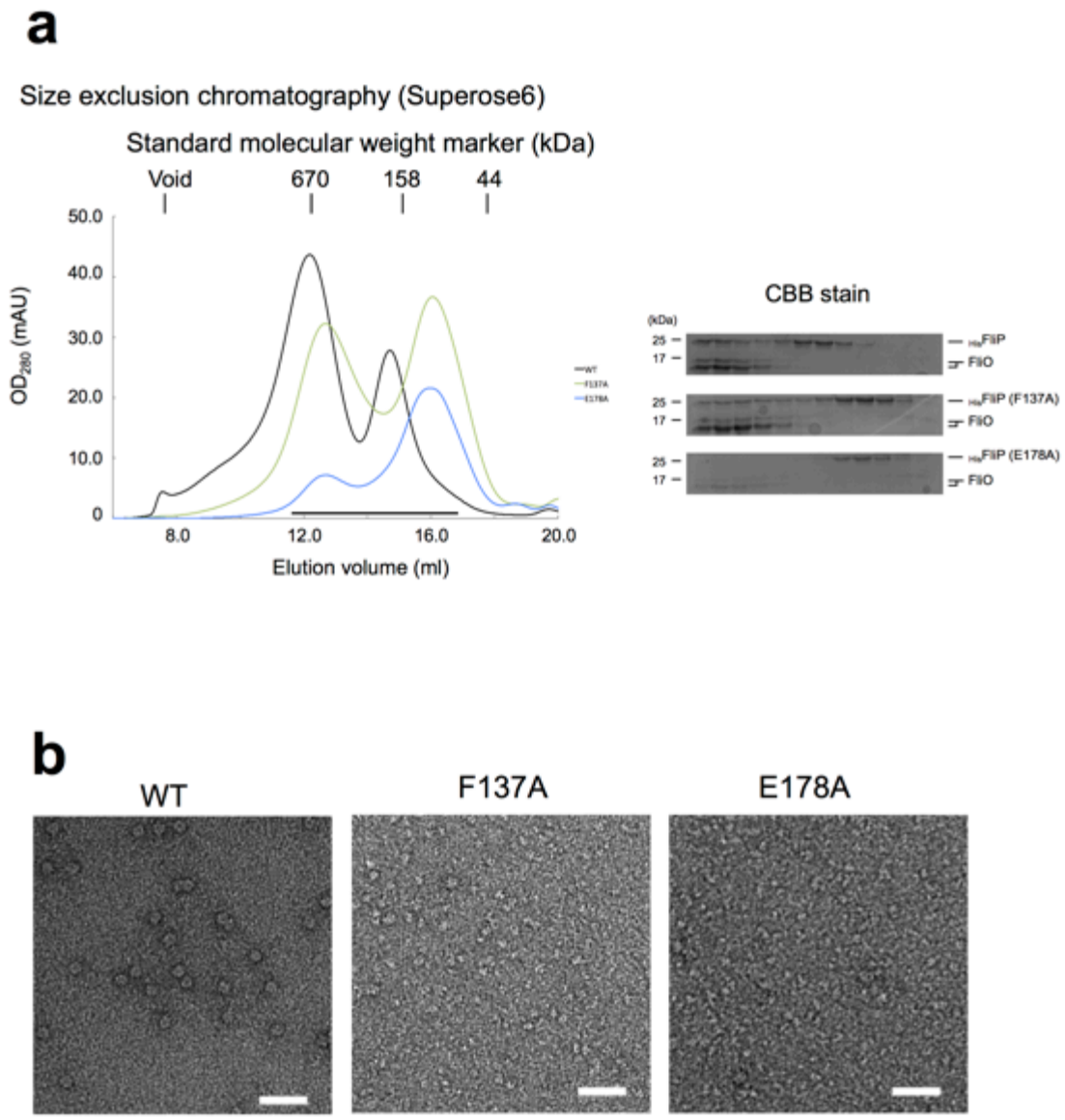

Figure 3-5. Purification of FliP variants

(a) Size exclusion chromatography profiles of FliO/P (black line), FliO/P(F137A) (green line) and FliO/P(E178A) (blue line). Eluted proteins were confirmed by SDS-PAGE. (b) Representative negatively stained EM images of the FliP fraction from each variant. Scale bar shows 50 nm.

3.4. Discussion

Biological unit of FliP and role of FliO

I showed that FliO directly interacts with FliP to facilitate FliP hexamer formation. I also found that a couple of the FliP rings connect with each other in the purified FliO/FliP complex. Interestingly, the $FliP_6$ ring dissociates from the FliO/P complex during size exclusion chromatography. These observations suggest that FliO acts as a scaffold to form FliP ring. Recent genetic study have shown that FliO dose not contribute to FliP protein stability because the bypass mutations isolated from the *fliO* null strain, FliP(R143H) and FliP(F170L), do not increase the protein stability of FliP, significantly. In contrast, I found that the co-expression of FliP with FliO increases the expression level of FliP, significantly. In agreement with this, FliO also stabilized point mutant variants of FliP. These results indicate that FliO has a role in stabilization of FliP *in vivo*. Therefore, I suggest that the bypass FliP (R143H) and FliP(F170L) mutations could increase the probability of FliP ring formation in the absence of FliO.

As discussed in chapter 2, the $FliP_P$-$FliP_P$ interaction is required for FliP dimer formation. Here, I showed that both FliP(F137A) and FliP(E178A) interact with FliO. However, they did not form the FliP ring structure, indicating that the $FliP_P$-$FliP_P$ interaction is also required for FliP ring formation. Furthermore, FliO easily dissociated from FliP(E178A) during size exclusion chromatography, indicating that the $FliP_P$-$FliP_P$ interaction stabilizes the FliO-FliP interaction. Taken all together, I suggest that the $FliP_6$ ring is a timer of dimer. Because FliP(E178A) did not restore motility to a considerable degree even under high expression condition, I propose that the $FliP_6$ ring is a functional unit in the export apparatus. This is in agreement with the previous observation that about 4 to 5 molecules of FliP associate with the FBB.

The central channel of the growing flagellar structure is a physical path for flagellar protein. Interestingly, the diameter of the central channel of the flagellar structure is only 2 nm, which is the same as that of the central pore of the $FliP_6$ ring. This raises the possibility that FliP acts as a peptide channel for export substrates. We need further experiments to confirm this hypothesis.

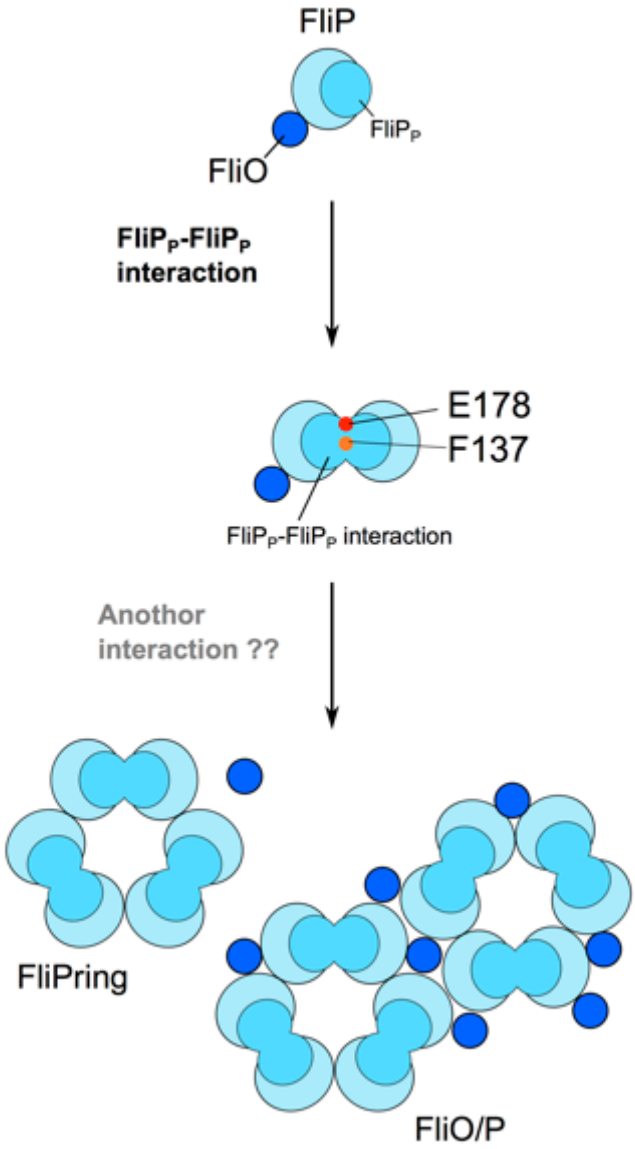

Fig 3-8 Assembly model of FliP

FliP self-assembles into a homo-dimer through the $FliP_P$-$FliP_P$ interaction in the cytoplasmic membrane. The hydrophobic interaction of F137-F137 plays an important role in this process. Although a counterpart of E178 for salt-bridge formation is not conserved, E178 is directly involved in the dimerization. The FliP dimer forms a timer of dimer with the help of FliO, which acts as scaffold for $FliP_6$ ring formation.

Chapter 4
Cryo-EM study of the FliP ring, and the construction of the export gate complex

4.1. Introduction

In chapter 3, I have shown that the FliP ring has a central pore with a diameter of 2 nm. This result gives rise to a new question of whether the FliP ring is a channel for export substrates. To clarify whether FliP interacts with export substrates, I would like to carry out *in vivo* photo-crosslinking experiments. I have to do two things conduct this experiment. One is that I have to obtain a high-resolution 3D structure of the FliP ring. That would be useful for me not only to make design for the photo-crosslinking experiment but also to discuss the obtained results more accurately based on the high-resolution structure. The other thing is that I have to develop the overexpression system of the entire export gate complex. So far, FliO, FliP, FliQ and FliR expressed from chromosmal DNA are unable to detected by western blotting. Overexpression of FliP alone is not sufficient since the export gate works as the complex. Furthermore, as I mentioned in chapter 1, to investigate the molecular mechanism how the export gate converts PMF to the mechanical work required for flagellar protein export in the future, the isolation of the complete export gate complex must be needed. Therefore, the overexpression system of the export gate complex must be developed.

In this chapter, I will show preliminary high-resolution structural analysis of

the FliP ring by cryo-EM and single particle image analysis. The FliP ring particles, of which detergent micelles are replaced by amphipol, are well mono-dispersed in the thin ice formed on the carbon grid. 2D-EM image classification shows a clear hexagonal ring shape, indicating structural analysis of FliP by single particle analysis could be possible. I will also show the construction of the export gate complex for the future research. All components of the export gate are sufficiently expressed. From this co-expression system, I can purify the FlhA/FliF/FliG complex.

4.2. Materials and Methods

4.2.1. Bacterial strains, plasmids and media

The bacterial strains and plasmids used in this chapter are listed in Table 4-1

4.2.2. DNA manipulation

The *Cla*I, *Eag*I and *Spe*I sites that are placed at 30 bp intervals were inserted into the pTc99A vector by invers PCR method, generating a plasmid named pTrc_CES01. To construct pTrc_SE01, the *Spe*I and *Eag*I sites were inserted into the 30bp upstream region of trc promoter and 30bp downstream region of rrnb terminator of pTrc99A, respectively by the Quick Change method. To construct pUC_CE01, a DNA fragment that contains both *Nde*I and *Bam*HI sites were removed from pUC19 by inverse PCR method. Then, the *Cla*I and *Eag*I sites were inserted by inverse PCR method, and a DNA fragment that contains a trc promoter, a multiple of cloning sites and a rrnb terminator derived from the pTrc99A vector was amplified by PCR and then inserted into the *ClaI*-*EagI* sites of the above vector.

4.2.3. Motility assay

Fresh transformant colonies were inoculated onto soft tryptone agar plates.

4.2.4. Preparation of whole cell fractions and immunoblotting

Salmonella cells were grown at 30°C with shaking exponentially. Aliquots of culture proteins containing a constant number of cells were clarified by centrifugation. Cell pellets were resuspended in SDS-loading buffer normalized by cell density to give a constant amount of cells. After sodium dodecyl sulfate-polyacrylamide gel electrophoresis (SDS-PAGE), immunoblot detection was done with an ECL immunoblotting detection kit (GE Healthcare).

4.2.5. Protein expression and purification

The FliP ring was purified in the same method as described in chapter 3. After size exclusion chromatography, total proteins were concentrated to 1 mg ml^{-1}, and supplemented with amphipol A8-35 (Anatrace) to a final concentration of 3 mg ml^{-1}. After incubation at 4 ºC for 4 h, 50 mg Bio-Beads SM-2 (Bio-Rad) was added and then incubated for 6 h. Free amphipol molecules were removed by size exclusion chromatography. Peak fractions were collected for cryo-EM studies.

The export gate complex was expressed and purified in the same method as described in chapter 3.

4.2.6. Data collection and image processing

Aliquots of 2.1 μl of purified FliP at a concentration of approximately 2 mg ml^{-1} were placed on glow-discharged holey carbon grids (Quantifoil Cu R1.2/1.3). Grids were blotted for 7 s and flash frozen in liquid ethane using an FEI Vitrobot. Grids were transferred to JEM-3200FSC electron microscope that was operating at 300 kV. Images were recorded manually using a K2 Summit detector at a super-resolution mode on the JEM-3200FSC microscope at a calibrated magnification of 40,000 (yielding a pixel size of 0.9798 $Å^2$). The K2 detector was mounted after a Gatan Imaging Filter (GIF), but the filter was not used to remove any inelastic scattering. A dose rate of approximately 16 electrons per $Å^2$ per s and exposure time of 12 s on the K2. Defocus values in the final K2 data set ranged from 1.5–3.5 mm, and 40 video frames were recorded.

RELION1.3 was used for automated selection of 37,655 particles from 112 mmicrographs. Contrast transfer function parameters were estimated using CTFFIND3

(Mindell J.A. and Grigorieff N, 2003) and then reference-free two-dimensional class averaging was carried out.

Table 4-1. Strains and plasmids used in this study of this chapter.

Strains or Plasmids	Relevant properties	Source or reference
Salmonella		
SJW1368	Δ(cheW-flhD); master operon mutant ΔfliP	(Ohnishi et al.,1994)
Plasmids		
pTrc99AFF4	Modified trc expression vector	(Ohnishi et al.,1994)
pTrc_ES01	Modified trc expression vector	This study
pTrc_CES01	Modified trc expression vector	This study
pUC_CE01	Modified cloning vector	This study
pKY076	pTrc99AFF4/FliO.$_{His}$FliP	Chapter 3
pKY077	pTrc99AFF4/FliO.$_{His}$FliP.$_{HA}$FliQ.FliR$_{FLAG}$	This study
pKY078	pTrc_CES01 /FlhB.FlhA_FliO.$_{His}$FliP.$_{HA}$FliQ.FliR$_{FLAG}$	This study
pKY079	pTrc_CES01 /FlhB.FlhA_FliO.FliP.$_{HA}$FliQ.FliR$_{FLAG}$_FliF.FliG$_{His}$	This study

Table 4-2. Primers used in this study of this chapter

Primers	Sequence
CES3.Fw	TcggccgAGTAAATAACCCCTTGCGGATCTATGCTAGactagtcggttctggcaaatattc
CES3.Re	CTGCCGCCCCAGctgctcgaagcggccACatcgatttatgatgtcg
E_pTrc99A.Fw	gttttttgcgccgacatcataacggccgcggttctggcaaatattc
E_pTrc99A.Re	gaatatttgccagaaccgcggccgttatgatgtcggcgcaaaaaac
pBAD24_S.Fw	tgtttatttttctaaatacaactagtttcaaatatgtatccgctc
pBAD24_S.Re	gagcggatacatatttgaaactagttgtatttagaaaaataaaca
C_pTrc99A.Fw	gttttttgcgccgacatcataaatcgataggttctggcaaatattc
C_pTrc99A.Re	gaatatttgccagaacctatcgatttatgatgtcggcgcaaaaaac
pTrc99A_E.Fw	tgtttatttttctaaatacacggccgttcaaatatgtatccgctc
pTrc99A_E.Re	gagcggatacatatttgaacggccgtgtatttagaaaaataaaca
trcP_EagI.Fw	tccggccgcggttctggcaaatattctg
rrnB_SpeI.Re	ggactagttgtatttagaaaaataaacaaaaag
trcP_ClaI.Fw	tcataaatcgataggttctggcaaatattctg
rrnB_SpeI.Re	tccggccgtgtatttagaaaaataaacaaaaag
pUC_MOD.Fw	atcgatgtcggccgagactagttttcttagacgtcaggtggcac
pUC_MOD.Re	tcttccgcttcctcgctcactgac
pUC_MOD2.Fw	TcggccgAGTAAATAACCCCTTGCGGATCTATGCTAGactagttttcttagacgtcaggtggc
pUC_MOD2.Re	CTGCCGCCCCAGctgctcgaagcggccACatcgattcttccgcttcctcgctcac
NdeI_FlhB.Fw	gggaattccatATGGCAGAAGAGAGCGACGAC
FlhA_BamI.Re	cgcggatccTTATTTTCCTCCAATGGTC
FliO_NdeI.Fw	gggaattccatATGATGAAGACAGAAGCCAC
FliR_FLAG_BamHI.Re	cgcggatccTTActtatcgtcgtcatccttgtaatcTGGGTTATTATTTATCGGCATC
FliF_NdeI.Fw	gggaattccatATGAGTGCGACTGCATCGAC
	cgcggatccTTAGTGATGATGATGATGATGATGATGATGgccctgaaaatacaggttttcGACATAGGT
FliG_His10_BamHI.Re	ATCCTCGCCG

4.3. Result

4.3.1. Purification and observation of the FliPring by cryo-EM

To succeed in high-resolution structural analysis by cryo-EM and single particle analysis, it is important to embed biomolecule particles into the thin ice on the grid to obtain their high contrast images. It has been reported that detergents in the protein solution make it difficult. To remove DDM from protein solution, I replaced DDM by amphipol. The membrane proteins with amphipol are known to behave larger size than those embedded in detergent micelles in general. The size exclusion chromatography indicated that the FliP ring with amphipol also behaved larger size as well, and was well mono-dispersed as well as the FliP ring with DDM micelle (**Fig4-1**). The FliP ring particles were also mono-dispersed in a thin layer of vitreous ice formed in the carbon holes, indicating that the FliP rings are not absorbed to the carbon grid and that the rings are still in a stable state in vitreous ice (**Fig.4-2a**).

4.3.2. Construction for the expression system of the entire export gate complex

To confirm the expression level of each export gate components, it must be necessary to detect each component by immunobloting. Among the export gate components, we did not have polyclonal anti-bodies specific for FliQ and FliR. Therefore, I fused a HA-tag to the N-terminus of FliQ and a FLAG-tag to the C-terminus of FliR. These tags did not affect the export function of these two proteins at all. It has been reported that the export gate is proposed to assemble in a coordinated manner during MS ring formation (Morimoto et al., 2014). A C-ring component protein FliG is required for efficient MS ring formation in vivo (Morimoto et al., 2014). Therefore, FlhA, FlhB, FliO, FliP, FliQ, FliR, FliF and FliG must be co-expressed to obtain the complete export gate complex associated with the MS ring. To simplify the

expression system, I expressed these eight proteins from a pTrc99A-based plasmid in a *Salmonella* Δ*flhDC* strain as a host. *flhA* and *flhB*, *fliO*, *fliP*, *fliQ* and *fliM*, *fliF* and *fliG* are transcribed as the *flhB*, *fliL* and *fliF* operons, respectively in *Salmonella* (Kutsukake *et al*., 1988). Three PCR products, *flhBA*, *fliOPQR*, and *fliFG*, were cloned into three distinct sites of the pTrc99A_CES01 vector. They were placed from a p*trc* promoter (**Fig.4-3**). I also constructed the FliO/P/Q/R and FlhB/A-FliO/P/Q/R, FlhB/A-FliO/P/Q/R-FliF/G co-expression system respectively.

As mentioned in Chapter 3, I attach a His-tag to FliP and so purification of the FliO/P/Q/R and FlhB/A-FliO/P/Q/R complexes was carried out by Ni-NTA affinity chromatography, followed by size exclusion chromatography (**Fig.4-4a**). The FliO/P/R complex was purified by Ni-ATA affinity chromatography from FliO/P/Q/R co-expression system and FliO was dissociated from this complex during gel filtration chromatography. The FliP/R complex showed a mono-dispersed peak. The FliO/P/R structure looked similar to the FliO/P complex (**Fig.4-4b**). The FliO/P/R-FlhB complex was affinity purified from the FlhB/A-FliO/P/Q/R co-expression system, indicating that FlhB directly binds to the FliO/P/R complex whereas FlhA does not. The molar ratio of FliR and FlhB seemed to be 1:1, in agreement with a previous observation that a FliR-FlhB fusion is functional (REF). However, FlhB was easily dissociated from this complex during size exclusion chromatography, indicating the interaction between FliO/P/R and FlhB could be weak. For FlhB/A-FliO/P/Q/R-FliF/G co-expression system, I fused a deca-histidine tag at the C-terminus of FliG and then the FlhA/FliF/FliG complex was able to be purified by Ni-NTA affinity chromatography, followed gel filtration chromatography (**Fig.4-4a**). This indicates that FlhB/FliO/P/Q/R easily dissociates from the FlhA/FliF/FliG complex during solubilization and puritication. Negatively stained EM observation of this complex revealed the MS-ring

structure, indicating that FlhA and FliG associate with the MS ring (**Fig.4-4b**). The stoichiometry of the FlhA/FliF/FliG complex seemed to be ~0.3 FlhA : 1 FliF : ~1.5 FliG.

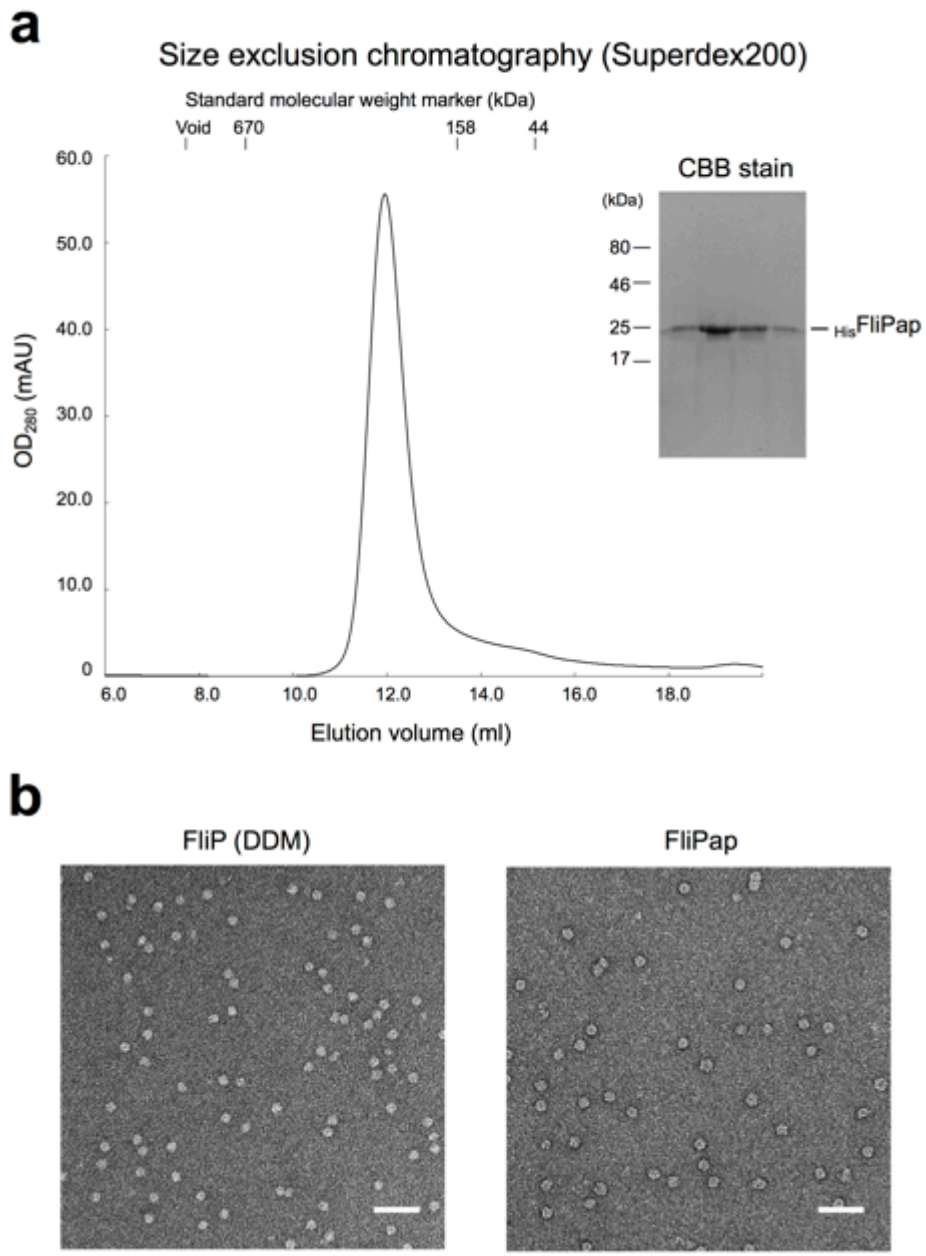

Figure 4-1. Purification profile of FliPap

(a) Size exclusion chromatography (Superdex200) after exchanging from DDM to amphipol. Eluted proteins in the peak was confirmed by SDS-PAGE. (b) Representative negatively stained EM images of purified FliP in DDM and in amphipol. Scale bar shows 50 nm.

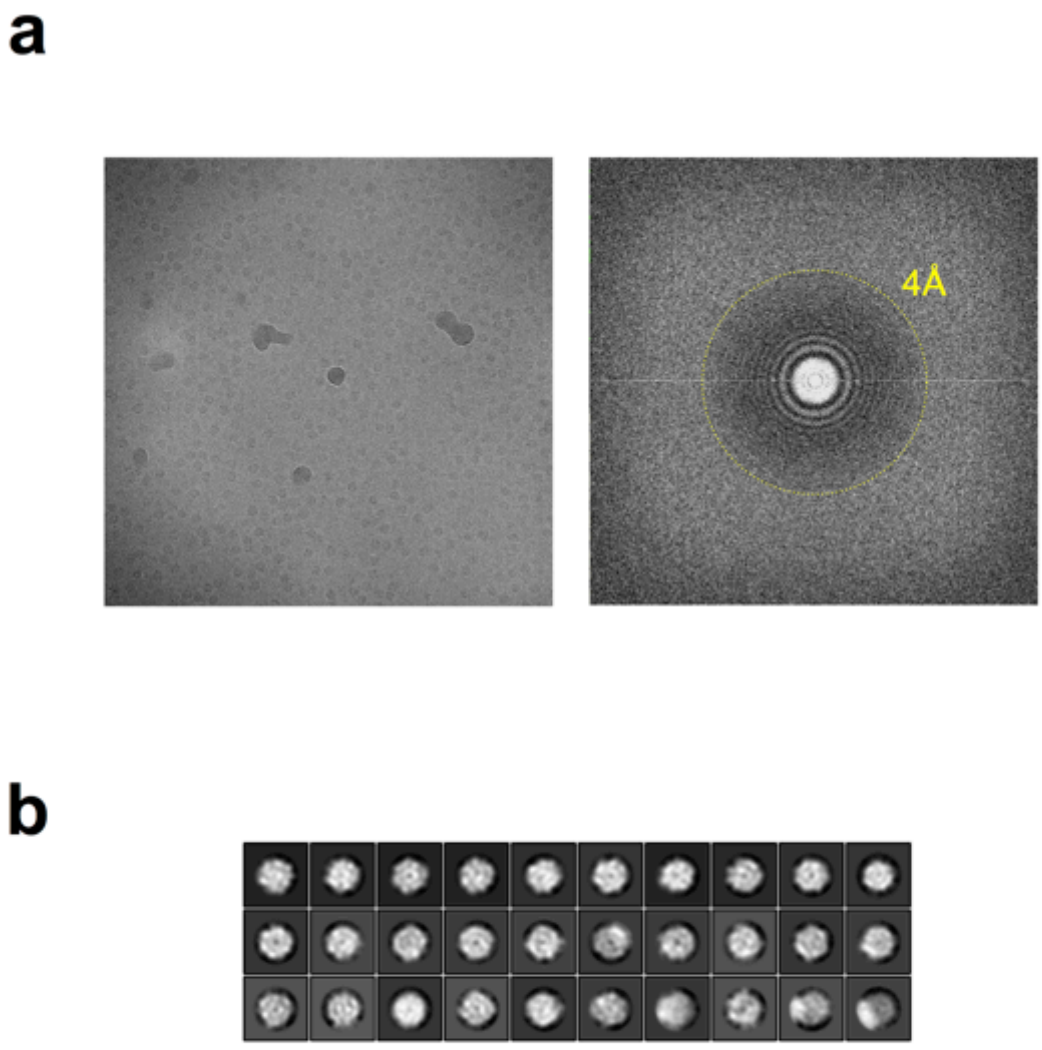

Figure 4-2. Cryo-EM images and 2-D classification

(a) Representative EM image of FliPap embedded in a thin layer of vitreous ice. Fourier transform of micrograph shown in right, with Thon rings extending beyond 4 Å. (b) Representative 2D class averages.

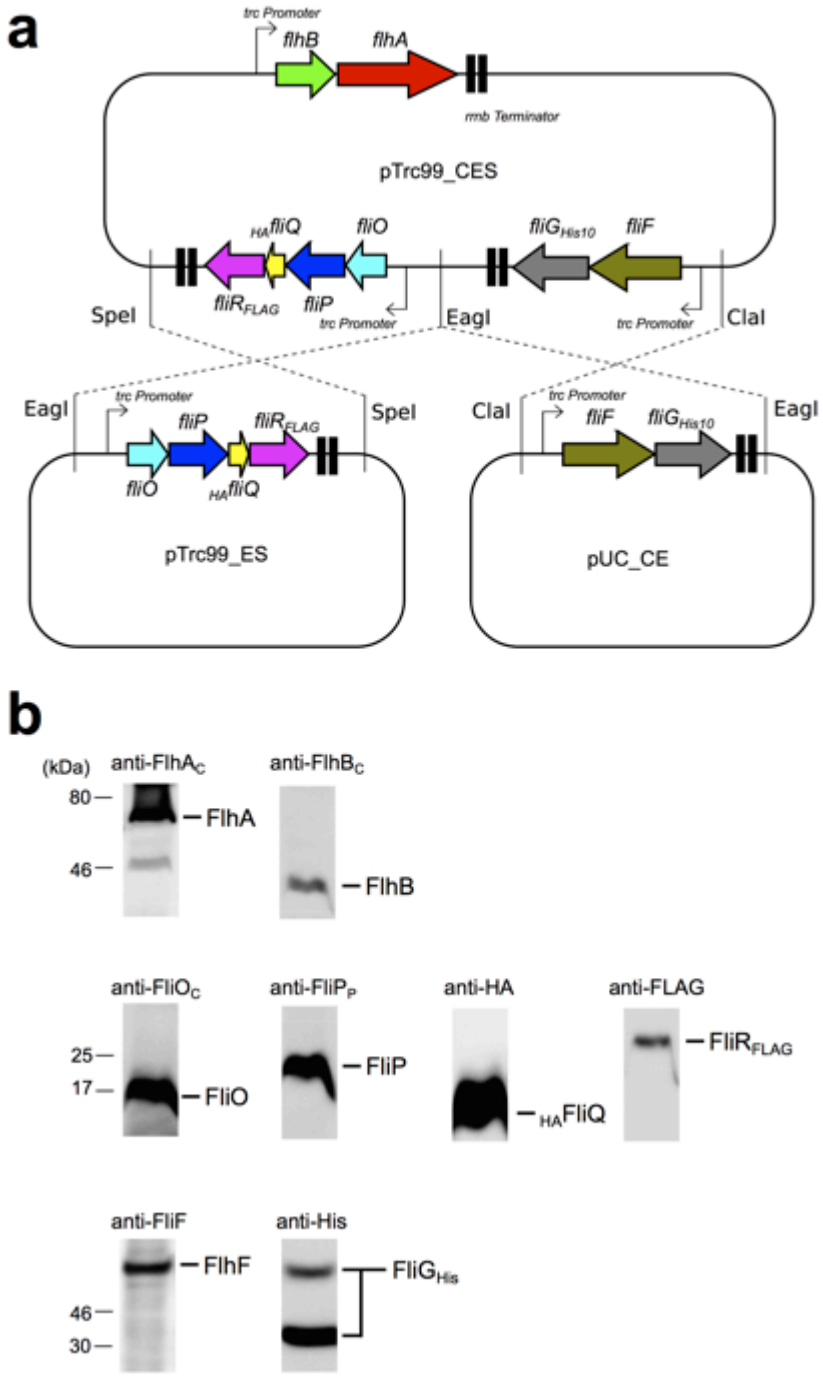

Figure 4-3. Construction and expressions

(a) Schematic diagram of co-expression plasmids of the export gate. (b) Westernblotting of membrane fraction by antibody to each export gate component and westernblotting of whole cell fraction by antibody to FliF and FliG.

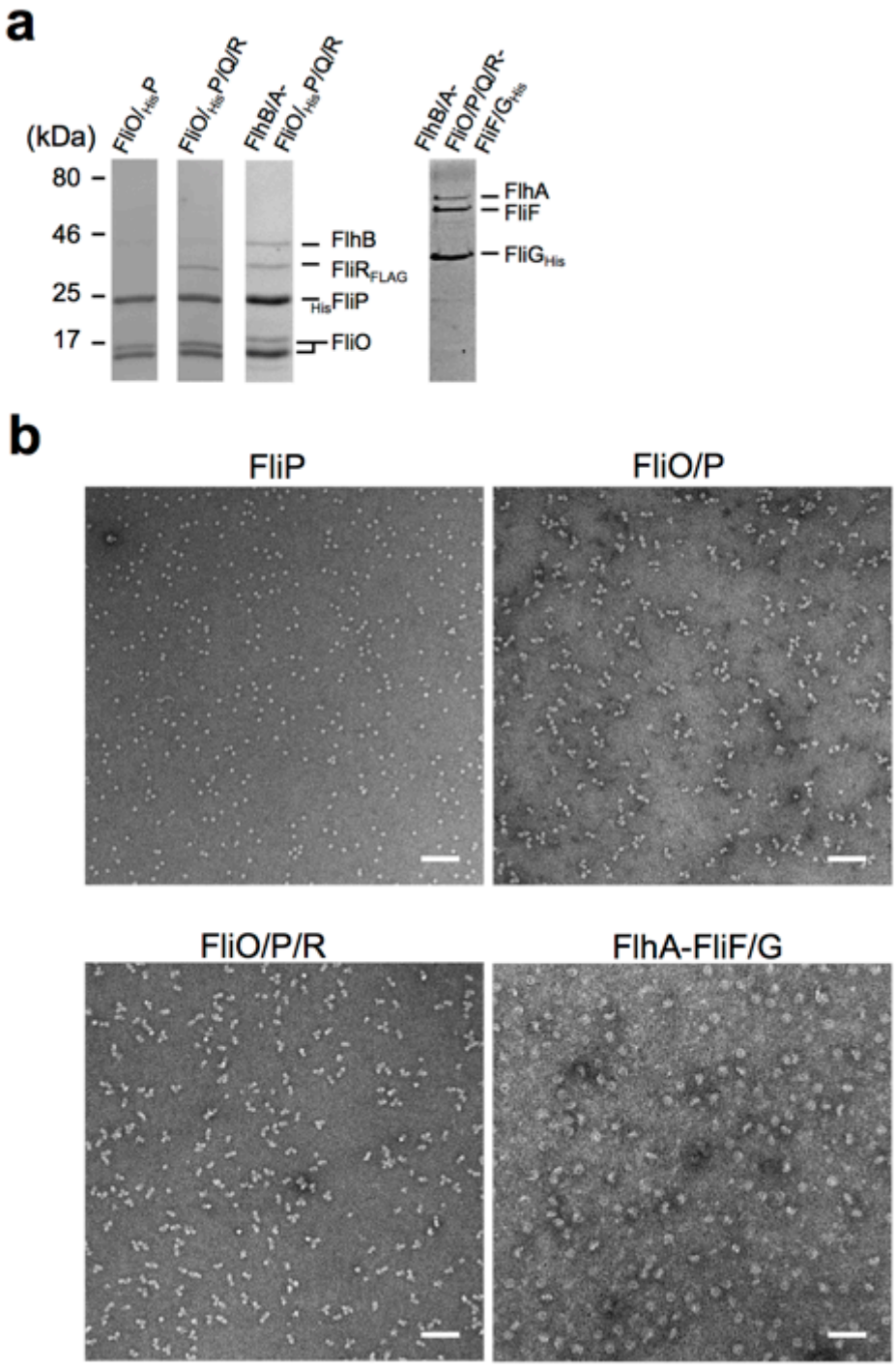

Figure 4-4. Purification and EM-observation

(a) SDS-PAGE results after Ni-NTA affinity chromatography from each co-expression system. (b) Representative negatively stained EM images FliP and complexes purified after size exclusion chromatography. Scale bar shows 50 nm.

4.4. Discussion

2D class averages of negatively stained FliP ring showed that the FliP ring is a hexagonal ring structure. Some 2D class averages of the FliP ring from cryo-EM data also showed a hexagonal ring structure (**Fig.4-2b**), indicating that the FliP ring is not distorted by negative staining. Therefore, I conclude that the $FliP_6$ ring is a physiological and functional relevant in the export apparatus. Since the biological unit of $FliP_P$ is proposed to be a dimer, the FliP ring is assumed to form a trimer of dimer. Indeed, many classes of the FliP ring showed three-fold symmetric structure.

The previous genetic and biochemical study of the flagellar homologue, the needle complex, revealed that an earlier assembly of SpaP, SpaQ and SpaR (correspond to FliP, FliQ, FliR respectively) is required for the assembly of InvA and SpaS (correspond to FlhA and FlhB) into the export gate. In addition, InvA and SpaS can assemble into the export gate after completion of the assembly of the needle complex base whereas neither SpaP, SpaQ nor SpaR can. These result indicated that in flagellar structure, FliO, FliP, FliQ and FliR forms a core complex for the following assembly of FlhA and FlhB into the export gate. Since SpaP and SpaR seemed to form a complex in the export gate and their assembly is required for the assembly of SpaQ into the export gate, SpaP and SpaR forms stable complex at the earliest stage of the export gate assembly. This is in agreement with my result that FliP and FliR forms a stable complex. Although the FliP/R complex was isolated from the FliO/P/R complex, it is still unclear that the FliO/P complex structure is required for efficient interaction of FliP with FliR. FliQ was assumed to form a complex with the FliO/P/R complex, however FliQ dissociated form the FliO/P/R complex during Ni-NTA affinity chromatography, indicating that an association between FliQ and the FliO/P/R complex could be weak .

Another previous genetic study showed that fusion protein of FlhB and FliR complemented their function, indicating FlhB and FliR interact with each other at a 1 to 1 molar ratio. In this study, co-expression and purification of FlhA/FlhB -FliO/P/Q/R revealed that FlhB interacts with FliO/P/R. Furthermore the molar ratio of FlhB and FliR seemed to be 1:1. Therefore FlhB was assumed to be associated with FliO/P/R complex through the transmembrane region of FliR at a 1:1 molar ratio. However, still FliQ and FlhA were dissociated from the complex.

When FlhB, FlhA, FliO/P/Q/R and FliF/G were expressed at the same time, I succeeded in purification of the FlhA/FliF/FliG complex by Ni-Affinity chormatography, followed by size exclusion chromatography. This result was consistent with the recent genetic and fluorescent microscopic analysis that the MS-ring component, FliF, and one of the C-ring components, FliG, are required for FlhA assembly into the export gate. Co-expression and affinity purification of by C-terminal His-tag of FliG resulted in the purification of FlhA-FliF/G complex. From the result of CBB stain, the molecular ratio of FliF and FliG seemed to be 1 : 1.5. It has been reported that FliF/FliG complex was purified from FliF/G co-expression system and the molecular ratio of FliF and FliG is 1 : 1. Therefore FlhA in the MS-ring might affect the conformation of FliF or FliG to change the interaction manner between the MS-ring and FliG. Other components except for FliO and FlhB were detected by immunoblotting, however almost all components were appeared in the flow through fractions, indicating those components were dissociated form the complex when they were solubilized from the membrane or the complete complex flew through from the affinity resin.

To clarify the detail assemble mechanism of the export gate, it is necessary to express any combinations of the export gate components, followed by purification and observation. Furthermore to confirm these biochemical data, it is important to observe

the localization and dynamics of each component by fluorescent microscope in the living cells. Moreover to isolate the complete export gate complex for understanding the molecular mechanism of the protein translocation, it is still necessary to examine the solubilization conditions from the membrane and the purification conditions.

Chapter 5
Conclusion

The PMF-driven export gate complex is located at the flagellar base to drive flagellar protein export for the construction of the flagellum beyond the cell membranes (Katayama et al. 1996; Kawamoto et al. 2013). It has been reported FliP and FliR are incorporated into the basal body along with FliF and FliG at the earliest stage (Jones and Macnab, 1990; Fan *et al*., 1997). Since FlhA assembles into the export gate complex along with other transmembrane export gate proteins during MS ring formation, it has been proposed that the assembly of the export gate complex may begin with FliO, FliP, FliQ and FliR, followed by FlhA and FlhB (Morimoto et al. 2014). However, it remains unknown how FliO, FliP, FliQ and FliR forms a core structure of the export gate for assembly of FlhA and FlhB. Therefore, I forced on the structure of FliP to understand the assembly mechanism of the export gate complex. Because FliP has a relatively large periplasmic domain, I first determined the structure of a periplasmic domain of $FliP_P$ from *Thermotoga maritima* at 2.4 Å resolution. Structure-based in vivo disulfide cross-linking experiment, revealed that FliP form a homo-dimer through the $FliP_P$-$FliP_P$ interaction. Highly conserved Phe-137 and Glu-178 residue located at the interface 1 contribute to the strong $FliP_P$-$FliP_P$ interaction in the crystal structure. In agreement with this, the FliP(F137A) and FliP(E178A) substitutions results in a significant reduction in motility. These results suggest that FliP forms a

dimer unit through the $FliP_P$-$FliP_P$ interaction for efficient assembly of the export gate complex.

It has been reported that about 4 or 5 copies of FliP associates with the basal body MS ring (Fan *et al*., 1997). To test whether if full-length FliP forms a higher oligomer in the MS ring, I overexpressed and purified full-length FliP. Although FliP did not show a mono-dispersed peak during size exclusion chromatography even though several detergents were examined for its solubilization, co-expression of FliP with FliO dramatically increased its homogeneity. FliO was co-purified with FliP, indicating FliO and FliP directly interact with each other. EM observation of FliP revealed that FliP forms a ring-shaped structure. 2D class averages of the FliP ring revealed the hexagonal ring structures, indicating FliP forms a homo-hexamer. EM observation of the FliO/P complex revealed that a couple of the FliP rings associate with each other through an interaction between FliO and the FliP ring. The FliP variants harboring a mutation that affects the $FliP_P$-$FliP_P$ interaction was unable to form the stable FliP ring structure, Based on these results, I propose that the FliP form a hexamer as a trimer of dimer, and that FliO act as a scaffold to facilitate FliP ring formation. Since the diameter of the MS-ring is estimated to be around 40 nm, it is difficult to insert the FliO/P complex into the MS-ring. On the bases of the result that FliP and FliP/R easily dissociate form FliO, and the fact that FliO is indispensable among the export gate components, I assume that FliO may not localize in the MS-ring.

Co-expressions of FliO/P/Q/R and FlhB/A-FliO/P/Q/R allowed me to purify the FliO/P/R and FliO/P/R-FlhB complexes, respectively. The stoichiometry of FlhB and FliR seemed to be 1:1 that is consistent with the previous genetic analysis. Although FlhB was easily dissociated from the FliO/P/R complex during gel filtration chromatography, indicating that an association between FlhB and the FliO/P/R complex

is weak. EM observation of the FliO/P/R complex revealed that its overall structure was almost the same as the FliO/P complex. The FliP/R complex was dissociated form the FliO/P/R complex during gel filtration chromatography in a way similar to FliP dissociated from the FliO/P complex, and its structure was also almost identical to the FliP ring. This suggests that FliR directly binds to the FliP ring. Co-expression of FlhB/A-FliO/P/Q/R-FliF/G allowed me to isolate the FlhA-FliF/G complex by gel filtration chromaotgraphy, suggesting that the FlhB/FliO/P/R and FliQ dissociates from the FlhA-FliF/G complex during solubilization , followed by Ni affinity chromatography. EM observation of the FlhA-FliF/G complex revealed that FliF forms the MS-ring and that FlhA and FliG associates with the MS ring . Although the stoichiometry of FliF and FliG is proposed to be 1:1, the stoichiometry of FliF and FliG in FlhA-FliF/G complex seemed to be 1:~1.5, indicating that the association of FlhA with the MS-ring might affect the interaction between FliF and FliG.

FliJ binds to the $FliI_6$ ring to form the $FliI_6$FliJ ring complex (Ibuki *et al*., 2011). ATP hydrolysis by the $FliI_6$FliJ ring complex activates the export gate complex through an interaction between FliJ and FlhA, allowing the gate to efficiently utilize PMF across the cytoplasmic membrane for rapid and efficient flagellar protein export (Minamino et al., 2014). The export gate complex is a proton-protein antipoter to couples the proton flow with protein translocation (Minamino *et al.*, 2011). FlhA is an energy transducer to conduct both H^+ and Na^+ (Minamino *et al*., unpublished data). ATP hydrolysis by FliI ATPase is coupled to proton translocation through the export gate (Morimoto *et al*., unpublished data). Since the FliP ring seems to be a core structure for export gate assembly, the FliP ring could be located at the center of the export gate complex. The central pore of the FliP ring is 2 nm, which is the same size as the central channel of the growing flagellar structure, I propose that the FliP ring acts as

a peptide channel and that ATP hydrolysis by FliI ATPase induces proton translocation through the FlhA proton channel, allowing export substrates to go into the FliP channel and then the central channel of the growing flagellar structure. To understand the detail molecular mechanism of PMF-driven protein transport by the export gate complex, further biochemical and high-resolution structural analysis must be necessary.

Acknowledgement

This study has been carried out in the Protonic NanoMachine Laboratory, Graduate School of Frontier Biosciences, Osaka University.

I would like to express my sincere gratitude to my supervisor, Prof. Keiichi Namba and Associate Prof. Tohru Minamino for incessant guidance, discussion and encouragement throughout my Ph.D work. I wish to express my sincere thanks to Prof. Yasushi Hiraoka, Prof. Katsumi Imada and Prof. Junichi Takagi in Osaka University for evaluating this work.

I am deeply grateful to Prof. Katsuimi Imada and assistant Prof. Saijo-Hamano Yumiko for teaching me crystallization, data collection and structural analysis for X-ray crystallographic analysis. I am grateful to Assistant Prof. Takayuki Kato, Dr. Takashi Fujii and Yurika Yamada for teaching me a lot of techniques of electron microscopy and discussion.

I cannot find any words to express my sincere gratitude to all the members of the Protonic NanoMachine Laboratory, including its former members, for a lot of technical help, extensive discussion and continuous encouragement.

In closing, I thank my family for their heartwarming encouragement and support.

March, 2016 Takuma Fukumura

Reference

Abrusci P, Vergara-Irigaray M, Johnson S, Beeby MD, Hendrixson DR, Roversi P, Friede ME, Deane JE, Jensen GJ, Tang CM, Lea SM. Architecture of the major component of the type III secretion system export apparatus. Nat Struct Mol Biol. 2013 Jan;20(1):99-104.

Adams PD, Afonine PV, Bunkóczi G, Chen VB, Davis IW, Echols N, Headd JJ, Hung LW, Kapral GJ, Grosse-Kunstleve RW, McCoy AJ, Moriarty NW, Oeffner R, Read RJ, Richardson DC, Richardson JS, Terwilliger TC, Zwart PH. PHENIX: a comprehensive Python-based system for macromolecular structure solution. Acta Crystallogr D Biol Crystallogr. 2010 Feb;66(Pt 2):213-21.

Aizawa SI, Dean GE, Jones CJ, Macnab RM, Yamaguchi S. Purification and characterization of the flagellar hook-basal body complex of Salmonella typhimurium. J Bacteriol. 1985 Mar;161(3):836-49.

Akiba T, Yoshimura H, Namba K. Monolayer crystallization of flagellar L-P rings by sequential addition and depletion of lipid. Science. 1991 Jun 14;252(5012):1544-6.

Aldridge P, Karlinsey J, Hughes KT. The type III secretion chaperone FlgN regulates flagellar assembly via a negative feedback loop containing its chaperone substrates FlgK and FlgL. Mol Microbiol. 2003 Sep;49(5):1333-45.

Aldridge PD, Karlinsey JE, Aldridge C, Birchall C, Thompson D, Yagasaki J, Hughes KT. The flagellar-specific transcription factor, sigma28, is the Type III secretion chaperone for the flagellar-specific anti-sigma28 factor FlgM. Genes Dev. 2006 Aug 15;20(16):2315-26.

Asakura S. Polymerization of flagellin and polymorphism of flagella. Adv Biophys. 1970;1:99-155. Review.

Auvray F, Thomas J, Fraser GM, Hughes C. Flagellin polymerisation control by a cytosolic export chaperone. J Mol Biol. 2001 Apr 27;308(2):221-9.

Auvray F, Ozin AJ, Claret L, Hughes C. Intrinsic membrane targeting of the flagellar

export ATPase FliI: interaction with acidic phospholipids and FliH. J Mol Biol. 2002 May 10;318(4):941-50.

Bai F, Branch RW, Nicolau DV Jr, Pilizota T, Steel BC, Maini PK, Berry RM. Conformational spread as a mechanism for cooperativity in the bacterial flagellar switch. Science. 2010 Feb 5;327(5966):685-9.

Bai F, Morimoto YV, Yoshimura SD, Hara N, Kami-Ike N, Namba K, Minamino T. Assembly dynamics and the roles of FliI ATPase of the bacterial flagellar export apparatus. Sci Rep. 2014 Oct 6;4:6528

Bange G, Kümmerer N, Engel C, Bozkurt G, Wild K, Sinning I. FlhA provides the adaptor for coordinated delivery of late flagella building blocks to the type III secretion system. Proc Natl Acad Sci U S A. 2010 Jun 22;107(25):11295-300.

Barker CS, Meshcheryakova IV, Kostyukova AS, Samatey FA. FliO regulation of FliP in the formation of the Salmonella enterica flagellum. PLoS Genet. 2010 Sep 30;6(9):e1001143.

Barker CS, Samatey FA. Cross-complementation study of the flagellar type III export apparatus membrane protein FlhB. PLoS One. 2012;7(8):e44030.

Barker CS, Meshcheryakova IV, Inoue T, Samatey FA. Assembling flagella in Salmonella mutant strains producing a type III export apparatus without FliO. J Bacteriol. 2014 Dec;196(23):4001-11.

Battye TG, Kontogiannis L, Johnson O, Powell HR, Leslie AG. iMOSFLM: a new graphical interface for diffraction-image processing with MOSFLM. Acta Crystallogr D Biol Crystallogr. 2011 Apr;67(Pt 4):271-81.

Bennett JC, Thomas J, Fraser GM, Hughes C. Substrate complexes and domain organization of the Salmonella flagellar export chaperones FlgN and FliT. Mol Microbiol. 2001 Feb;39(3):781-91.

Berg HC. Constraints on models for the flagellar rotary motor. Philos Trans R Soc Lond B Biol Sci. 2000 Apr 29;355(1396):491-501.

Berg HC, Anderson RA. Bacteria swim by rotating their flagellar filaments. Nature. 1973 Oct 19;245(5425):380-2.

Berg HC, Brown DA. Chemotaxis in Escherichia coli analysed by three-dimensional tracking. Nature. 1972 Oct 27;239(5374):500-4.

Berg HC. The rotary motor of bacterial flagella. Annu Rev Biochem. 2003;72:19-54. Epub 2002 Dec 11. Review.

Blair DF, Kim DY, Berg HC. Mutant MotB proteins in Escherichia coli. J Bacteriol. 1991 Jul;173(13):4049-55.

Blair DF, Berg HC. The MotA protein of E. coli is a proton-conducting component of the flagellar motor. Cell. 1990 Feb 9;60(3):439-49.

Blair DF, Berg HC. Mutations in the MotA protein of Escherichia coli reveal domains critical for proton conduction. J Mol Biol. 1991 Oct 20;221(4):1433-42.

Braun TF, Blair DF. Targeted disulfide cross-linking of the MotB protein of Escherichia coli: evidence for two H(+) channels in the stator Complex. Biochemistry. 2001 Oct 30;40(43):13051-9.

Braun TF, Al-Mawsawi LQ, Kojima S, Blair DF. Arrangement of core membrane segments in the MotA/MotB proton-channel complex of Escherichia coli. Biochemistry. 2004 Jan 13;43(1):35-45.

Brown PN, Hill CP, Blair DF. Crystal structure of the middle and C-terminal domains of the flagellar rotor protein FliG. EMBO J. 2002 Jul 1;21(13):3225-34.

Brown PN, Mathews MA, Joss LA, Hill CP, Blair DF. Crystal structure of the flagellar rotor protein FliN from Thermotoga maritima. J Bacteriol. 2005 Apr;187(8):2890-902.

Chen S, Beeby M, Murphy GE, Leadbetter JR, Hendrixson DR, Briegel A, Li Z, Shi J, Tocheva EI, Müller A, Dobro MJ, Jensen GJ. Chen S, Beeby M, Murphy GE, Leadbetter JR, Hendrixson DR, Briegel A, Li Z, Shi J, Tocheva EI, Müller A, Dobro

MJ, Jensen GJ. EMBO J. 2011 Jun 14;30(14):2972-81.

Chevance FF, Hughes KT. Coordinating assembly of a bacterial macromolecular machine. Nat Rev Microbiol. 2008 Jun;6(6):455-65.

Claret L, Calder SR, Higgins M, Hughes C. Oligomerization and activation of the FliI ATPase central to bacterial flagellum assembly. Mol Microbiol. 2003 Jun;48(5):1349-55.

Datsenko KA, Wanner BL. One-step inactivation of chromosomal genes in Escherichia coli K-12 using PCR products. Proc Natl Acad Sci U S A. 2000 Jun 6;97(12):6640-5.

DePamphilis ML, Adler J. Attachment of flagellar basal bodies to the cell envelope: specific attachment to the outer, lipopolysaccharide membrane and the cyoplasmic membrane. J Bacteriol. 1971 Jan;105(1):396-407.

Dickson VK, Silvester JA, Fearnley IM, Leslie AG, Walker JE. On the structure of the stator of the mitochondrial ATP synthase. EMBO J. 2006 Jun 21;25(12):2911-8.

Dreyfus G, Williams AW, Kawagishi I, Macnab RM. Genetic and biochemical analysis of Salmonella typhimurium FliI, a flagellar protein related to the catalytic subunit of the F0F1 ATPase and to virulence proteins of mammalian and plant pathogens. J Bacteriol. 1993 May;175(10):3131-8.

Emsley P, Lohkamp B, Scott WG, Cowtan K. Features and development of Coot. Acta Crystallogr D Biol Crystallogr. 2010 Apr;66(Pt 4):486-501.

Evans P. Scaling and assessment of data quality. Acta Crystallogr D Biol Crystallogr. 2006 Jan;62(Pt 1):72-82. Epub 2005 Dec 14. Review.

Evdokimov AG, Phan J, Tropea JE, Routzahn KM, Peters HK, Pokross M, Waugh DS. Similar modes of polypeptide recognition by export chaperones in flagellar biosynthesis and type III secretion. Nat Struct Biol. 2003 Oct;10(10):789-93. Epub 2003 Sep 7.

Fan F, Ohnishi K, Francis NR, Macnab RM. The FliP and FliR proteins of Salmonella typhimurium, putative components of the type III flagellar export apparatus, are located in the flagellar basal body. Mol Microbiol. 1997 Dec;26(5):1035-46.

Fan F, Macnab RM. Enzymatic characterization of FliI. An ATPase involved in flagellar assembly in Salmonella typhimurium. J Biol Chem. 1996 Dec 13;271(50):31981-8.

Ferris HU, Furukawa Y, Minamino T, Kroetz MB, Kihara M, Namba K, Macnab RM. FlhB regulates ordered export of flagellar components via autocleavage mechanism. J Biol Chem. 2005 Dec 16;280(50):41236-42. Epub 2005 Oct 24.

Fraser GM, Bennett JC, Hughes C. Substrate-specific binding of hook-associated proteins by FlgN and FliT, putative chaperones for flagellum assembly. Mol Microbiol. 1999 May;32(3):569-80.

Francis NR, Irikura VM, Yamaguchi S, DeRosier DJ, Macnab RM. Localization of the Salmonella typhimurium flagellar switch protein FliG to the cytoplasmic M-ring face of the basal body. Proc Natl Acad Sci U S A. 1992 Jul 15;89(14):6304-8.

Francis NR, Sosinsky GE, Thomas D, DeRosier DJ. Isolation, characterization and structure of bacterial flagellar motors containing the switch complex. J Mol Biol. 1994 Jan 28;235(4):1261-70.

Fraser GM, Bennett JC, Hughes C. Substrate-specific binding of hook-associated proteins by FlgN and FliT, putative chaperones for flagellum assembly. Mol Microbiol. 1999 May;32(3):569-80.

Fraser GM, Hirano T, Ferris HU, Devgan LL, Kihara M, Macnab RM. Substrate specificity of type III flagellar protein export in Salmonella is controlled by subdomain interactions in FlhB. Mol Microbiol. 2003 May;48(4):1043-57.

Fraser GM, González-Pedrajo B, Tame JR, Macnab RM. Interactions of FliJ with the Salmonella type III flagellar export apparatus. J Bacteriol. 2003 Sep;185(18):5546-54.

Fujii T, Kato T, Namba K. Specific arrangement of alpha-helical coiled coils in the core

domain of the bacterial flagellar hook for the universal joint function. Structure. 2009 Nov 11;17(11):1485-93.

Fujime S, Maruyama M, Asakura S. Flexural rigidity of bacterial flagella studied by quasielastic scattering of laser light. J Mol Biol. 1972 Jul 21;68(2):347-59.

González-Pedrajo B, Fraser GM, Minamino T, Macnab RM. Molecular dissection of Salmonella FliH, a regulator of the ATPase FliI and the type III flagellar protein export pathway. Mol Microbiol. 2002 Aug;45(4):967-82.

Hara N, Namba K, Minamino T. Genetic characterization of conserved charged residues in the bacterial flagellar type III export protein FlhA. PLoS One. 2011;6(7):e22417.

Hara N, Morimoto YV, Kawamoto A, Namba K, Minamino T. Interaction of the extreme N-terminal region of FliH with FlhA is required for efficient bacterial flagellar protein export. J Bacteriol. 2012 Oct;194(19)

Hirano T, Yamaguchi S, Oosawa K, Aizawa S. Roles of FliK and FlhB in determination of flagellar hook length in Salmonella typhimurium. J Bacteriol. 1994 Sep;176(17):5439-49.

Hirota N, Imae Y. Na+-driven flagellar motors of an alkalophilic Bacillus strain YN-1. J Biol Chem. 1983 Sep 10;258(17):10577-81.

Hizukuri Y, Yakushi T, Kawagishi I, Homma M Role of the intramolecular disulfide bond in FlgI, the flagellar P-ring component of Escherichia coli. J Bacteriol. 2006 Jun;188(12):4190-7.

Hizukuri Y, Kojima S, Homma M. Disulphide cross-linking between the stator and the bearing components in the bacterial flagellar motor. J Biochem. 2010 Sep;148(3):309-18.

Homma M, Komeda Y, Iino T, Macnab RM. The flaFIX gene product of Salmonella typhimurium is a flagellar basal body component with a signal peptide for export. J Bacteriol. 1987 Apr;169(4):1493-8.

Hu B, Morado DR, Margolin W, Rohde JR, Arizmendi O, Picking WL, Picking WD, Liu J. Visualization of the type III secretion sorting platform of Shigella flexneri. Proc Natl Acad Sci U S A. 2015 Jan 27;112(4):1047-52.

Hueck CJ. Type III protein secretion systems in bacterial pathogens of animals and plants. Microbiol Mol Biol Rev. 1998 Jun;62(2):379-433.

Imada K, Minamino T, Tahara A, Namba K. Structural similarity between the flagellar type III ATPase FliI and F1-ATPase subunits. Proc Natl Acad Sci U S A. 2007 Jan 9;104(2):485-90.

Imada K, Minamino T, Kinoshita M, Furukawa Y, Namba K. Structural insight into the regulatory mechanisms of interactions of the flagellar type III chaperone FliT with its binding partners. Proc Natl Acad Sci U S A. 2010 May 11;107(19):8812-7.

Ibuki T, Imada K, Minamino T, Kato T, Miyata T, Namba K. Common architecture of the flagellar type III protein export apparatus and F- and V-type ATPases. Nat Struct Mol Biol. 2011 Mar;18(3):277-82.

Ibuki T, Uchida Y, Hironaka Y, Namba K, Imada K, Minamino T. Interaction between FliJ and FlhA, components of the bacterial flagellar type III export apparatus. J Bacteriol. 2013 Feb;195(3):466-73.

Imada K, Minamino T, Kinoshita M, Furukawa Y, Namba K. Structural insight into the regulatory mechanisms of interactions of the flagellar type III chaperone FliT with its binding partners. Proc Natl Acad Sci U S A. 2010 May 11;107(19):8812-7.

Jones CJ, Homma M, Macnab RM. Identification of proteins of the outer (L and P) rings of the flagellar basal body of Escherichia coli. J Bacteriol. 1987 Apr;169(4):1489-92.

Jones CJ, Homma M, Macnab RM. L-, P-, and M-ring proteins of the flagellar basal body of Salmonella typhimurium: gene sequences and deduced protein sequences. J Bacteriol. 1989 Jul;171(7):3890-900.

Jones PC, Hermolin J, Jiang W, Fillingame RH. Insights into the rotary catalytic mechanism of F0F1 ATP synthase from the cross-linking of subunits b and c in the Escherichia coli enzyme. J Biol Chem. 2000 Oct 6;275(40):31340-6.

Karlinsey JE, Tanaka S, Bettenworth V, Yamaguchi S, Boos W, Aizawa SI, Hughes KT. Completion of the hook-basal body complex of the Salmonella typhimurium flagellum is coupled to FlgM secretion and fliC transcription. Mol Microbiol. 2000 Sep;37(5):1220-31.

Kawamoto A, Morimoto YV, Miyata T, Minamino T, Hughes KT, Kato T, Namba K. Common and distinct structural features of Salmonella injectisome and flagellar basal body. Sci Rep. 2013 Nov 28;3:3369.

Kazetani K, Minamino T, Miyata T, Kato T, Namba K. ATP-induced FliI hexamerization facilitates bacterial flagellar protein export. Biochem Biophys Res Commun. 2009 Oct 16;388(2):323-7.

Khan S, Meister M, Berg HC. Constraints on flagellar rotation. J Mol Biol. 1985 Aug 20;184(4):645-56.

Kihara M, Minamino T, Yamaguchi S, Macnab RM. Intergenic suppression between the flagellar MS ring protein FliF of Salmonella and FlhA, a membrane component of its export apparatus. J Bacteriol. 2001 Mar;183(5):1655-62.

Kinoshita M, Hara N, Imada K, Namba K, Minamino T. Interactions of bacterial flagellar chaperone-substrate complexes with FlhA contribute to co-ordinating assembly of the flagellar filament. Mol Microbiol. 2013 Dec;90(6):1249-61.

Kishikawa J, Ibuki T, Nakamura S, Nakanishi A, Minamino T, Miyata T, Namba K, Konno H, Ueno H, Imada K, Yokoyama K. Common evolutionary origin for the rotor domain of rotary ATPases and flagellar protein export apparatus. PLoS One. 2013 May 28;8(5):e64695.

Kojima S, Blair DF. Solubilization and purification of the MotA/MotB complex of Escherichia coli. Biochemistry. 2004 Jan 13;43(1):26-34.

Kojima S, Imada K, Sakuma M, Sudo Y, Kojima C, Minamino T, Homma M, Namba K. Stator assembly and activation mechanism of the flagellar motor by the periplasmic region of MotB. Mol Microbiol. 2009 Aug;73(4):710-8.

Kubori T, Shimamoto N, Yamaguchi S, Namba K, Aizawa S. Morphological pathway of flagellar assembly in Salmonella typhimurium.J Mol Biol. 1992 Jul 20;226(2):433-46.

Kutsukake K, Okada T, Yokoseki T, Iino T. Sequence analysis of the flgA gene and its adjacent region in Salmonella typhimurium, and identification of another flagellar gene, flgN. Gene. 1994 May 27;143(1):49-54.

Larsen SH, Reader RW, Kort EN, Tso WW, Adler J. Change in direction of flagellar rotation is the basis of the chemotactic response in Escherichia coli. Nature. 1974 May 3;249(452):74-7.

Lee J, Harshey RM. Loss of FlhE in the flagellar Type III secretion system allows proton influx into Salmonella and Escherichia coli. Mol Microbiol. 2012 May;84(3):550-65.

Lee J, Monzingo AF, Keatinge-Clay AT, Harshey RM. Structure of Salmonella FlhE, conserved member of a flagellar type III secretion operon. J Mol Biol. 2015 Mar 27;427(6 Pt B):1254-62.

Lee LK, Ginsburg MA, Crovace C, Donohoe M, Stock D. Structure of the torque ring of the flagellar motor and the molecular basis for rotational switching. Nature. 2010 Aug 19;466(7309):996-1000.

Li H, Sourjik V. Assembly and stability of flagellar motor in Escherichia coli. Mol Microbiol. 2011 May;80(4):886-99.

Ludtke SJ, Baldwin PR, Chiu W. EMAN: semiautomated software for high-resolution single-particle reconstructions. J Struct Biol. 1999 Dec 1;128(1):82-97.

Macnab RM. How bacteria assemble flagella. Annu Rev Microbiol. 2003;57:77-100.

Manson MD, Tedesco P, Berg HC, Harold FM, Van der Drift C. A protonmotive force drives bacterial flagella. Proc Natl Acad Sci U S A. 1977 Jul;74(7):3060-4.

Maki-Yonekura S, Yonekura K, Namba K. Conformational change of flagellin for polymorphic supercoiling of the flagellar filament. Nat Struct Mol Biol. 2010 Apr;17(4):417-22.

Malakooti J, Komeda Y, Matsumura P. DNA sequence analysis, gene product identification, and localization of flagellar motor components of Escherichia coli. J Bacteriol. 1989 May;171(5):2728-34.

McMurry JL, Van Arnam JS, Kihara M, Macnab RM. Analysis of the cytoplasmic domains of Salmonella FlhA and interactions with components of the flagellar export machinery. J Bacteriol. 2004 Nov;186(22):7586-92.

McMurry JL, Murphy JW, González-Pedrajo B. The FliN-FliH interaction mediates localization of flagellar export ATPase FliI to the C ring complex. Biochemistry. 2006 Oct 3;45(39):11790-8.

Minamino T, Iino T, Kutuskake K. Molecular characterization of the Salmonella typhimurium flhB operon and its protein products. J Bacteriol. 1994 Dec;176(24):7630-7.

Minamino T, Imada K, Kinoshita M, Nakamura S, Morimoto YV, Namba K. Structural insight into the rotational switching mechanism of the bacterial flagellar motor. PLoS Biol. 2011 May;9(5):e1000616.

Minamino T, Chu R, Yamaguchi S, Macnab RM. Role of FliJ in flagellar protein export in Salmonella. J Bacteriol. 2000 Aug;182(15):4207-15.

Minamino T, González-Pedrajo B, Oosawa K, Namba K, Macnab RM. Structural properties of FliH, an ATPase regulatory component of the Salmonella type III flagellar export apparatus. J Mol Biol. 2002 Sep 13;322(2):281-90.

Minamino T, González-Pedrajo B, Kihara M, Namba K, Macnab RM. The ATPase FliI can interact with the type III flagellar protein export apparatus in the absence of its regulator, FliH. J Bacteriol. 2003 Jul;185(13):3983-8.

Minamino T, Macnab RM. Domain structure of Salmonella FlhB, a flagellar export component responsible for substrate specificity switching. J Bacteriol. 2000 Sep;182(17):4906-14.

Minamino T, Kazetani K, Tahara A, Suzuki H, Furukawa Y, Kihara M, Namba K. Oligomerization of the bacterial flagellar ATPase FliI is controlled by its extreme N-terminal region. J Mol Biol. 2006 Jul 7;360(2):510-9.

Minamino T, Ferris HU, Moriya N, Kihara M, Namba K. Two parts of the T3S4 domain of the hook-length control protein FliK are essential for the substrate specificity switching of the flagellar type III export apparatus. J Mol Biol. 2006 Oct 6;362(5):1148-58.

Minamino T, Imada K, Namba K. Molecular motors of the bacterial flagella. Curr Opin Struct Biol. 2008 Dec;18(6):693-701.

Minamino T, Imada K, Namba K. Mechanisms of type III protein export for bacterial flagellar assembly. Mol Biosyst. 2008 Nov;4(11):1105-15.

Minamino T, Yoshimura SD, Morimoto YV, González-Pedrajo B, Kami-Ike N, Namba K. Roles of the extreme N-terminal region of FliH for efficient localization of the FliH-FliI complex to the bacterial flagellar type III export apparatus. Mol Microbiol. 2009 Dec;74(6):1471-83.

Minamino T, Macnab RM. Components of the Salmonella flagellar export apparatus and classification of export substrates. J Bacteriol. 1999 Mar;181(5):1388-94.

Minamino T, MacNab RM. Interactions among components of the Salmonella flagellar export apparatus and its substrates. Mol Microbiol. 2000 Mar;35(5):1052-64.

Minamino T, MacNab RM. FliH, a soluble component of the type III flagellar export apparatus of Salmonella, forms a complex with FliI and inhibits its ATPase activity. Mol Microbiol. 2000 Sep;37(6):1494-503.

Minamino T, Namba K. Self-assembly and type III protein export of the bacterial flagellum. J Mol Microbiol Biotechnol. 2004;7(1-2):5-17.

Minamino T, Namba K. Distinct roles of the FliI ATPase and proton motive force in bacterial flagellar protein export.Nature. 2008 Jan 24;451(7177):485-8.

Minamino T, Morimoto YV, Hara N, Namba K. An energy transduction mechanism used in bacterial flagellar type III protein export. Nat Commun. 2011 Sep 20;2:475.

Minamino T, Kinoshita M, Imada K, Namba K. Interaction between FliI ATPase and a flagellar chaperone FliT during bacterial flagellar protein export. Mol Microbiol. 2012 Jan;83(1):168-78.

Minamino T, Kinoshita M, Hara N, Takeuchi S, Hida A, Koya S, Glenwright H, Imada K, Aldridge PD, Namba K. Interaction of a bacterial flagellar chaperone FlgN with FlhA is required for efficient export of its cognate substrates. Mol Microbiol. 2012 Feb;83(4):775-88.

Minamino T, Morimoto YV, Kinoshita M, Aldridge PD, Namba K. The bacterial flagellar protein export apparatus processively transports flagellar proteins even with extremely infrequent ATP hydrolysis. Sci Rep. 2014 Dec 22;4:7579.

Mindell JA, Grigorieff N. Accurate determination of local defocus and specimen tilt in electron microscopy. J Struct Biol. 2003 Jun;142(3):334-47.

Morimoto YV, Ito M, Hiraoka KD, Che YS, Bai F, Kami-Ike N, Namba K, Minamino T. Assembly and stoichiometry of FliF and FlhA in Salmonella flagellar basal body. Mol Microbiol. 2014 Mar;91(6):1214-26.

Moriya N, Minamino T, Hughes KT, Macnab RM, Namba K. The type III flagellar export specificity switch is dependent on FliK ruler and a molecular clock. J Mol Biol. 2006 Jun 2;359(2):466-77.

Murphy GE, Leadbetter JR, Jensen GJ. In situ structure of the complete Treponema primitia flagellar motor. Nature. 2006 Aug 31;442(7106):1062-4. Epub 2006 Aug 2.

Namba K, Vonderviszt F. Molecular architecture of bacterial flagellum. Q Rev Biophys. 1997 Feb;30(1):1-65.

Nambu T, Minamino T, Macnab RM, Kutsukake K. Peptidoglycan-hydrolyzing activity of the FlgJ protein, essential for flagellar rod formation in Salmonella typhimurium. J Bacteriol. 1999 Mar;181(5):1555-61.

Nambu T, Kutsukake K. The Salmonella FlgA protein, a putativeve periplasmic chaperone essential for flagellar P ring formation. Microbiology. 2000 May;146 (Pt 5):1171-8.

Natale P, Brüser T, Driessen AJ. Sec- and Tat-mediated protein secretion across the bacterial cytoplasmic membrane--distinct translocases and mechanisms. Biochim Biophys Acta. 2008 Sep;1778(9):1735-56. Epub 2007 Aug 9. Review.

Ohnishi K, Ohto Y, Aizawa S, Macnab RM, Iino T. FlgD is a scaffolding protein needed for flagellar hook assembly in Salmonella typhimurium. J Bacteriol. 1994 Apr;176(8):2272-81.

Ohnishi K, Fan F, Schoenhals GJ, Kihara M, Macnab RM. The FliO, FliP, FliQ, and FliR proteins of Salmonella typhimurium: putative components for flagellar assembly. J Bacteriol. 1997 Oct;179(19):6092-9.

Pallen MJ, Bailey CM, Beatson SA. Evolutionary links between FliH/YscL-like proteins from bacterial type III secretion systems and second-stalk components of the FoF1 and vacuolar ATPases. Protein Sci. 2006 Apr;15(4):935-41.

Pradel N, Ye C, Wu LF. A cleavable signal peptide is required for the full function of the polytopic inner membrane protein FliP of Escherichia coli. Biochem Biophys Res Commun. 2004 Jul 9;319(4):1276-80.

Park SY, Lowder B, Bilwes AM, Blair DF, Crane BR. Structure of FliM provides

insight into assembly of the switch complex in the bacterial flagella motor. Proc Natl Acad Sci U S A. 2006 Aug 8;103(32):11886-91. Epub 2006 Aug 1.

Paul K, Harmon JG, Blair DF. Mutational analysis of the flagellar rotor protein FliN: identification of surfaces important for flagellar assembly and switching. J Bacteriol. 2006 Jul;188(14):5240-8.

Paul K, Erhardt M, Hirano T, Blair DF, Hughes KT. Energy source of flagellar type III secretion. Nature. 2008 Jan 24;451(7177):489-92. EMBO J. 2011 Jun 14;30(14):2962-71.

Paul K, Gonzalez-Bonet G, Bilwes AM, Crane BR, Blair D. Architecture of the flagellar rotor.

Raddi G, Morado DR, Yan J, Haake DA, Yang XF, Liu J. Three-dimensional structures of pathogenic and saprophytic Leptospira species revealed by cryo-electron tomography. J Bacteriol. 2012 Mar;194(6):1299-306.

Saijo-Hamano Y, Uchida N, Namba K, Oosawa K. In vitro characterization of FlgB, FlgC, FlgF, FlgG, and FliE, flagellar basal body proteins of Salmonella. J Mol Biol. 2004 May 28;339(2):423-35.

Saijo-Hamano Y, Imada K, Minamino T, Kihara M, Shimada M, Kitao A, Namba K. Structure of the cytoplasmic domain of FlhA and implication for flagellar type III protein export. Mol Microbiol. 2010 Apr;76(1):260-8.

Saijo-Hamano Y, Matsunami H, Namba K, Imada K. Expression, purification, crystallization and preliminary X-ray diffraction analysis of a core fragment of FlgG, a bacterial flagellar rod protein. Acta Crystallogr Sect F Struct Biol Cryst Commun. 2013 May 1;69(Pt 5):547-50.

Samatey FA, Imada K, Nagashima S, Vonderviszt F, Kumasaka T, Yamamoto M, Namba K. Structure of the bacterial flagellar protofilament and implications for a switch for supercoiling. Nature. 2001 Mar 15;410(6826):331-7.

Samatey FA, Matsunami H, Imada K, Nagashima S, Shaikh TR, Thomas DR, Chen JZ, Derosier DJ, Kitao A, Namba K. Structure of the bacterial flagellar hook and implication for the molecular universal joint mechanism. Nature. 2004 Oct 28;431(7012):1062-8.

Sarkar MK, Paul K, Blair DF. Subunit organization and reversal-associated movements in the flagellar switch of Escherichia coli. J Biol Chem. 2010 Jan 1;285(1):675-84.

Sarkar MK, Paul K, Blair D. Chemotaxis signaling protein CheY binds to the rotor protein FliN to control the direction of flagellar rotation in Escherichia coli. Proc Natl Acad Sci U S A. 2010 May 18;107(20):9370-5.

Schoenhals GJ, Macnab RM. Physiological and biochemical analyses of FlgH, a lipoprotein forming the outer membrane L ring of the flagellar basal body of Salmonella typhimurium. Bacteriol. 1996 Jul;178(14):4200-7.

Shaikh TR, Thomas DR, Chen JZ, Samatey FA, Matsunami H, Imada K, Namba K, Derosier DJ. A partial atomic structure for the flagellar hook of Salmonella typhimurium. Proc Natl Acad Sci U S A. 2005 Jan 25;102(4):1023-8. Epub 2005 Jan 18.

Shioi JI, Matsuura S, Imae Y. Quantitative measurements of proton motive force and motility in Bacillus subtilis. J Bacteriol. 1980 Dec;144(3):891-7.

Silva-Herzog E, Dreyfus G. Interaction of FliI, a component of the flagellar export apparatus, with flagellin and hook protein. Biochim Biophys Acta. 1999 May 18;1431(2):374-83.

Stock D, Namba K, Lee LK. Nanorotors and self-assembling macromolecular machines: the torque ring of the bacterial flagellar motor. Curr Opin Biotechnol. 2012 Aug;23(4):545-54.

Suzuki H, Yonekura K, Namba K. Structure of the rotor of the bacterial flagellar motor revealed by electron cryomicroscopy and single-particle image analysis. J Mol Biol. 2004 Mar 12;337(1):105-13.

Suzuki T, Iino T, Horiguchi T, Yamaguchi S. Incomplete flagellar structures in nonflagellate mutants of Salmonella typhimurium. J Bacteriol. 1978 Feb;133(2):904-15.

Suzuki T, Komeda Y. Incomplete flagellar structures in Escherichia coli mutants. J Bacteriol. 1981 Feb;145(2):1036-41.

Terahara N, Krulwich TA, Ito M. Mutations alter the sodium versus proton use of a Bacillus clausii flagellar motor and confer dual ion use on Bacillus subtilis motors. Proc Natl Acad Sci U S A. 2008 Sep 23;105(38):14359-64.

Thomas DR, Francis NR, Xu C, DeRosier DJ. The three-dimensional structure of the flagellar rotor from a clockwise-locked mutant of Salmonella enterica serovar Typhimurium. J Bacteriol. 2006 Oct;188(20):7039-48.

Thomas J, Stafford GP, Hughes C. Docking of cytosolic chaperone-substrate complexes at the membrane ATPase during flagellar type III protein export. Proc Natl Acad Sci U S A. 2004 Mar 16;101(11):3945-50.

Yokoseki T, Kutsukake K, Ohnishi K, Iino T. Functional analysis of the flagellar genes in the fliD operon of Salmonella typhimurium. Microbiology. 1995 Jul;141 (Pt 7):1715-22.

Yonekura K, Maki-Yonekura S, Namba K. Complete atomic model of the bacterial flagellar filament by electron cryomicroscopy. Nature. 2003 Aug 7;424(6949):643-50.

Yonekura K, Maki-Yonekura S, Homma M. Structure of the flagellar motor protein complex PomAB: implications for the torque-generating conformation. J Bacteriol. 2011 Aug;193(15):3863-70.

Van Arnam JS, McMurry JL, Kihara M, Macnab RM. Analysis of an engineered Salmonella flagellar fusion protein, FliR-FlhB. J Bacteriol. 2004 Apr;186(8):2495-8.

Vogler AP, Homma M, Irikura VM, Macnab RM.Salmonella typhimurium mutants defective in flagellar filament regrowth and sequence similarity of FliI to F_0F_1, vacuolar, and archaebacterial ATPase subunits. J Bacteriol. 1991 Jun;173(11):3564-72.

von Ballmoos C, Cook GM, Dimroth P. Unique rotary ATP synthase and its biological diversity. Annu Rev Biophys. 2008;37:43-64.

Wagner S, Königsmaier L, Lara-Tejero M, Lefebre M, Marlovits TC, Galán JE. Organization and coordinated assembly of the type III secretion export apparatus. Proc Natl Acad Sci U S A. 2010 Oct 12;107(41):17745-50.

Wickner W, Schekman R. Protein translocation across biological membranes. Science. 2005 Dec 2;310(5753):1452-6.

Winn MD, Ballard CC, Cowtan KD, Dodson EJ, Emsley P, Evans PR, Keegan RM, Krissinel EB, Leslie AG, McCoy A, McNicholas SJ, Murshudov GN, Pannu NS, Potterton EA, Powell HR, Read RJ, Vagin A, Wilson KS. Overview of the CCP4 suite and current developments. Acta Crystallogr D Biol Crystallogr. 2011 Apr;67(Pt 4):235-42.

Williams AW, Yamaguchi S, Togashi F, Aizawa SI, Kawagishi I, Macnab RM. Mutations in fliK and flhB affecting flagellar hook and filament assembly in Salmonella typhimurium. J Bacteriol. 1996 May;178(10):2960-70.

Zhou J, Blair DF. Residues of the cytoplasmic domain of MotA essential for torque generation in the bacterial flagellar motor. J Mol Biol. 1997 Oct 24;273(2):428-39.

Zhou J, Lloyd SA, Blair DF. Electrostatic interactions between rotor and stator in the bacterial flagellar motor. Proc Natl Acad Sci U S A. 1998 May 26;95(11):6436-41.

Zhou J, Sharp LL, Tang HL, Lloyd SA, Billings S, Braun TF, Blair DF. Function of protonatable residues in the flagellar motor of Escherichia coli: a critical role for Asp 32 of MotB. J Bacteriol. 1998 May;180(10):2729-35.

Zhu K, González-Pedrajo B, Macnab RM. Interactions among membrane and soluble components of the flagellar export apparatus of Salmonella. Biochemistry. 2002 Jul 30;41(30)

Publication

Original paper

1. Fukumura T., Furukawa Y., Kawaguchi T., Saijo-Hamano Y., Namba, K., Imada K. & Minamino T. (2014) Crystallization and preliminary X-ray analysis of the periplasmic domain of FliP, an integral membrane component of the bacterial flagellar type III protein export apparatus. **Acta Cryst.** F70, 1215-1218. 査読有

2. Fukumura T., Makino F., Namba K., Imada K. & Minamino T. Structural characterization of FliP, a component of type III flagellar protein export gate. 投稿準備中

Conferrence

○福村拓真、古川進郎、西條由見子、今田勝巳、難波啓一、南野徹. バクテリアべん毛 輸送ゲート構成蛋白質 FliP の機能構造解析, 第 19 回べん毛研究交流会、群馬、2013 年 3 月

三谷理恵、川村真結子、福村拓真、竹原清日、松岡信、○上口美弥子. ジベレリン 核内受容体の GID1 の機能解析, 第 53 回日本植物生理学会、名古屋、2012 年 3 月,

○福村拓真、古川進郎、西條由見子、今田勝巳、難波啓一、南野徹. べん毛輸送装置 構成因子 FliP ペリプラズム領域の機能構造解析, 第 9 回 21 世紀大腸菌研究会、滋賀県、 2012 年 6 月

○福村拓真、古川進郎、西條由見子、今田勝巳、難波啓一、南野徹. べん毛輸送装置 構成因子 FliP ペリプラズム領域の機能構造解析, 第 50 回日本生物物理学会、愛知県、 2012 年 9 月

○福村拓真、古川進郎、西條由見子、今田勝巳、難波啓一、南野徹. べん毛 III 型輸送 装置構成タンパク質 FliP のペリプラズム領域の結晶化と機能解析, 日本生体エネルギ ー研究会　第 38 回討論会、岡山県、2012 年 12 月

○福村拓真、川口辰也、古川進郎、今田勝巳、難波啓一、南野徹. べん毛輸送装置構 成蛋白質 FliP ペリプラズミックループの結晶化と遺伝学的解析, 第四回箱島領域全体 会議、山梨、2013 年 6 月

○福村拓真、古川進郎、西條由見子、今田勝巳、難波啓一、南野徹. Crystallization and genetic analyses of a periplasmic loop of FliP, a component of the flagellar protein export apparatus, 第 51 回日本生物物理学会、京都府、2013 年 10 月

○福村拓真、川口辰也、古川進郎、今田勝巳、難波啓一、南野徹. X-ray crystallographic analysis of a peri plasmic domain of FliP, a component of the bacterial flagellar type III export gate, 第 20 回べん毛研究交流会、広島、2014 年 3 月

○福村拓真、今田勝巳、難波啓一、南野徹. バクテリアべん毛輸送ゲート構成因子 FliP の機能構造解析, 新学術領域研究「構造細胞生物学」第五回班会議、北海道、2014 年 6 月

○Takuma Fukumura, Fumiaki Makino, Takayuki Kato, Katsumi Imada, Keiichi Namba1 and Toh ru Minamino. STRUCTURAL CHARACTERIZATION OF FLIP, A COMPONENT OF THE TY PE III FLAGELLAR PROTEIN EXPORT APPARATUS, BLAST XIII , Tucson Arizona USA, 2 015年1月

○Takuma Fukumura, Fumiaki Makino, Takayuki Kato,Katsumi Imada, Keiichi Namba and Tohru Minamino. Structural characterization of FliP, a component of the type III flagellar protein expo rt apparatus, 第 53 回日本生物物理学会、金沢、2015 年 9 月